Imperial College London

CHANGES IN BONE'S NANOSTRUCTURE ASSOCIATED WITH BONE FRAGILITY & BISPHOSPHONATE TREATMENT

A thesis submitted in fulfilment of the requirements for the degree of Doctor of Philosophy and the Diploma of Imperial College London

Tabitha Jia Hui TAY

Department of Surgery & Cancer

Imperial College London

Statement of Originality

This is to certify that the content of this thesis is original and of my own work. All assistance received has been acknowledged and sources of material have been appropriately referenced. Finally this work has not been submitted for any other degree or other purposes.

Copyright Declaration

Acknowledgements

Firstly I would like to express my upmost gratitude to my supervisor, Dr Richard Abel for his support and guidance throughout the research. During the three years, he was not only a supervisor for the project but also a mentor and advisor for my life outside of academics. His immense knowledge, motivation and patience have shown me how to be a good researcher as well as how to excel in life. I am also pleased to say thank you to Dr Ulrich Hansen, my secondary supervisor, who has given me much support and valuable insights in the engineering side of the project. Apart from my supervisors, I would also express gratitude to Professor Justin Cobb, who constantly gave me valuable support at different stages of the research.

Secondly, I owe sincere thanks to all my collaborators and fellow researchers, with whom I would not have been able to produce this research. I would like to acknowledge Mr Rajarshi Bhattachrya from St Mary's Hospital for his full support in collecting samples for the research, Dr Himadri Gupta from Queen Mary University of London for his guidance in the concepts of synchrotron imaging and the use of his tensile testing rig, and Professor Anthony Bull for the loan of equipment used for synchrotron experiments. I also want to thank my other collaborators, Professor Edward Guo and Miss Yizhong Hu from Columbia University, and Professor Peter Zioupos and Mr Andrea Bonicelli from Cranfield University. I am extremely grateful to all my colleagues, the hardworking fellow PhDs and post-docs from the MSK Lab in the School of Medicine, as well as the Bioengineering Department. In addition, I would like to thank the staff and technicians at Diamond Light Source for their assistance with experiments, as well as the staff at the Imperial Tissue Bank with ethical approvals for specimen collection.

Moreover, I would like to thank my friends who supported me throughout the research program, who listened to my never-ending complaints and motivated me during difficult times. I especially want to thank Kwai Pang for all his love and support.

Finally, and most importantly, I would like to thank my parents and siblings who always kept me their prayers. Their unfailing love and support helped me through the toughest times during the PhD and motivated me to pursue my goals, and I would consider myself nothing without them.

Conference Presentations

1. Tay, T.; You, A.; Ma, S.; Churchwell, J.; Hansen, U.; Cobb, J.; Abel, R. (2017), The effects of bisphosphonate therapy on bone nanostructure.
   British Orthopaedic Research Society, 4-5 September 2017, London, UK

2. Tay, T.; Gupta, H.; Cobb, J.; Hansen, U.; Abel, R. (2019), The effects of osteoporosis and bisphosphonate treatment on bone's nanostructure.
   25th Congress of the European Society of Biomechanics, 7-10 July 2019, Vienna, Austria

Publications

1. Bone Building Blocks. Tabitha Tay & Richard Abel
   Osteoporosis Review, Volume 28, Number 1, Winter 2018, Pages 17-19

Abstract

The contribution of the nanostructure to whole bone strength has long been debated. However the impact of the collagen-mineral matrix on whole bone mechanics has yet to be tested. At the start of the study, bone volume and microarchitecture were found to not entirely account for bone strength, even though new ITS techniques were included, and thus it seemed possible that the gap could be attributed to the nanostructure.

State-of-the-art synchrotron imaging was used to compare nanomechanics between bones from ageing non-fracture donors and ageing fracture patients, half of whom had been prescribed bisphosphonate. Fracture patients exhibited with lower tissue, collagen and mineral strains than non-fracture patients, suggesting that their nanostructures were less deformable. In addition, the fracture patients exhibited with wider mineral crystals, providing for larger surface areas for interfacial bonding with collagen fibrils, and thus preventing the unwinding and sliding of the matrix during loading. The less deformable matrix may reduce macroscopic strength via a cascade effect by easier initiation and growth of microcracks in the collagen-mineral matrix and limiting the bone's ability to bend and absorb energy during a trip or fall.

This new knowledge of the importance of the nanoscale deformation to whole bone strength could fill gaps in current diagnostics and treatments, if it were possible to measure deformation properties *in vivo.* Nanoindentation was developed to measure such deformations, and as such, a benchtop system was used to measure material properties of

the three groups, and the data was correlated with nanostrain data. However, nanoindentation material properties and fibril and mineral strains were not correlated. In addition to the lack of correlation to microstructure and macro level strength and stiffness, it seems that nanoindentation does not measure material properties accurately and thus other alternatives need to be looked into for *in-vivo* measurements at the nanoscale.

Contents

List of Equations

$\beta = 1 - \Delta\chi$ Equation 2.1

$Connectivty\ density = \frac{\beta}{stack\ volume}$ Equation 2.2

$n\lambda = 2d \sin\theta$ Equation 3.1

$q = \frac{2\pi n}{D}$ Equation 3.2

$S = \frac{\Delta d}{D}$ Equation 3.3

$\psi = \frac{\phi}{z}$ Equation 4.1

$E_\rho = \psi \times 1.6 \times 10^{-19} J/eV \times E$ Equation 4.2

$T = e^{-\alpha\rho l}$ Equation 4.3

$D = \frac{AE_\rho}{m}$ Equation 4.4

$Total\ irradiation\ dose = D \times t$ Equation 4.5

$$D = \frac{K\lambda}{\beta_{1/2}\cos(\theta)}$$ Equation 5.1

$$I(q) = Pq^{-4}$$ Equation 5.2

$$T = \frac{4}{\pi P}\int_0^\infty q^2 I(q)\, dq$$ Equation 5.3

$$T = \frac{4v(1/v)}{\sigma}$$ Equation 5.4

$$H = \frac{P_{max}}{A_r}$$ Equation 6.1

$$E_r = \frac{1}{\beta}\frac{\sqrt{\pi}}{2}\frac{S}{\sqrt{A_p h_c}}$$ Equation 6.2

$$A_p h_c = C_0 h_c^2 + C_1 h_c^1 + C_2 h_c^{1/2} + \cdots + C_8 h_c^{1/128}$$ Equation 6.3

$$\frac{1}{E_r} = \frac{(1-v_i^2)}{E_i} + \frac{(1-v_s^2)}{E_s}$$ Equation 6.4

List of Figures

List of Tables

Chapter 1. Motivation and Structure of Thesis

1.1 Background

1.1.1 Bone fragility

Bone fragility affects 200 million people worldwide and causes 8.9 million fractures annually (International Osteoporosis Foundation, 2017). A major disease of the bone that results in fragility fractures is osteoporosis which is associated with aging and is a severe, growing problem worldwide. The disease makes bone susceptible to fracture by causing the loss of bone mass, mineral density and structure (Raisz & Rodan, 2003). 1 in 2 women and 1 in 5 men over the age of 50 will suffer a fracture due to osteoporosis and result in an estimated £1.8 billion spent on direct medical costs in the UK and £40.5 billion globally (International Osteoporosis Foundation, 2017).

1.1.2 Bisphosphonate

The frontline therapy for treating and preventing fragility fractures is a family of medicines called bisphosphonate (BP), which includes alendronate, risendronate, ibandronate and zolendronate. The most commonly prescribed form of therapy is the once weekly oral medication, alendronate. Bisphosphonates act to reduce remodelling rate and resorption of bone, increasing bone mass and mineral density (BMD), thereby reducing fracture risks (Kenkre & Bassett, 2018). Clinical trials and follow-ups have shown that bisphosphonates are effective at reducing the number of vertebral and hip fractures in postmenopausal women with osteoporosis (Black et al., 1996; Cummings et al., 1998; Harris et al., 1999; McClung et al., 2001). These studies have shown that BP increases BMD or bone mineral content, however, there is a poor correlation between BMD and incidence of fractures (Cummings et al., 2002). Cummings *et al.* conducted a meta-analysis of 12 clinical trials to estimate the reduction in risk vertebral fractures with improvements in BMD. They reported that changes in BMD only accounted for 9% of the observed 52% risk reduction (Cummings et al., 2002). However, the clinical trials included in the study all lasted less than 5 years and BMD improvements occur slowly, possibly even after 5 years of treatment. Thus the estimation of the correlation between BMD and fracture risk reduction could have been underestimated.

1.1.3 Loss of mass, mineral density & structure

Bone has a complex hierarchical structure, as shown in Figure 1.1.1, from the macrostructure to the nanostructure, and deterioration occurs at every level with a disease like osteoporosis.

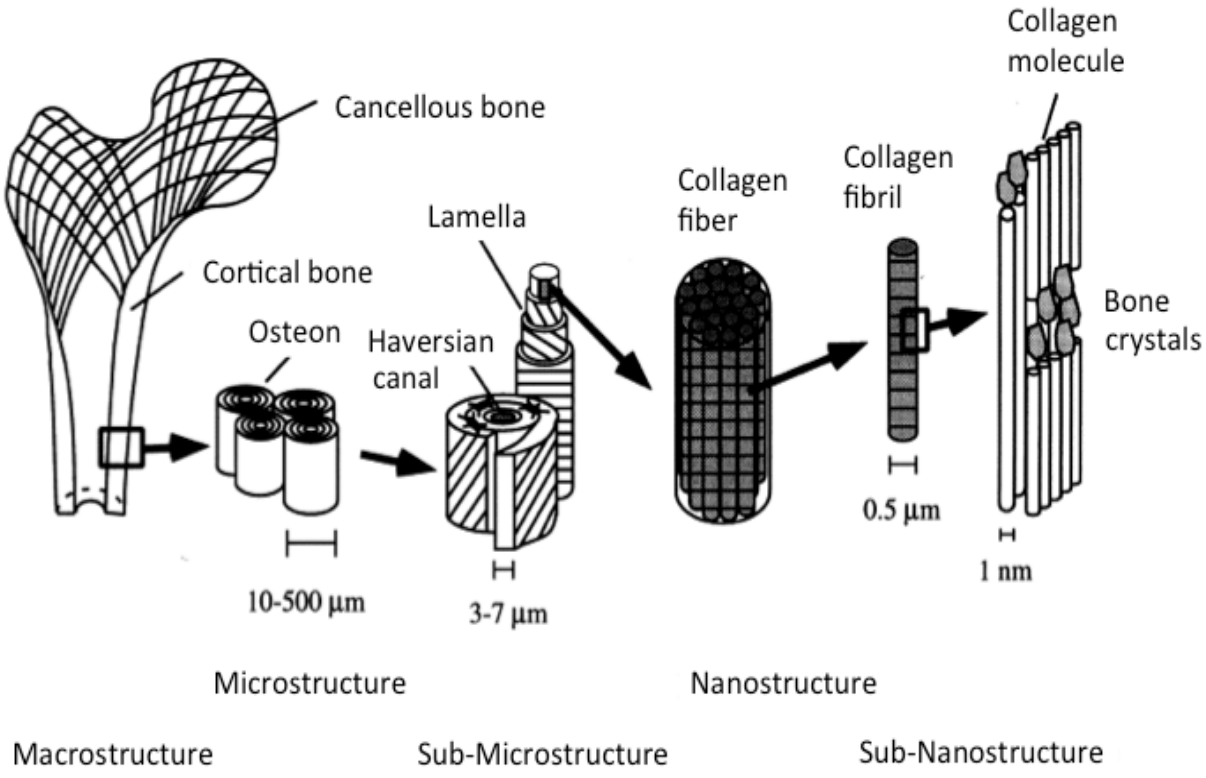

Figure 1.1.1 Depiction of the hierarchical structure of bone adapted from (Rho et al., 1998)

At the macro level, osteoporosis results in the loss of bone mass and density. As such the most common identification of osteoporosis is the measurement of BMD. However, half of people who fracture have healthy BMDs. This lack of correlation of BMD with fragility fractures could be due to the fact that osteoporosis is not just associated with the loss of mass and mineral density but also the loss of structure at lower levels.

At the micro level, overactive osteoclasts (to be further explained in section 1.1.4.4) in osteoporotic bone result in the impairment of the bone's microstructure, by altering trabecular connectivity, thickness, number and shape, which in turn reduce bone strength (Thürlimann, 2012). Further down the hierarchy, research has also brought about a growing consensus that the basic building blocks, namely the collagen and mineral, are damaged due to osteoporosis (Vashishth, 2007). However, there has been little work done on the understanding of their role to whole bone strength.

1.1.4 Bone's Basic Building Blocks

At the nano length scale, bone is made up of a collagen-mineral matrix, consisting of a mesh of overlapping collagen fibres, held together by chemical bonds known as crosslinks, and embedded with mineral crystals (Figure 1.1.2).

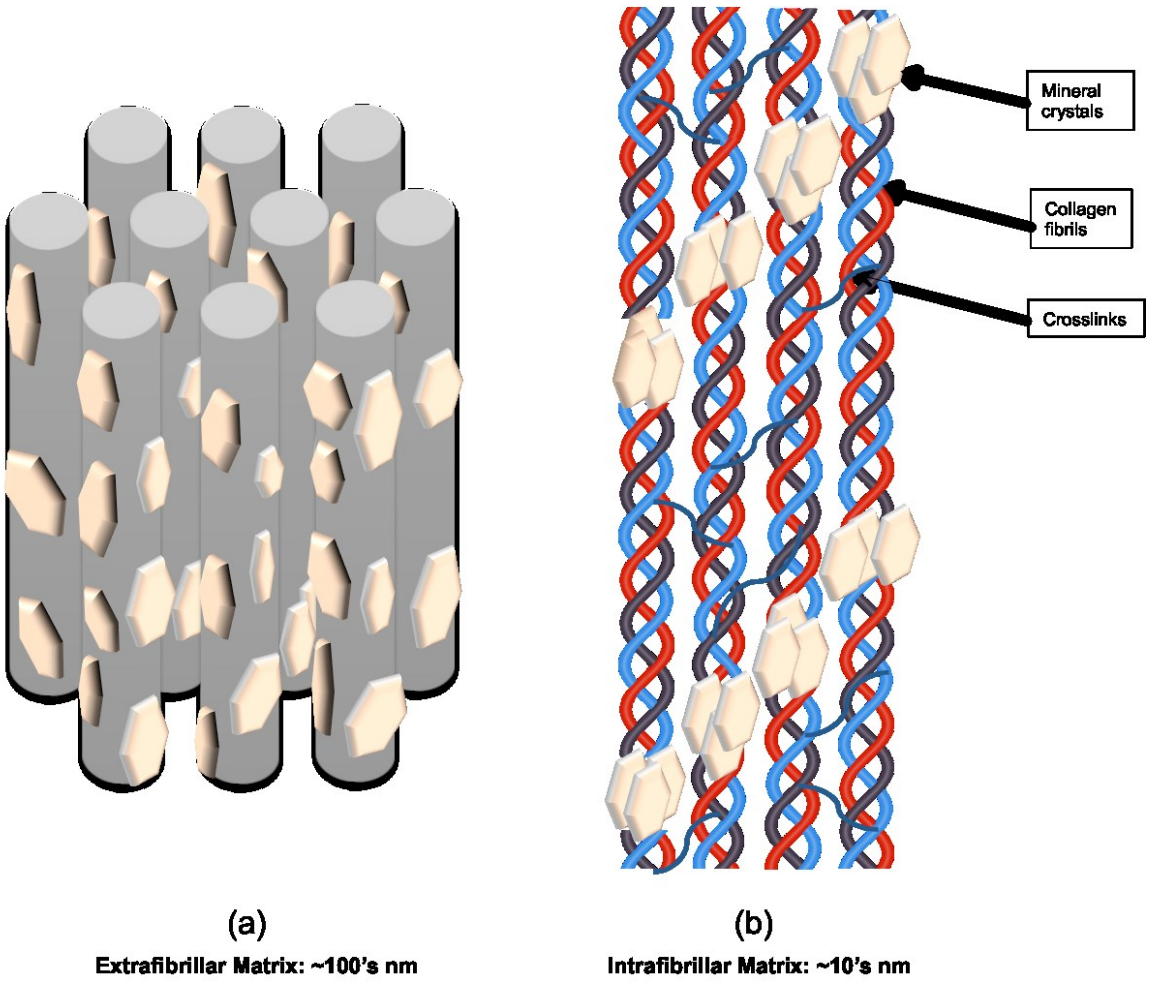

Figure 1.1.2 The collagen-mineral's extrafibrillar and intrafibrillar matrices .

1.1.4.1 The mineral phase

The mineral make-up of bone is carbonated hydroxyapatite, in the form of plate-shaped crystals roughly 50nm by 25nm by 2nm in dimensions (Robinson, 1952; Fratzl et al., 1992). The unit cell of hydroxyapatite $Ca_{10}(PO_4)_6(OH)_2$ crystallises into a hexagonal structure forming the apatite crystals which provide structural stability to the bone by reinforcing collagen fibrils.

1.1.4.2 Collagen

In bone, type I collagen is the most abundant protein, although other types including types III, VI and V are also present (Keene et al., 1991; Hert et al., 1994). Type I collagen is comprised of tropocollagen molecules that are about 300nm in length and are composed of 3 polypeptide chains (two α1 and one α2). The three peptide chains with repeating motifs of Gly-X-Y (Gly: Glycine, and X, Y can be either proline or hydroxyproline) wind together via hydrogen bonds between the -NH2 and -COOH terminals to form a triple helix. The staggered arrangement of the tropogollagen molecules result in the formation of spaces, where the intrafibrilllar crystals form (Hodge & Petruska, 1963; Traub et al., 1989).

The collagen fibrils typically merge with neighbouring fibrils, forming a diameter of about 50-200nm, and are connected by inter- and intra-molecular covalent crosslinks. These crosslinks can be categorised into two types: enzymatic crosslinks and nonenzymatic crosslinks.

Enzymatic crosslinks, also known as physiological crosslinks because they are naturally occurring, can also be subcatergorised into mature and immature crosslinks. Immature enzymatic crosslink formation is controlled by the enzyme, lysl oxidase, at specific lysline (Lys) and hydroxylysine (Hyl) residues at the N- and C- telopeptide terminals of the collagen molecules. This oxidation process produces lysl and hydroxyl aldehydes which subsequently condense to form the immature crosslinks,

Dihydroxylysinonorleucine (DHLNL) and Hydroxylysinonorleucine (HLNL) (Vashishth, 2007). These crosslinks later mature into more stable interfibrillar crosslinks such as the pyridinolines (Hydroxylysyl pyridinoline (HL-Pyr) and Lysyl-pyridinoline (L-Pyr)) and pyrrolic crosslinks (Zimmerman et al., 2012).

Nonenzymatic crosslinks, also known as advanced glycation end products (AGEs), form intra- and interfibrillarly along the collagen backbone with their formation induced by the glycation or oxidation between the Hyl or Lys residues and sugar (Zimmerman et al., 2012). The commonly identified AGEs include pentosidine, versperlysine, and nonfluorescent component-1 (NFC-1) (Vashishth, 2007). Although, at present time it has not been reported, another AGE, glucosepane, may also be an important AGE in bone type I collagen which forms in a parallel pathway as pentosidine, and is thought to have a significant presence in skin to affect the mechanical properties (Saito & Marumo, 2010).

1.1.4.3 Non-collagenous proteins

Besides the collagen and mineral, a phase of non-collagenous proteins (NCPs) makes up less than 10% of the total protein content that is present in bone. The most abundant NCPs in bone include osteonectin and osteocalcin and are thought to play crucial roles in bone formation, by affecting the regulation of osteoblast and osteoclast activity, as well as determining bone quality and fracture resistance (Robey, 1995; Morgan et al., 2016). Although the precise locations of specific NCP macromolecules in bone are not well known, they have been suggested to accumulate in the spaces between collagen fibrils

(Nanci, 1999). The NCPs act as glue between the mineralised collagen fibrils during crack formation and separation, via the sacrificial bonding mechanism (Fantner et al., 2005). This mechanism involves NCPs interacting with calcium (Ca^{2+}) ions to form and reform bonds, which are weak and thus break before the stronger bonds that hold the structure together. This mechanism increases the total energy required to fracture bone thereby dissipating loading energy and increasing bone's fracture toughness (Fantner et al., 2007).

1.1.4.4 Bone cells

Further down at the cellular level, there are four types of bone cells: the osteoblasts, the bone lining cells, the osteocytes and the osteoclasts (Figure 1.1.3).

The osteoblasts are bone forming cells and are located all along the surface of bone. These cells synthesise and secrete collagen proteins, NCPs and other proteoglycans to form the bone's organic matrix (Capulli et al., 2014). As osteoblasts mature, some become inactive and eventually form bone lining cells or become encapsulated in the bone matrix to form osteocytes (Manolagas, 2000).

Bone lining cells are formed once osteoblasts activities have terminated. The initial cuboidal osteoblasts, flatten and elongate to attach to the bone surface in a thin continuous layer (Miller et al., 1989). These cells act as a membrane, controlling the

transfer of ions between bone and the interstitial fluid (Andersen et al., 2009; Mosley, 2000).

The formation of osteocytes also only occur after osteoblasts activity has stopped and the cells are entrapped in the mineralised bone matrix. Osteocytes are the most abundant type of bone cells, comprising of 90-95% of the total bone cells and have long lifespans of up to 25 years (Franz-Odendaal et al., 2006). Osteocytes have a mechanosensitive function which is thought to activate osteoblasts and osteoclasts activity during external mechanical loading (Florencio-Silva et al., 2015; Hemmatian et al., 2017).

Finally, the osteoclasts are responsible for bone resorption, and with the osteoblasts, they make up the basic mutlicellular unit (BMU) which are in charge of the bone's remodelling process. Osteoclasts are larger than the other aforementioned bone cells and each cell contains multiple nuclei (Florencio-Silva et al., 2015). During bone resorption, these cells release proteases and acids to dissolve the bone's mineralised matrix (Charles & Aliprantis, 2014).

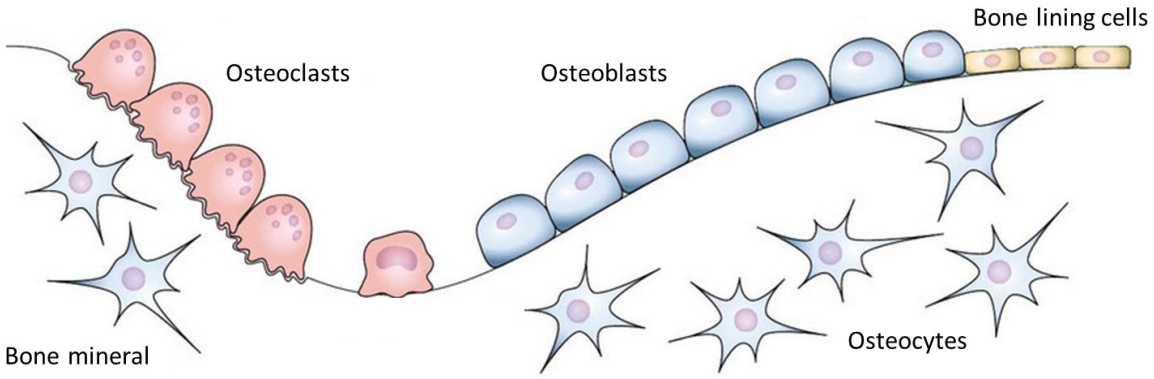

Figure 1.1.3 Schematic representation of the four types of bone cells (adapted from Corte, et al., 2019).

1.1.5 Effects of ageing & osteoporosis

The changes due to ageing and osteoporosis at the macro and micro levels of bone during ageing have been well studied to understand how the changes in material properties at these two levels affect whole bone mechanics (Zimmerman et al., 2015; Ritchie et al., 2009; Brandi, 2009). However, the research has still been unable to explain why only some people fracture while others do not, given that their bone quality, as defined by measurements at the tissue level, such as bone mineral density, are the same. For example, a patient with a healthy T-score, defining a normal BMD, might suffer a fracture, yet another with an unhealthy T-score (-2.5 or lower), who had not or is unable to receive treatment, does not fracture.

As such research recently has moved to focus on lower levels, at the nanostructure, looking at the collagen fibrils and mineral crystals, and the relative importance on the

bone's mechanical integrity. The basic building blocks of bone affect how flexible and strong the material is, with the collagen mesh allowing bone to bend and flex, while mineral crystals providing for rigidity. (National Institutes of Health Osteoporosis and Related Bone Diseases National Resource Center, 2018). As the basic building blocks of bone, they are important structures probably contributing to whole bone strength (both directly on macroscopic properties and indirectly via effects at the micro level) and thus any changes at this basic structural level due to disease or treatment could affect whole bone mechanics (Vashishth, 2007). It is thus possible that the most important changes that occur during aging and osteoporosis, that are currently not targeted for diagnosis and treatments, are actually the changes at the nanostructural level.

Despite the importance of the nanostructure to whole bone mechanics, people had not studied them in depth due to the lack of technology. However, with advancing imaging techniques such as synchrotron imaging, we are now in a good position to expand our understanding at this level.

1.2 Aims and objectives

1.2.1 Aims

The aim of this PhD thesis is to investigate the role of fibril and mineral mechanics in age-related fractures. The nano level of bone is the most understudied and thus a major focus in this thesis is placed on understanding how the nanoscale differs and how that differentiation affects whole bone strength. However it is impossible to understand the contribution of one level in isolation as the structures are interrelated. Thus the thesis investigated how the hierarchical levels of bone differed in bone that had suffered a fracture and non-fractured bone, working our way down from the microstructure to the nanostructure.

1.2.2 Objectives

To achieve the aim, the following chapters will:

1. Assess what portion of bone strength is unexplained after bone volume and microarchitecture are taken into account
2. Compare the nanomechanics in non-fracture controls, non-treated fracture controls and bisphosphonate treated fracture patients
3. Compare the mineral crystal dimensions in non-fracture controls, non-treated fracture controls and BP treated fracture patients
4. Assess the use of nanoindentation and the feasibility of measuring nanomechanics

1.3 Structure of the thesis

The thesis is divided into 7 chapters. Chapter 1 introduces the background, motivation, aims and objectives of the entire thesis. Chapter 2 investigates the differences in microarchitecture among the groups and the contribution to whole bone compressive strength. Chapter 3 investigates the differences in nanostrains between the aforementioned three groups as well as the effects of treatment on the nanomechanics. Chapter 4 validates the use synchrotron imaging by looking at the effects of irradiation on mechanics. Chapter 5 investigates the reason for the lower strains in the fracture groups by looking at the differences in mineral crystal size across the groups. Chapter 6 compares the nanoscale material properties using nanoindentation between the three groups and correlates the findings to nanostrain data collected in Chapter 3. Finally Chapter 7 synthesises all the findings of the research and proposes future work.

Chapter 2. Role of Microstructure in Bone Strength

2.1 Introduction

Published evidence has shown that the microarchitecture is an important determinant of bone strength (Dalle Carbonare & Giannini, 2004; Brandi, 2009; van der Linden, 2007). As such researchers have delved into looking at the microarchitecture to understand this process, with the idea that bone volume might be of importance to whole bone strength, but that the structural arrangement of tissue could also be of key importance. Such detailed arrangements include trabecular number, thickness, spacing, connectivity and orientation (Eastell & Walsh, 2018). However these studies have not looked at some key aspects such as trabecular shape, which could be of importance since it has been shown that shape, changes with age and disease. Hence there is more to learn with regards to the effect of the microstructure on macromechanics.

2.1.1 Trabecular Shape

It is possible that there might be other important aspects of the trabecular structure that have not been but could be important determinants of strength, such as the shape of the trabecular struts. Trabecular bone comprises of plates and rods, with fundamental differences between the two shapes. During aging, due to remodelling, trabecular plates transition to rods (Akhter et al., 2007; Liu et al., 2008; Thomsen et al., 2002; Walker et al., 2013). As plate-like trabeculae are thought to resist higher loads than rod-like trabculae, these geometrical structures have been thought to play a critical role in

determining bone strength and could be important for understanding effects of disease and treatment.

2.1.2 Quantifying trabecular shape

Researchers traditionally used the structural model index (SMI) to capture the trabecular rods and plates, however this technique has been widely criticised not to be a good measure (Salmon et al., 2015). Salmon *et al.* states that the SMI is heavily dependent on bone volume fraction and the index relies on the assumption that the entire bone surface is convex, which is not true of real trabecular bone structures. Moreover, the analysis does not separate trabecular plates and rods, even though the two structures are very differently shaped. As such recently, new tools have been developed to assess the shape of trabeculae. A new technique developed by Liu *et al*. is an individual trabeculae segmentation (ITS)-based morphological analysis (Liu et al., 2008). ITS is a complete decomposition technique which segments the trabecular bone microstructure into individual plates and rods. Previous techniques could not separate, in particular, plate-like elements into individual elements. Without the segmentation, the orientation, thickness, and number of such structures, which are considered mechanically important to the anisotropic material, cannot be determined. ITS is able to identify smaller elements and categorise them into individual plates and rods, allowing for the contribution of the elements in different orientations to anisotropic mechanical properties to be quantified.

2.1.3 Aims & Objectives

It is unclear which microstructure parameters are the most important for bone strength. Therefore, in this chapter, the new measures of microstructure, the individual quantification of rods and plates, will be added to determine whether they can improve the prediction of mechanical properties. In order to achieve this, the trabecular microstructures will be compared across non-fracture ageing controls, non-treated fracture controls and BP treated fracture groups. In relation to the bone strengths of the three groups, it will also be determined if the addition of ITS measurements will increase the association of microstructure with strength. In subsequent chapters, the microstructure data from this study will be also be used to understand the nanostructural importance by looking at unexplained gap in strength.

2.2 Sample Preparation

2.2.1 Sample Groups

Bone cores were drilled from femoral heads of 3 groups of patients: an ageing non-fracture control group (NFC), a fracture control group (FC), and a BP treated fracture group. Imperial College Tissue Bank (R13004) approved the collection and research of the tissue at Imperial College Healthcare NHS Trust. Both the untreated and BP treated fracture groups' samples were obtained from patients who had suffered femoral neck fractures and had undergone hip arthroplasty surgery at Imperial College Healthcare National Service Trust in London, United Kingdom between May 2015 and September 2017. The NFC samples were acquired from cadavers who were deemed to have aged healthily since they had no histories of hip fractures, metabolic bone disease or treatments known to affect bone. All individuals with histories of primary bone diseases or underlying disorders, such as cancer, which could lead to secondary bone disease, were excluded from the study.

The BP treated group included patients who had suffered a femoral neck fracture after they had received BP therapy. The type of treatment undergone was with one type of BP, Alendronate, with a dosage of 70mg weekly. Only samples from patients whom had undergone treatment for a minimum of a year were included in the BP treated group.

In total, there were 17 female patients included, of which 4 NFC, 6 FC and 7 BP. The samples were matched for sex and age (Table 2.2.1). It is arguable that the BP specimens in the study represent a subgroup of patients for whom the therapy did not prevent a fracture. However the concern could be valid as it suggests the importance of the results for this particular subgroup of patients that need to be identified for alternative treatment.

Table 2.2.1 Demography of samples

Donor Group	Sex	Age	Age years (Median)	1st Quart	2nd Quart	Treatment Years
NFC	F	73	77.5	73	82	
	F	73				
	F	82				
	F	82				
FC	F	82	83	76	90	
	F	74				
	F	90				
	F	76				
	F	84				
	F	95				
BP	F	88	79	73.5	82	8
	F	79				5
	F	82				5
	F	82				5
	F	61				2
	F	68				1
	F	79				1

2.2.2 Sample processing

The sample preparation in this chapter was conducted by Jin (Jin, 2016). The cores were obtained by first removing the top third of the femoral head to leave a flat surface (step 1), which then allowed for a low speed bench pillar drill to drill out cores of diameter 7mm and depth of 13-15mm (step 2). The femoral head was then sawed again in another parallel plane to the first cut at an offset of 12mm (step 3). The cores were then removed from the femoral head and put in a mould of height 10mm to standardise the height for all cores, by removing the excess outside of the mould (step 4).

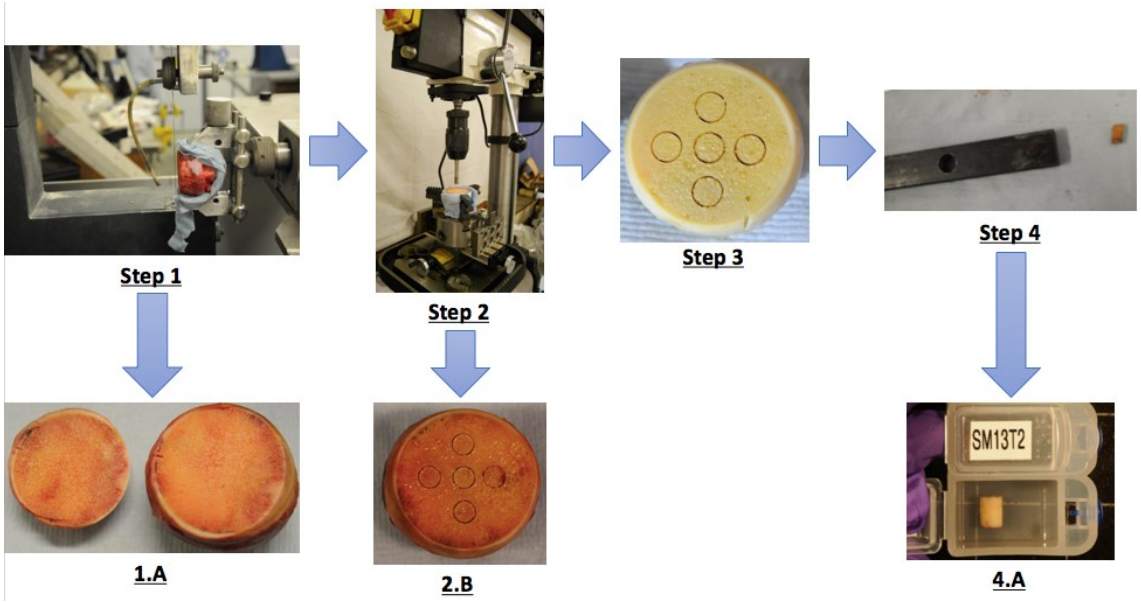

Figure 2.2.1 Shows a picture summary of the steps involved in the sample preparation. Step 1 is the sawing of the femoral head to allow for a flat surface to drill and 1.A shows the output of the sawing. Step 2 is the drilling of the 5 cores in the femoral head and 2.B is the output of this drilling. Step 3 shows the second sawing at an offset of 12mm from the first line. Step 4 shows the mould that was used to allow for exact sizing of the cores at a height of 10mm and 4.A shows the final core fully prepared.

2.3 Methodology

In this chapter, the work done was on the image analysis of the CT scans as well as the statistical analysis of the relation of the microarchitecture to the compressive strength of the samples. The mechanical tests and collection of scans were conducted by Jin as part of his PhD work and are outlined in this section as well (Jin, 2016; Jin et al., 2017).

2.3.1 Micro-CT & Mechanical Tests

Jin scanned cylinder samples using micro-CT of resolution 30μm using the scanner (Nikon X-Tek HMXST-225, Japan) (Jin, 2016). After scanning, Jin conducted uniaxial compression testing on the samples using an Instron 5866 (Instron Engineering Cooperation, US) and a load cell (Serial Number 83169; Instron Engineering Cooperation, US) of maximum load of 10KN (Jin, 2016). The samples were compressed to 50% of its original height to obtain the apparent compressive strengths as seen in Figure 2.3.1.

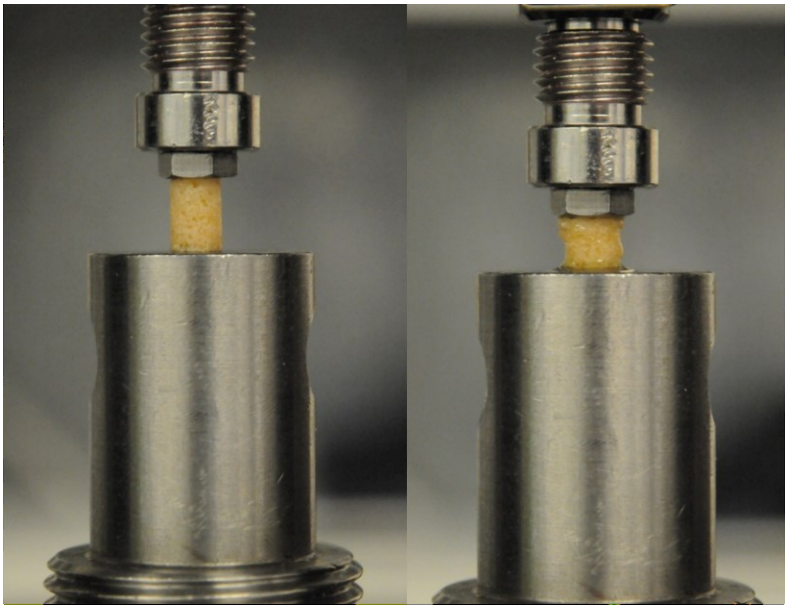

Figure 2.3.1 Example of compressive testing of a sample.

2.3.2 Image Analysis of micro-CT scans

Measurements of microstructural parameters were performed using ITS and Bone J, which is a plug-in for ImageJ (Doube et al., 2010).

2.3.2.1 Thresholding

Since ITS and BoneJ required binary inputs in order for analysis, the initial micro-CT stacks required thresholding in ImageJ.

To threshold the images, artefacts that would affect the thresholding values were first cropped out at the start and end of the stacks. The stacks were then converted into binary

images using the following series in ImageJ: *plugins* → *BoneJ* → *optimise threshold*. With the binary image stack output, a region of interest (ROI) was set so that only the area of the core was being measured using the next following series: *analyse* → *tools* → *ROI manager*. The ROI manager window would then open the circular tool to set points throughout the stack which were interpolated throughout the entire stack to set the ROI.

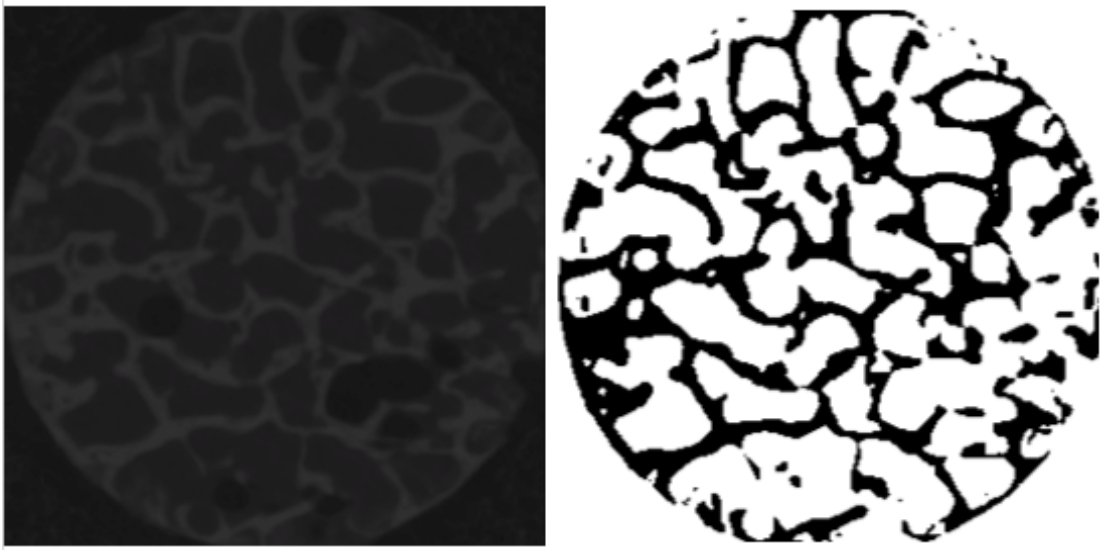

Figure 2.3.2 Micro CT images before thresholding (left) and the binary input after thresholding (right).

2.3.3 ITS Analysis

Individual plate and rods were quantified using ITS which was developed and validated by Liu *et al*. (Liu et al., 2008). During the process of ITS, digital topological analysis, including skeletonisation and topological classification, is performed to transform the micro-CT images of trabecular bone into a 1-voxel-thick skeleton while preserving the

trabecular bone topology (Saha & Chaudhuri, 1994; Saha et al., 1994). The skeleton is topologically typed into surface and curve, which correspond to plates and rods respectively. Finally, volumetric reconstruction of individual trabecular plates and rods was performed to produce a 3D image of the trabecular network with each bone voxel labelled as belonging to an individual plate or rod.

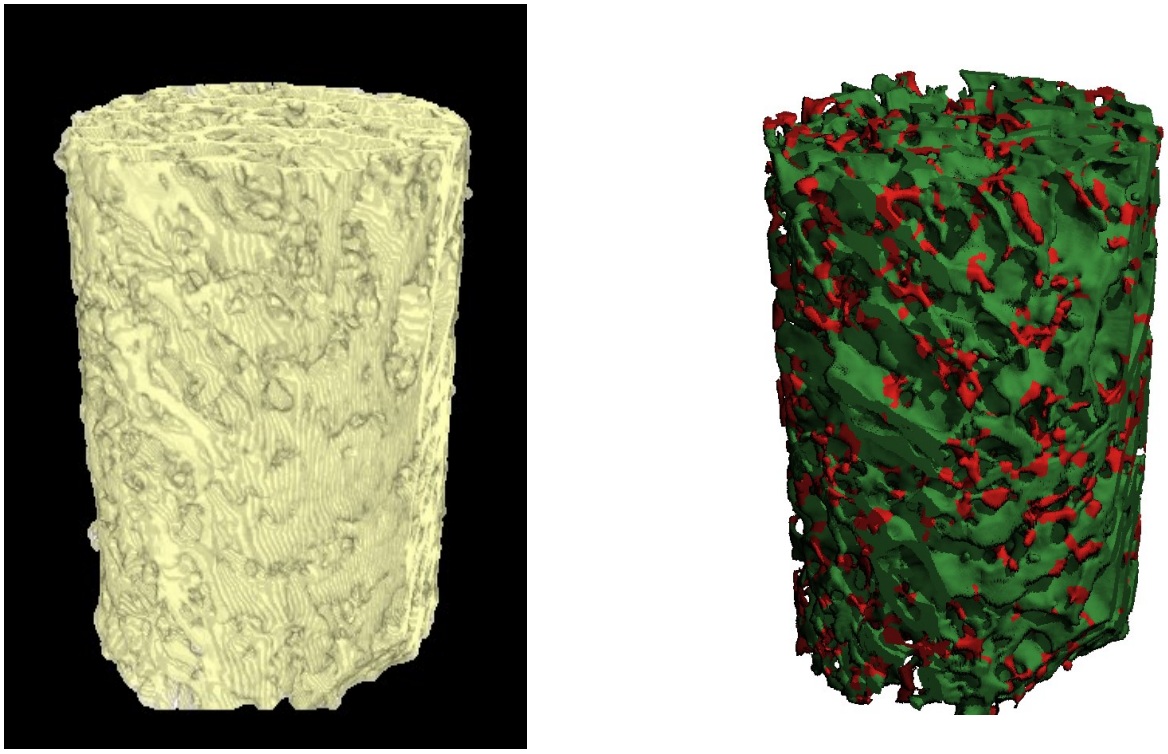

Figure 2.3.3 3D reconstruction of trabecular cores before (left) and after ITS analysis (right). The red voxels represent rods while the green voxels represent plates.

From the reconstructed trabecular bone network, the following parameters were evaluated: plate and rod bone volume fractions (pBV/TV and rBV/TV); axial bone volume fraction (aBV/TV), which is defined as the amount of bone in the loading

direction; axial plate and rod bone volume fractions. (apBV/TV and arBV/TV), defined as the amount of plates and rods in the loading direction respectively.

2.3.4 BoneJ Analysis of microarchitecture

Typical microarchitecture analysis was conducted in ImageJ using the BoneJ plugin. Each measure is outlined below with how the software computes them.

2.3.4.1 Bone Volume Fraction

Bone volume fraction (BV/TV) is a measure of the proportion of bone present within its volume. It is calculated using a proportion of the number of black voxels that represent bone to the number of white voxels that represent non-bone.

2.3.4.2 Trabecular Thickness

Trabecular thickness (Tb.Th) is a measure of the mean thickness of all the trabeculae, and is calculated by fitting spheres inside trabeculae and measuring their diameter, then using all the spheres to work out a mean as shown in Figure 2.3.4. The thickness of each

individual trabecular branch is then further averaged to get the trabecular thickness of the entire bone sample.

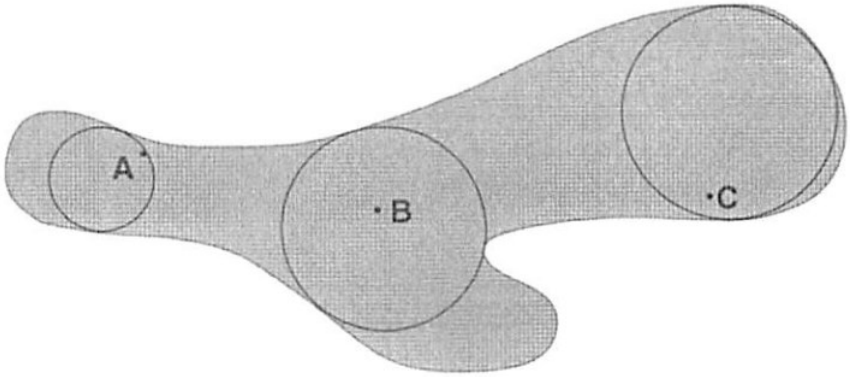

Figure 2.3.4 Illustration of the 2D measurement of trabecular thickness (Cowin, 2009). The mean trabecular thickness would be the mean of the diameter of spheres A, B & C.

2.3.4.3 Trabecular spacing

Trabecular spacing (Tb.Sp) is a measure of the mean space between all of the trabeculae. It is calculated similarly to Tb.Th as a mean of the spheres that are fitted in the space between trabeculae as shown in Figure 2.3.5. The average trabecular space is calculated by averaging the diameters of the largest spheres that fit within the structure.

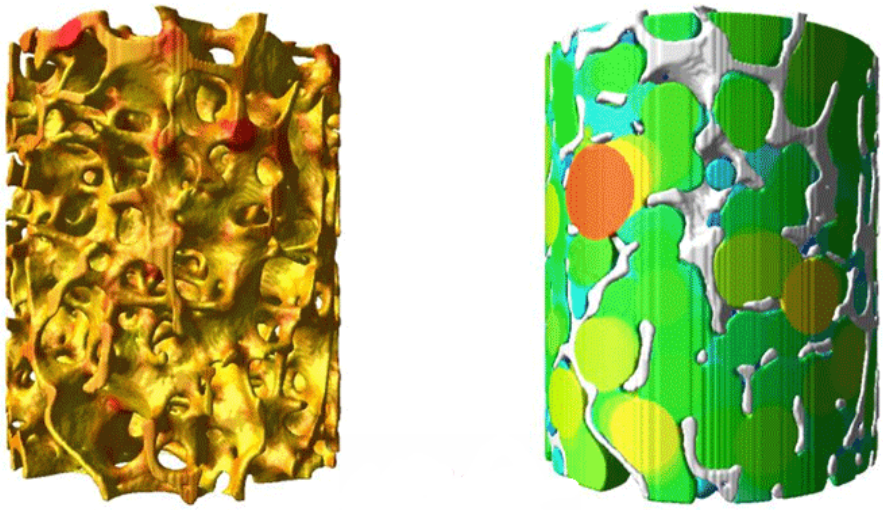

Figure 2.3.5 Illustration of spheres fitted into the spaces throughout the entire structure (microCT world, n.d.).

2.3.4.4 Connectivity Density

Connectivity density gives a quantification of the number of connections between trabeculae in a given area. It is determined using the Euler characteristic to estimate the connectivity, and then dividing this by the total volume of the sample. The Euler characteristic (χ) of a structure is a function of the number of vertices (V), edges (E) and faces (F). For example, a triangle would have an Euler characteristic, χ = V-E+F = (3-3+1) = 1.

The Euler characteristic is calculated for each voxel and recorded as $\delta\chi$ and is calculated for all image slices of the micro-CT stack. All the $\delta\chi$ are then summed up to give the Euler Characteristic for the whole bone sample. Since the samples are taken from a larger

femoral head, a modified Euler characteristic ($\Delta\chi$) is calculated (in BoneJ) to take into account the changed connectivity, as the cylinder samples were originally connected to other parts of the femoral head.

Connectivity is calculated using Equation 2.1:

$$\beta = 1 - \Delta\chi \qquad \text{Equation 2.1}$$

Connectivity density is then calculated as the equation below:

$$Connectivty\ density = \frac{\beta}{stack\ volume} \qquad \text{Equation 2.2}$$

2.3.4.5 Bone surface density

There is no direct output for bone surface density (BS/BV) with ImageJ, but there is an output for bone surface area. The software calculates the bone surface area using a mesh of triangles and determining the surface area as the sum of the areas of all the triangles. To subsequently calculate BS/BV the bone surface area is divided by the bone volume, which was given within the output of the bone volume fraction.

2.3.4.6 Specific bone surface

Similar to BS/BV, specific bone surface (BS/TV) is calculated using the bone surface area divided by the total volume, which was given within the output of the bone volume fraction.

2.3.4.7 Structure model index

The structural model index (SMI) is a technique used to measure the plate-like or rod-like structure of trabeculae. A value of 0 indicates a plate-like geometry whereas a value of 3 demonstrates a rods-like structure. The structural model index of trabecular bone should be between 0 and 3.

2.3.4.8 Anisotropy

Anisotropy (DA) is a method used to establish the orientation of the trabeculae within their volume. This is achieved using the mean intercept length, whereby many vectors originating from a random point are drawn, and when a vector hits a boundary an intercept is counted. The mean intercept length is then calculated using the vector length by the number of boundary hits. In the output, a value of 0 is isotropic and 1 is anisotropic.

2.3.5 Statistical Analysis

Since the parameters were not normally distributed, non-parametric statistical tests were used to compare the 3 groups within each test variable in the form of Kruskal-Wallis for whole group comparison and Mann-Whitney U for pairwise comparison and multiple regressions graphs were produced using GraphPad Prism 7.

PAST version 3.2 was used to perform principle component analysis (PCA). PCA was used as many of the microarchitecture parameters are highly correlated since they are calculated using similar algorithms from the same bone volume. If we input all the parameters into the multiple regression with such high collinearity, the regression will be skewed. PCA was conducted to reduce this collinearity by determining principal components from all the micro parameters. Only the parameters that were highly loaded in the main principle components were then added into the multiple regression in SPSS to determine the contribution to strength.

2.4 Results

2.4.1 Rods & Plates quantification

There were no significant differences in plate bone volumes and rod bone volume in all and axial directions between the groups ($p<0.05$).

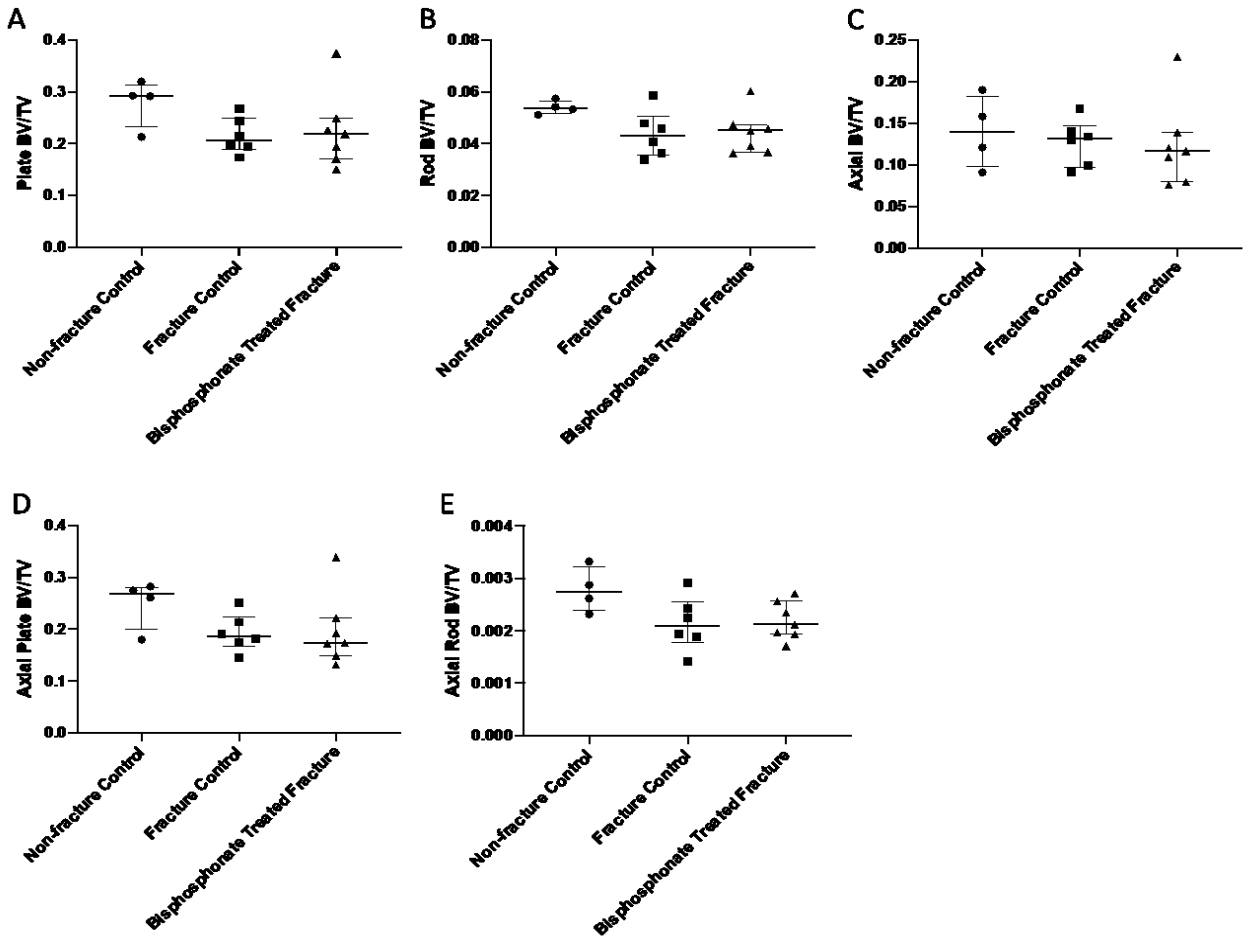

Figure 2.4.1 Comparing plate and rod bone volume fractions of cores. Kruskal-Wallis and post-hoc Mann-Whitney U tests showed that there were no significant differences in plate, rod, axial, axial plate and axial rod volume fractions between the three groups.

2.4.2 Microarchitecture Comparison

Kruskal-Wallis tests and Mann-Whitney U pairwise analysis show that there were significant differences between NFC and fracture groups in bone volume fraction ($p<0.01$), trabecular spacing ($p<0.05$), total bone surface density ($p<0.05$), and connectivity density ($p<0.05$). However, there were no significant differences in any of the parameters between the FC and BP treated fracture ($p>0.05$) (Figure 2.4.2 & 2.4.3).

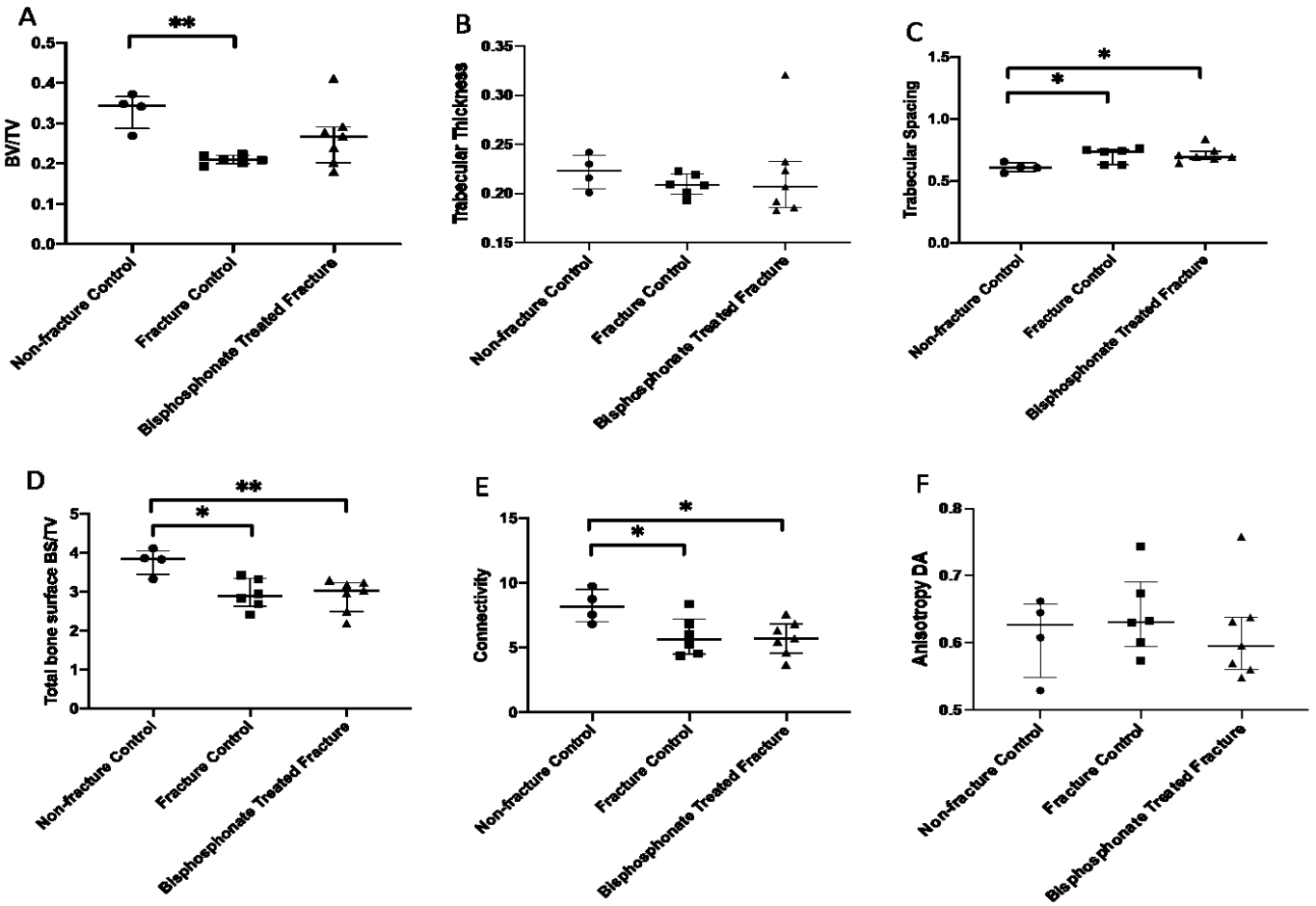

Figure 2.4.2 The parameters assessed are (A) bone volume fraction (B) trabecular thickness (C) trabecular spacing (D) bone surface density (E) connectivity density and (F) anisotropy. Kruskal-Wallis and post-hoc Mann-Whitney U tests were conducted, and the asterisks indicates significant pairwise differences * $p<0.05$, ** $p<0.01$.

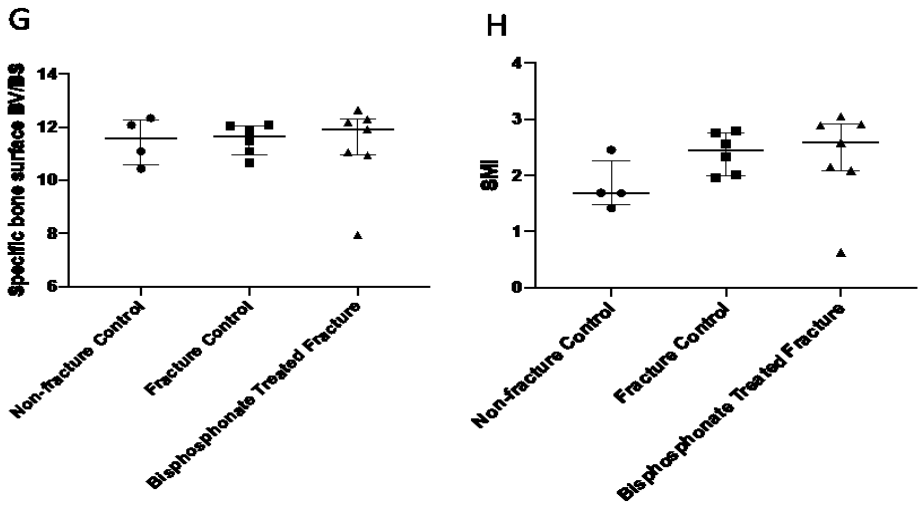

Figure 2.4.3 The parameters assessed are (G) bone specific surface and (H) structural model index. Kruskal-Wallis and post-hoc Mann-Whitney U tests were conducted.

2.4.3 Microarchitecture relation to mechanical strength

PCA of the microarchitecture parameters gave an output of 2 principal components (Figure 2.4.4), which showed that the principal components of the microarchitecture of the non-fracture controls were different from the fracture groups but they did not seem to be any distinguishable differences between the fracture groups (Figure 2.4.5).

The loadings of the 2 principal components indicated that the parameters that explain the variability in bone strength include connectivity, total bone surface density, specific bone surface and SMI (Figure 2.4.6).

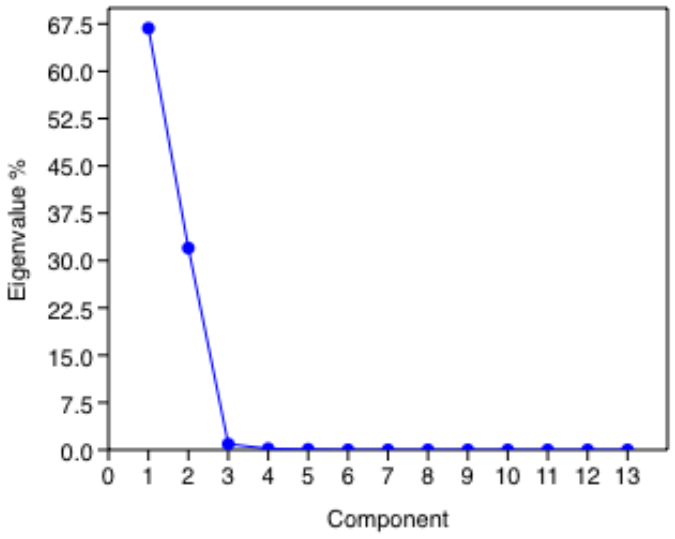

Figure 2.4.4 Eigenvalues from PCA show 2 principal components that account for more than 5% of the variability in microarchitecture between the groups.

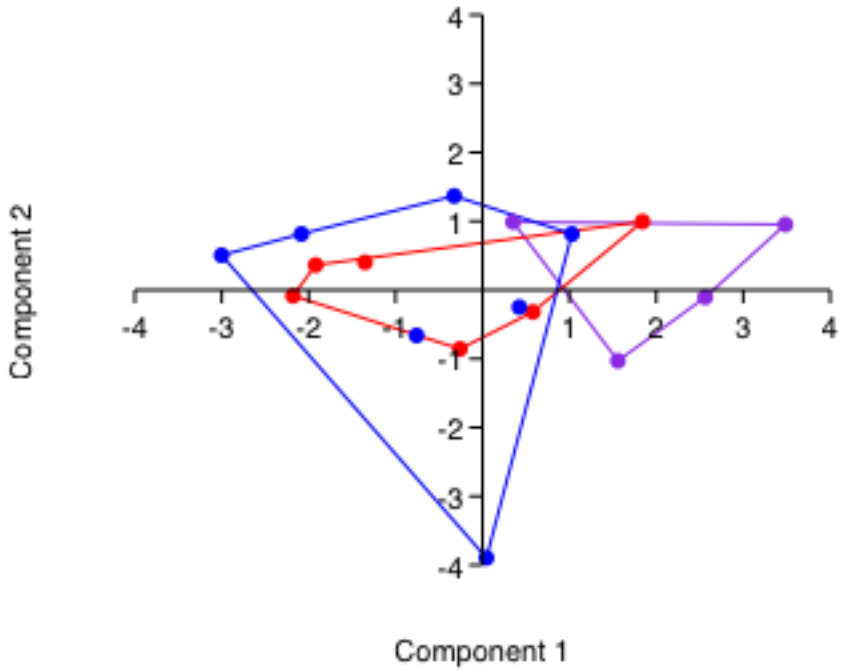

Figure 2.4.5 The 2 principal components of the microarchitecture of NFC (purple) are different from the fracture groups. However, FC (dark red) is not different from BP (blue).

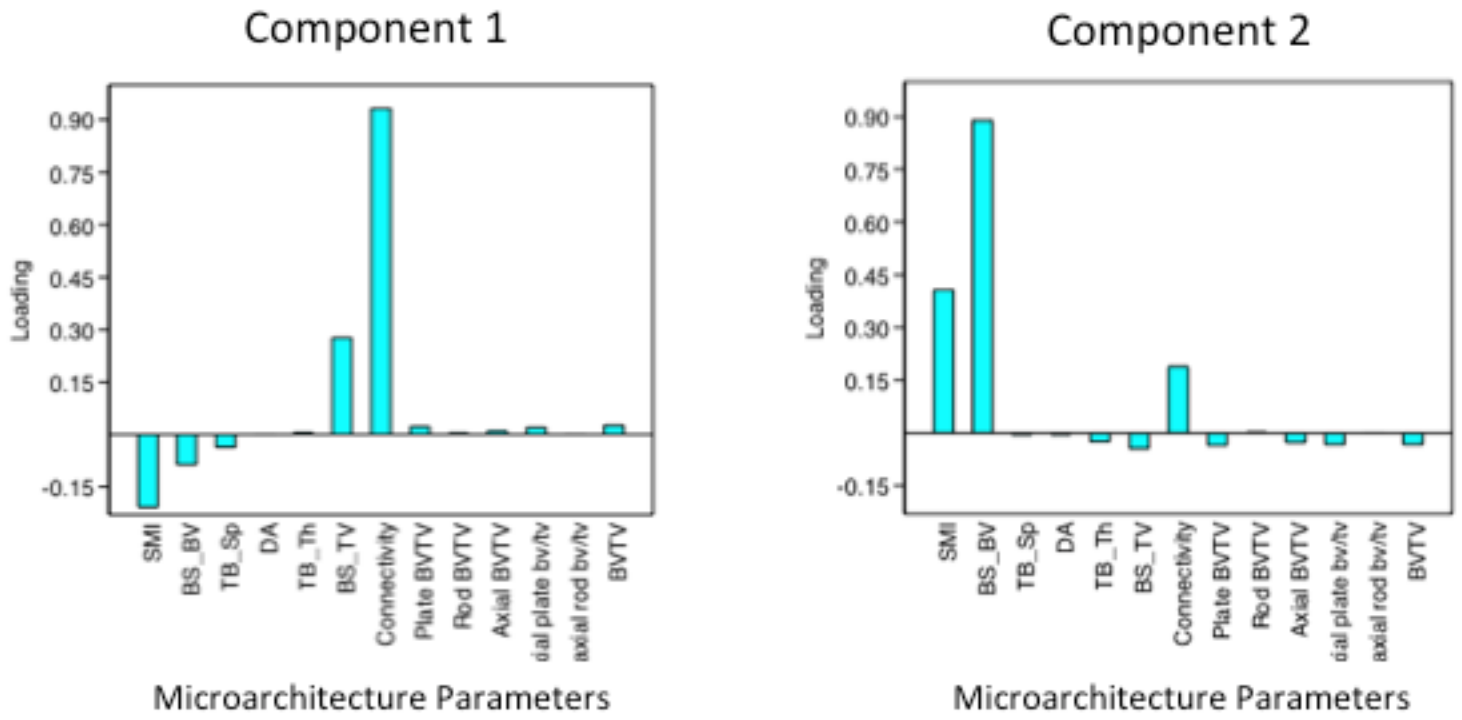

Figure 2.4.6 Principal component 1 (left) where connectivity, bone surface density and SMI are highly loaded. Principal component 2 (right) where connectivity, specific bone surface and SMI are highly loaded.

In relation to the compression tests conducted by Jin (Figure 2.4.7), a multiple linear regression was calculated to predict bone's mechanical strength based on the microarchitecture parameters that loaded highly in the principal components (IBM SPSS Statistics version 24). Only 29.1% (adjusted R square =0.291) of the variability in bone strength was accounted for by the microarchitecture parameters.

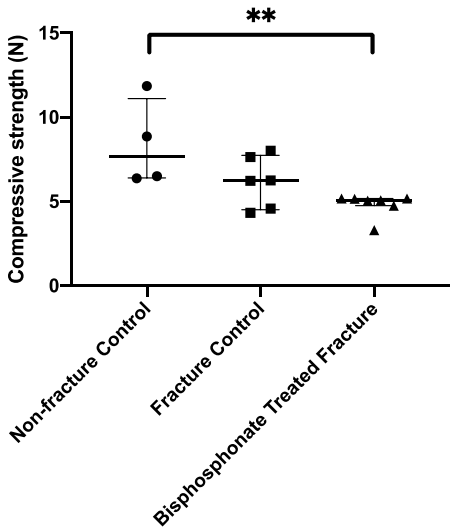

Figure 2.4.7 Compressive strength of the samples from compression test conducted by Jin (Jin, 2016).

Model Summary

Model	R	R Square	Adjusted R Square	Std. Error of the Estimate
1	.685[a]	.469	.291	1.72124

a. Predictors: (Constant), Connectivity, BSBV, BSTV, SMI

Table 2.4.1 Multiple regression for predicting apparent compressive strength with connectivity, specific bone surface, bone surface density & SMI. The parameters only account for 29.1% of variability in bone strength (adjusted $r^2 = 0.291$).

2.5 Discussion

In this chapter, the microarchitecture of trabecular cores were compared across the NFC, FC and BP groups. A new measure of rods and plates using ITS analysis software was added to the traditional parameters measured using BoneJ. There were significant differences in microarchitecture between the NFC and both fracture groups. However there were no differences in any of the parameters between diseased bone that had or had not been treated with BP. This shows that at the microstructural level, there is a fundamental difference between non-fractured bone and bone that has suffered a fracture. In relation to apparent compressive strength, the microarchitecture parameters account for less than 50% in the variability in all 3 groups, irrespective of health or treatment ($p<0.05$), leaving a substantial amount of variation in strength unexplained.

2.5.1 Effects of bone fragility on microarchitecture

The microarchitecture of NFC was significantly different from both the fracture groups. Many of the microarchitecture parameters assessed in this chapter are correlated and measure similar outputs. Thus to assess key the differences in microarchitecture, only the parameters highlighted in the principal components will be discussed, namely: connectivity, total bone surface density, specific bone surface and SMI (Figure 2.4.6). These parameters were determined by conducting PCA, mentioned in *section 2.4.3*. The other parameters were not included at they did not improve the variance on strength.

The connectivity density of the fracture groups was much lower than NFC. Studies have shown that during aging, the connectivity density in the femoral neck and vertebra decreases, contributing to the lack of maintenance of bone strength (Chen et al., 2008; Thomsen et al., 2002). In bone diseases that lead to fragility such as osteoporosis, it has been theorised that rod-shaped trabeculae are resorbed and lost, reducing connectivity, while plate-like trabeculae become thinner, hence resulting in a reduction in bone volume and trabecular number (Kinney & Ladd, 1998). Thereafter, the remaining trabeculae thicken to return to their original thickness, but the lost trabeculae cannot be re-established. The data in this chapter supports this theory as the lower bone volume fraction in the fracture groups are associated with fewer trabeculae, as inferred from trabecular spacing, but same mean trabeculae thickness as well as lower bone surface density and loss of connectivity.

Osteoporosis also leads to trabecular perforation, resulting in the loss of connectivity through the perforation of trabecular plates or rod breakage (Brandi, 2009; Altman et al., 2015). Perforation of plates results in a transition of plate-like to rod-like trabeculae, while rod breakage leads to a reduced number of trabeculae. Studies have shown that in fragile bone, there is a transition from trabecular plates to rods (Akhter et al., 2007; Liu et al., 2008; Thomsen et al., 2002; Walker et al., 2013). However in this study, the SMI was not significantly different between fracture patients and non-fracture patients. This is also supported by the more sophisticated ITS analysis showing that the fracture groups had the same volume fraction of rods and plates as the non-fracture controls. It is likely that the observation of increased rods and decreased plates in fracture patients were not

observed because the overall bone volume fractions were already significantly lower than NFC.

2.5.2 Microarchitecture contribution to strength

The regression between microarchitecture and strength showed that microarchitecture parameters combined accounted for only 29.1% (adjusted R^2=0.291) of the variability in mechanical strength. In contrast, other studies have found that bone volume fraction accounts for 74% in bone stiffness and strength (Nazarian et al., 2007). However, Nazarian *et al.* only compared samples from cadavers that did not have any skeletal pathology and the age range of the samples was not specified in the study. The samples were not affected by disease, or possibly even age, that could affect the microarchitecture. In our study, the fractured samples were compared against the non-fractured samples, giving a better variation in strength and stiffness. Moreover, bone volume fraction neglects architecture, morphology and geometry of the anisotropic material that bone is. It can be argued that one parameter cannot fully describe bone quality, as a complex hierarchical structure such as bone would have other parameters that should also be used to determine bone strength.

Other studies have published correlations of microarchitecture parameters to bone strength and found that the best predictors of bone strength were connectivity (Pearson's correlation coefficient R^2=0.70) and bone volume fraction (R^2=0.78) (Hulme et al., 2007). However, the resolution of the micro-CT analysis was 82μm, which resulted in the

overestimation of bone volume fraction by 28%. The low resolution could have thus resulted in inaccuracies in the measurement of the parameters. Moreover the parameters were evaluated separately and not together to determine the accountability of the entire microstructure.

As many of the parameters are highly correlated, only connectivity, total bone surface density, specific bone surface and SMI were added into the multiple regressions to reduce the problem of collinearity in this study. Although the new ITS measures of rods and plates were added into the microarchitecture comparisons, they were not highly loaded in the principle components and thus did not contribute further to the prediction of whole bone strength. Instead, the parameters that were identified from PCA, connectivity, total bone surface density, specific bone surface and SMI, were ones that were previously extensively researched (Ding et al., 2003; Kinney & Ladd, 1998; Chen et al., 2008). It is possible that the microarchitecture of bone has already been fully studied and there are no new parameters that could be researched that could further the understanding of the changes at the micro level.

Since there is a lot of unexplained variance (71%) in strength at the micro level for the samples in this thesis, it is possible that the other structural levels in the bone's hierarchy play an important role in whole bone strength. There could be changes in other lower levels: the micron level and the nano level, where the basic building blocks lay.

2.6 Conclusion

This chapter compared the microarchitecture parameters between non-fracture controls, fracture controls and BP treated fracture, and included a new analysis of trabecular rods and plates. The results showed that there were significant differences between the non-fracture and fracture groups. However, the trabecular architectures were comparable in every aspect between non-treated and treated fracture patients. Moreover, these differences in microarchitecture only accounted for about 30% of mechanical strength variability, and the newly developed ITS analysis also did not improve prediction of bone strength.

With over 50% of variability in mechanical strength unaccounted for by bone volume and microarchitectural parameters, it is possible that other structural levels account for the unknown. Bone has a complex hierarchical structure, recent research showing up to 12 levels, and during ageing, deterioration occurs at every structural level (Reznikov et al., 2018). Therefore the next step should be to look at the lower structural levels at the micron and the nanostructure.

Chapter 3. Nanomechanics of Collagen-Mineral Matrix

3.1 Introduction

The influence of the macro and microscale properties of bone on its mechanical competence has been extensively investigated, but less is known about possible contributions from bone's nanoscale (Yosibash et al., 2007; Rudman et al., 2006). These nanoscale properties, particularly the arrangement of the collagen network, size and shape of hydroxyapatite mineral crystals, and interactions between the two, are often cited as key determinants of whole bone mechanical properties such as strength and stiffness (Wang ZX, 2016; Wen et al., 2015; Burstein et al., 1975; Ammann & Rizzoli, 2003). In the previous chapter, a substantial amount of the variation in bone strength was not explained by the microstructure and could be attributed to the nanostructure. Yet only a few small studies have focused on the interactions of the fundamental nanoscale building blocks of bone and how they affect whole bone mechanics (i.e. strength and fragility) or their role in bone fragility and treatment (Allen et al., 2008; Bailey et al., 1998; Burr, 2002).

3.1.1 The Basic Building Blocks

Understanding the role of the matrix in whole bone mechanics could be important because researchers have suggested that the basic building blocks of bone at the nanostructural level are affected by ageing and disease (Vashishth, 2007). The basic building blocks consist of the collagen fibrils, linked together by crosslink molecules, and mineral crystals, embedded within the fibrils, making up the collagen-mineral matrix. During loading, the load transfers from the nanoscale level, propagating up to the tissue level, allowing the entire hierarchical structure to undergo deformation (Gupta et al., 2006). When the nanostructural level experiences a load, the neighbouring fibrils slide across one another and individual collagen molecules stretch and unwind, while crosslinks restrict the sliding of molecules (Depalle et al., 2015). Bone's stiffness and elasticity to resist fracture under compression or tension is derived from this sliding mechanism (Figure 3.1.1).

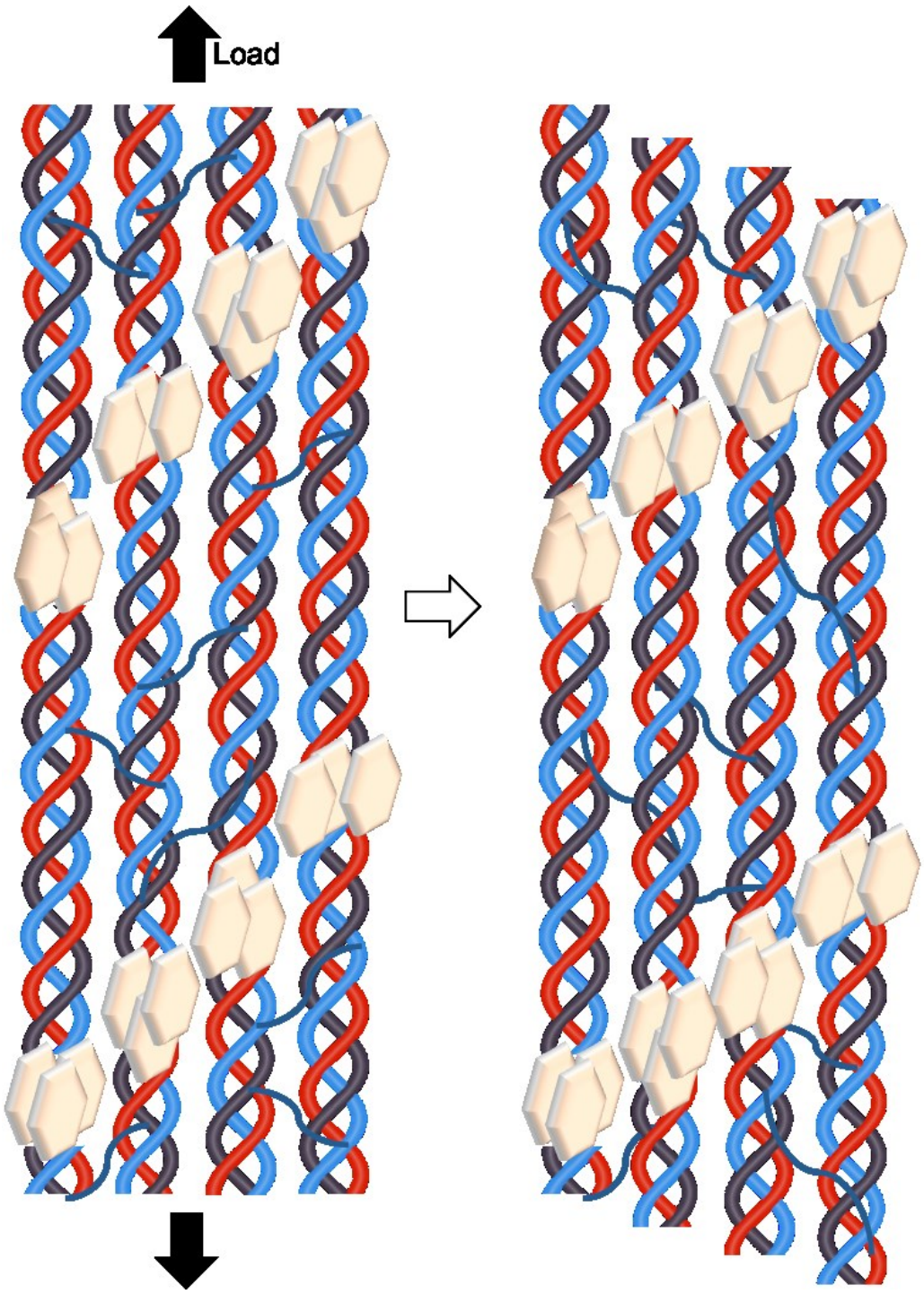

Figure 3.1.1 Depiction of sliding mechanism when the collagen-mineral matrix experiences a load. The collagen fibrils embedded with mineral crystals slide across one another while still being held together by crosslinks.

Bone stiffness is proportional to mineral content, hence mineral crystals likely play an important role in bone's mechanical behaviour (Currey, 1984; Currey, 2003). Currey obtained mineral content by ashing bone samples and reported that bone with low values of mineralisation corresponded with low values of Young modulus, a measure of stiffness, while highly mineralised bone produced high values of Young modulus.

Ageing bone has shown to exhibit with increased number of collagen crosslinks (Wang et al., 2002; Saito & Marumo, 2010; Garnero, 2012). As such the collagen crosslinking within the matrix may also affect elasticity and bone's fracture toughness. Wang *et al.* assessed the fracture toughness of human bone samples, comparing young, middle-aged and old bone, and used high performance liquid chromatography (HPLC) to quantify the amount of crosslinks in the samples (Wang et al., 2002). This study concluded that a 35% decrease in bone strength was observed with increasing age and this was also associated with an increase in crosslinks. The increase in crosslinking could reduce the sliding mechanism's elasticity, reducing strain, and ultimately the bone's fracture toughness.

Moreover, tissue mineral content and non-enzymatic crosslinks have also been reported to increase with BP treatment (Gourion-Arsiquaud et al., 2010; Saito et al., 2008). Gourion-Arsiquaud *et al.* used Fourier Transform Infrared imaging (FTIRI) to quantify and compare the amount of crosslinks in canine bone that had been treated with BP for a year against untreated controls. FTIRI analysis showed that there was significantly higher crosslink ratios in the bone treated with BP (Gourion-Arsiquaud et al., 2010). However the dogs were not osteoporotic and thus the study is not representative of how BP would affect osteoporotic bone. Moreover, the doses given to the canine models were 5-6 times

higher than clinical doses and this could further suppress remodelling and affect the matrix. Similarly, Saito *et al,* using density fractionation, also found that canine models treated with BP for 3 years exhibited with more crosslinks (Saito et al., 2008). However the dogs in the study were also non-ovariectomised (not osteoporotic) and therefore limit translating the results to post-menopausal women. Moreover, the bone samples were taken from the rib cortex and thus the remodelling could be different from other loading bone regions. Therefore it is possible that changes occurred during osteoporosis and treatment at the nanostructural level could be a significant contributor to whole bone strength.

3.1.2 Imaging at the Nanostructural Level

Aside from these insights, to date there has been little research into the function or role of the nanostructure, in part because of the extreme difficulty in visualising the collagen-mineral matrix, especially under *in-situ* loading, whilst simultaneously measuring macroscale mechanical properties such as strength and stiffness. Recently cutting-edge synchrotron imaging techniques have been developed, which employ high-energy x-ray beams that allow for high spatial resolution (to a few nm) and detailed investigation of nanostructure and mechanics. Synchrotron x-ray beams interact with the collagen fibrils and mineral crystals respectively to create scattering and diffraction patterns. Under loading, the ordered collagen-mineral matrix deforms, causing the diffraction patterns to

shift, and thus allowing for the measurement of collagen and mineral strains (Gupta et al., 2006).

3.1.3 X-ray Diffraction and Scattering

In this chapter, synchrotron x-ray diffraction (SAXD & WAXD) will be introduced, however there is also another technique commonly seen in synchrotron research known as scattering (SAXS & WAXS). Many studies have used the terms interchangeably, however it is unclear what the difference between scattering and diffraction are. The possible reason for the blurred line between the two phenomena is that diffraction is essentially a form of scattering. When x-rays interact with atoms or molecules in a crystalline structure, they are scattered in all directions. The scattered beams reinforce each other constructively when in phase and cancel one another out when out of phase, creating a diffracted beam. Scattering can occur in 3 ways:

1. Diffuse scattering, when scattering occurs in all directions due to the interaction with randomly arranged atoms in space.
2. By interaction with perfectly ordered atoms in space, like in a perfect crystal
3. Strong scattering or diffraction, when scattering occurs in only a few directions, satisfying Bragg's law.

Thus diffraction is a type of scattering but dependant on the organisation of the material, such as bone, which has periodic repetition units. The ordered molecular packing of a material leads to the reinforcement of scattering signals, creating a diffraction pattern.

3.1.4 Bragg's Law

For diffraction to occur, Bragg's law states the essential condition that needs to be met:

$$n\lambda = 2d \sin\theta \qquad \text{Equation 3.1}$$

where n is an integer, λ is the wavelength of the x-ray, d is the interplanar spacing and θ is the incident angle.

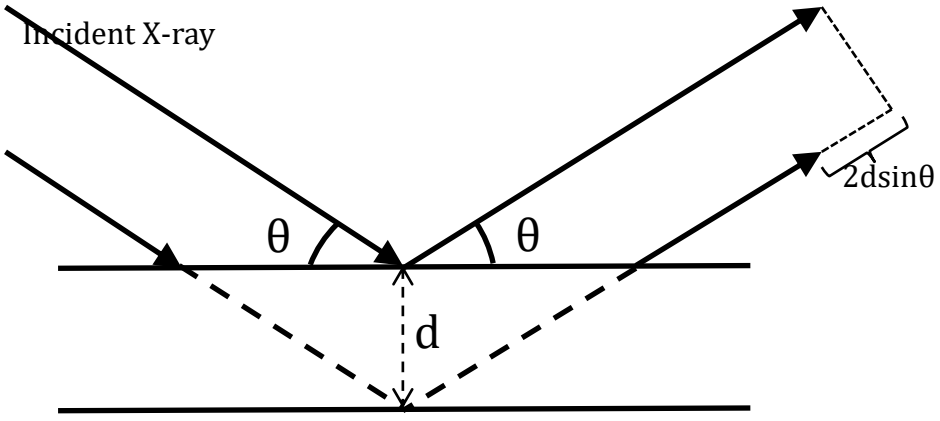

Figure 3.1.2 Bragg's law explains that x-rays deflected from different parallel planes of the crystal interfere constructively when the total path difference $2d \sin\theta$ equals to $n\lambda$.

Since bone has an ordered nanostructure resulting in diffraction patterns, in accordance with Bragg's law, the abbreviations in this thesis for synchrotron techniques have been

denoted as SAXD and WAXD. The interaction of x-ray beams with the mineralised collagen matrix and mineral crystals, and resulting diffraction patterns have been depicted in Figure 3.1.3 and 3.1.4 respectively.

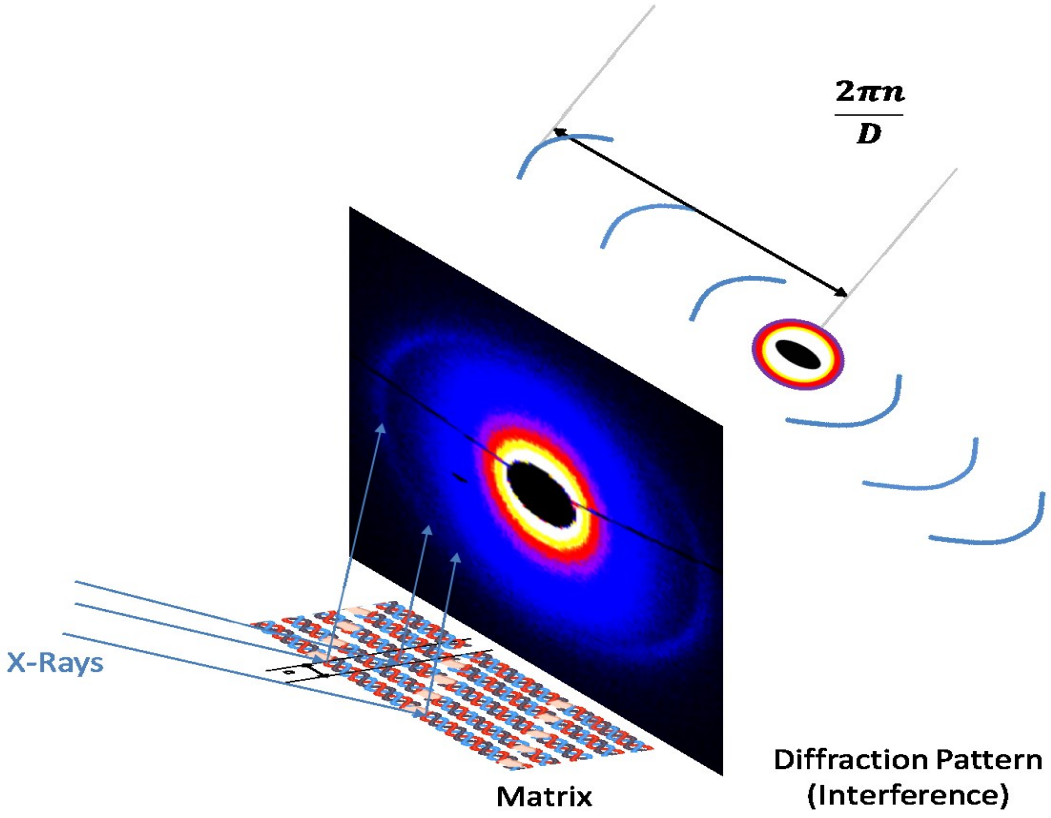

Figure 3.1.3 Depiction of the interaction of the x-rays with the mineralised matrix and in accordance to Bragg's Law, the subsequent SAXD pattern that is formed.

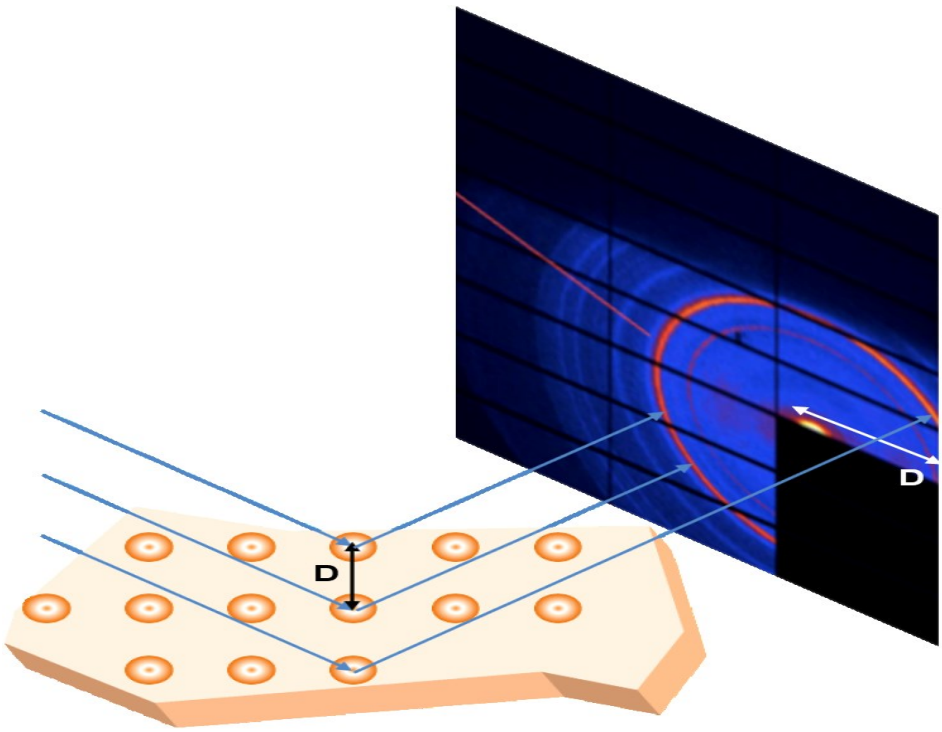

Figure 3.1.4 Depiction of the interaction of x-rays with the mineral crystal. Due to the periodic D-spacings in the crystal, the diffraction pattern (WAXD) is formed.

3.1.5 Aims & Objectives

Thus the present study aims to assess the role of the nanostructure in whole bone mechanics as well as investigate the effects of bone fragility and BP therapy on the collagen-mineral matrix strains using synchrotron x-ray scattering and diffraction techniques. To assess nano and macroscale properties in relation to each other, the collagen, mineral and tissue deformations will be measured simultaneously under *in-situ* loading.

3.1.6 Hypotheses

The hypothesis is that in comparison to ageing non-fracture patients, fracture patients, will exhibit with lower tissue, collagen and mineral strain. Fracture patients that have taken BP will exhibit with even lower strains than untreated fracture patients. Finally increases in mineral density brought about by BP could make the nanostructure more mineralised, making the collagen-mineral matrix stiffer, as such it is also hypothesised that tissue, collagen and mineral strains will decrease with BP treatment duration.

3.2 Material and Methods

3.2.1 Sample Groups

For this study, trabecular bone samples were collected from the femoral heads of 3 individual groups, namely NFC, the FC and the BP groups. Both the FC and BP groups' samples were obtained from patients who had suffered femoral neck fractures and had undergone hip arthroplasty surgery at Imperial College Healthcare National Service Trust in London, United Kingdom between May 2015 and February 2018. The NFC samples were acquired from cadavers who had no histories of hip fractures. All individuals with histories of primary bone diseases or underlying disorders, such as cancer, which could lead to secondary bone disease, were excluded from the study. Ethical approval was granted by the Imperial College Tissue Bank (R13004) for the collection of the femoral heads with additional patient consent to use their tissue for the study.

The BP treated group included patients who had suffered a femoral neck fracture after they had received BP therapy. The type of treatment undergone was with one type of BP, Alendronate, with a dosage of 70mg weekly. Only samples from patients whom had undergone treatment for a minimum of a year were included in the BP treated group.

In total, 33 samples were attained from donors for this study (including those presented in Chapter 2): 12 from BP treated fracture patients, 13 from untreated fracture patients and 8 from ageing non-fracture cadavers. The samples were matched for sex and age and the breakdown of the demography for the sample groups is presented in Table 3.2.1. Additional samples were collected and used in this study to give a better representation of the groups.

Table 3.2.1 Demography of Samples

Donor Group	Sex	Age	Age years (Median)	1st Quart	2nd Quart	Treatment Years
NFC	F	73	75	72.8	78	
	F	73				
	F	82				
	F	82				
	F	77				
	F	77				
	F	72				
	F	72				
FC	F	82	78	74	82	
	F	71				
	F	78				
	F	78				
	F	73				
	F	90				
	F	82				
	F	81				
	F	75				
	F	74				

	F	76				
	F	82				
	F	74				
BP	F	74	80	74.8	82.5	11
	F	88				9
	F	90				7.5
	F	61				6
	F	79				5
	F	84				5
	F	82				5
	F	75				3
	F	81				3
	F	82				2
	F	68				1
	F	79				1

3.2.2 Sample Processing

Rectangular shaped samples were systematically sectioned from the region directly superior to the trabecular chiasma. For tensile loading purposes, the samples were also ensured to have been cut from the same primary tensile trabecular arcade of the femoral heads (Figure 3.2.1).

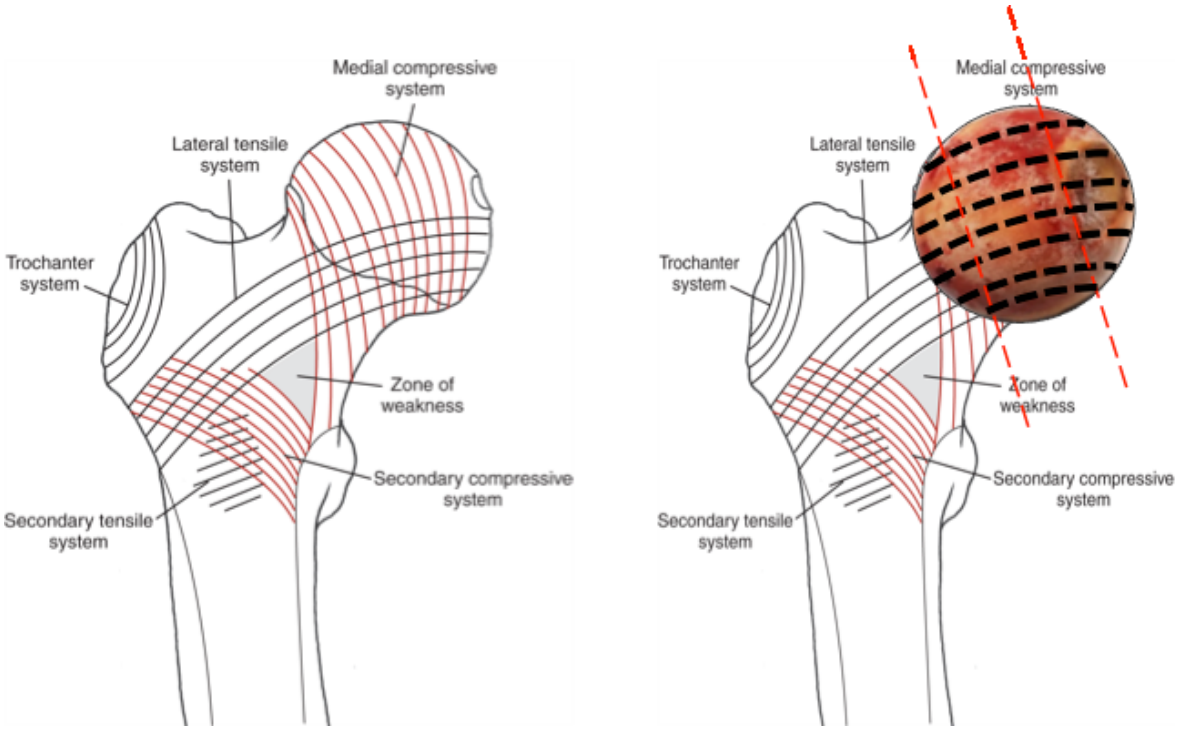

Figure 3.2.1 Depiction of the region in which the samples were cut, in the direction of the primary tensile arcade of the femoral heads.

From each femoral head sample, one third of the head from the top was removed using an EXAKT saw (Figure 3.2.2).

Figure 3.2.2 EXAKT saw used to cut two flat surfaces on the samples with a thickness of 10mm between the two surfaces.

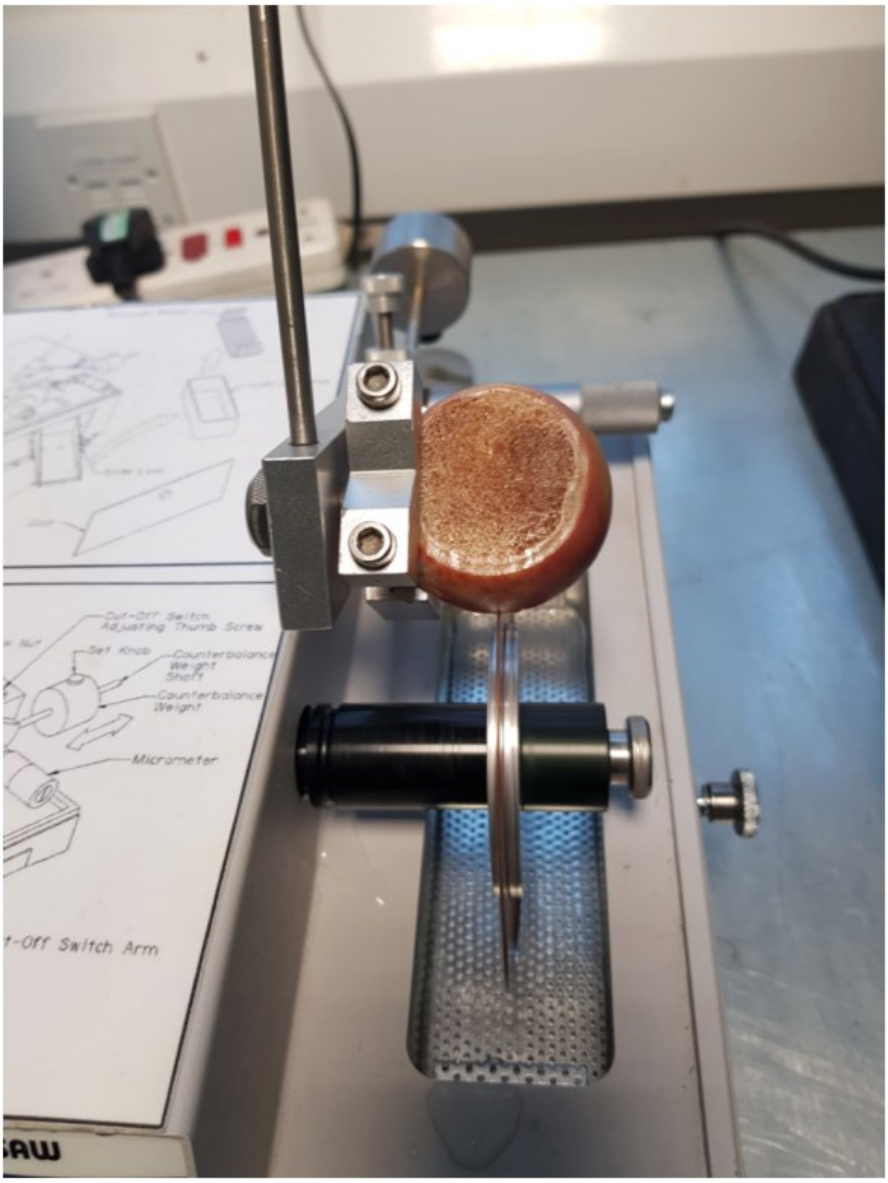

Figure 3.2.3 Diamond saw used to cut the sample into quarters

Moving further down the femoral head by 10mm, another cut was made to produce a slice with two flat surfaces. A diamond saw was then used to cut the 10mm slice into quarters (Figure 3.2.4).

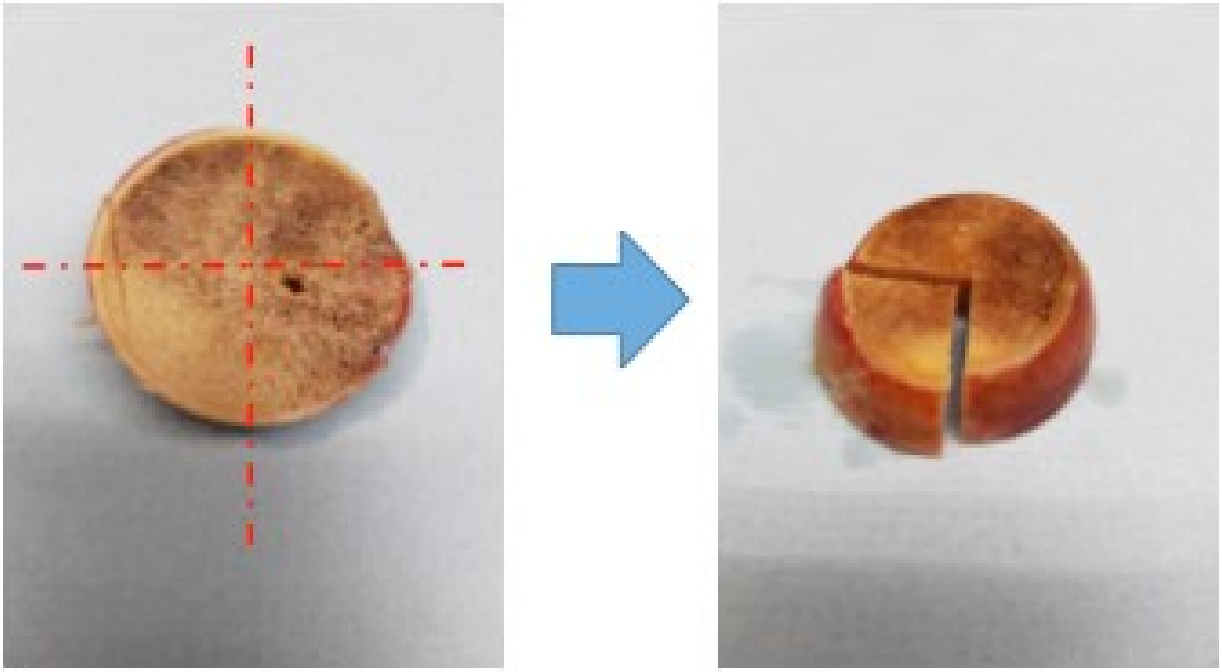

Figure 3.2.4 Depiction of where the quarter cuts were made and the resulting quarter piece.

The quarter slice was then further cut into 1mm thick pieces (Figure 3.2.5), and finally into the targeted sub-samples of dimensions 10mm in length, 2.5mm in width and 1mm in thickness (Figure 3.2.6). The ends of the samples were embedded into 3D printed holders, which served as clamps during loading, using dental cement (Figure 3.2.8).

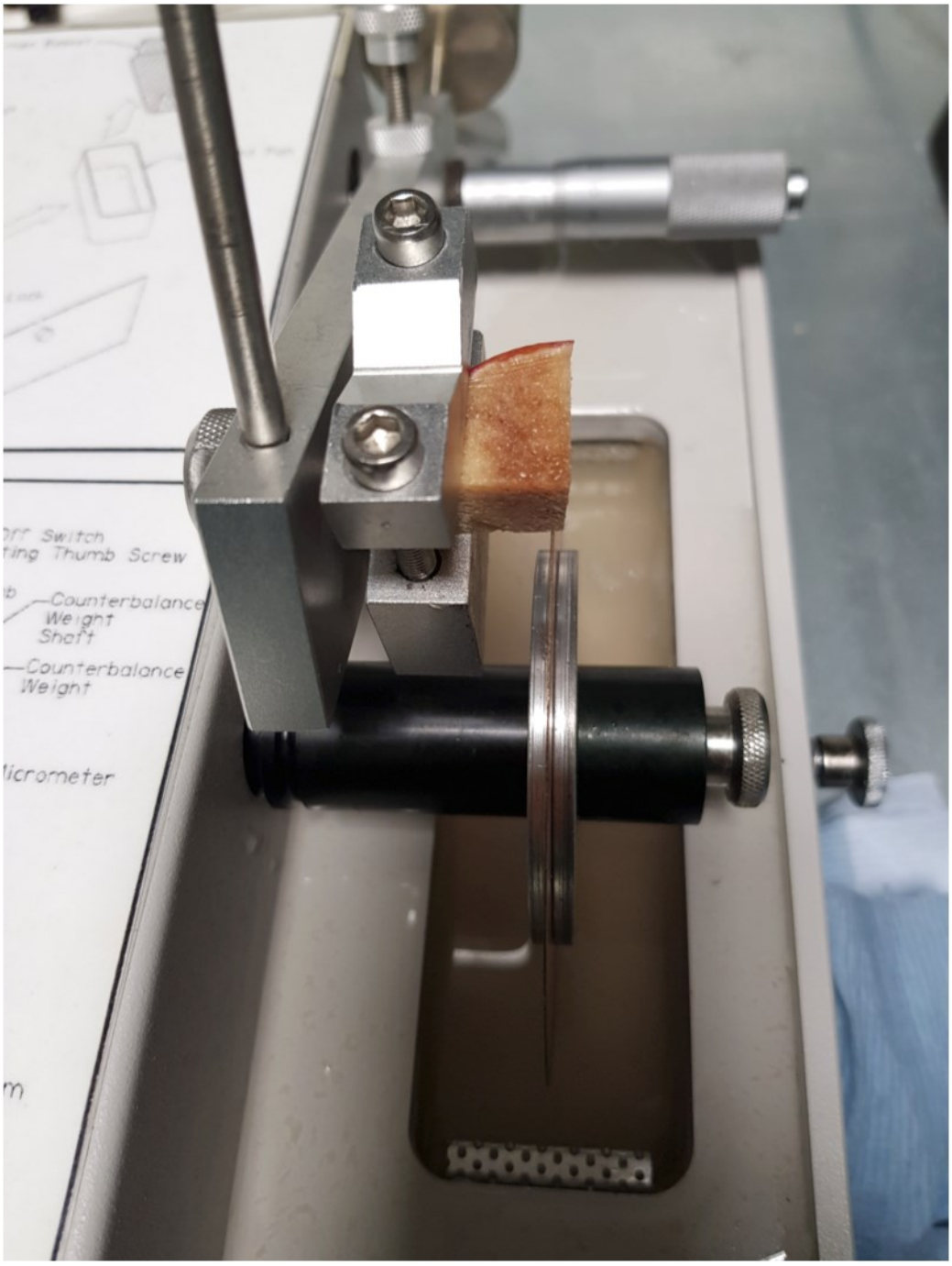

Figure 3.2.5 Diamond saw used again to slice the quarter into 1mm thick pieces.

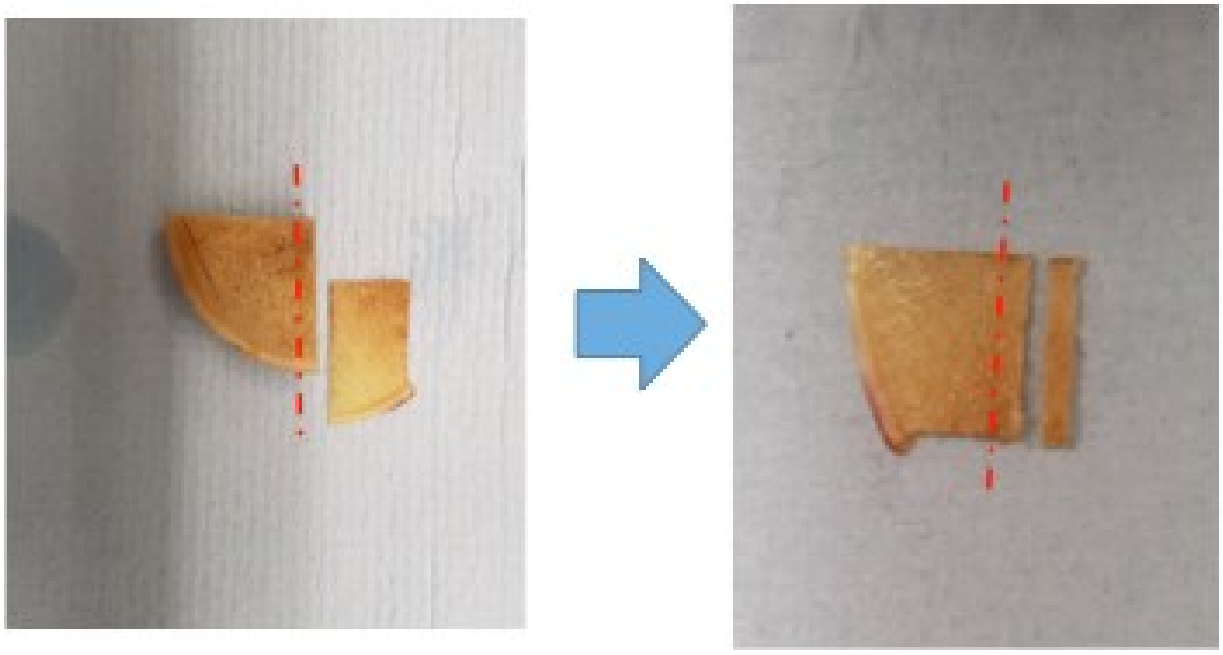

Figure 3.2.6 Depiction of where the cuts were made to result in samples of 1mm thickness and 2.5mm widths.

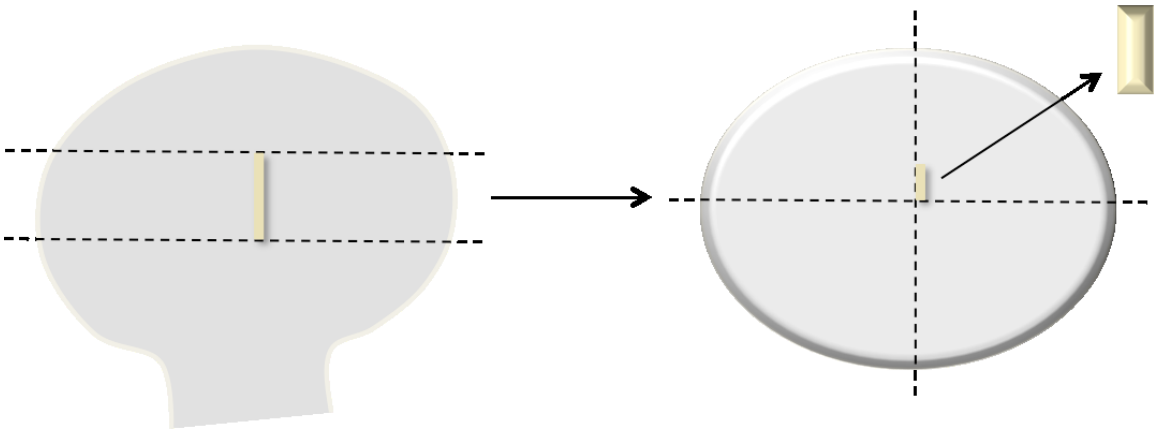

Figure 3.2.7 Simple depiction of the final sample in relation to the original femoral head.

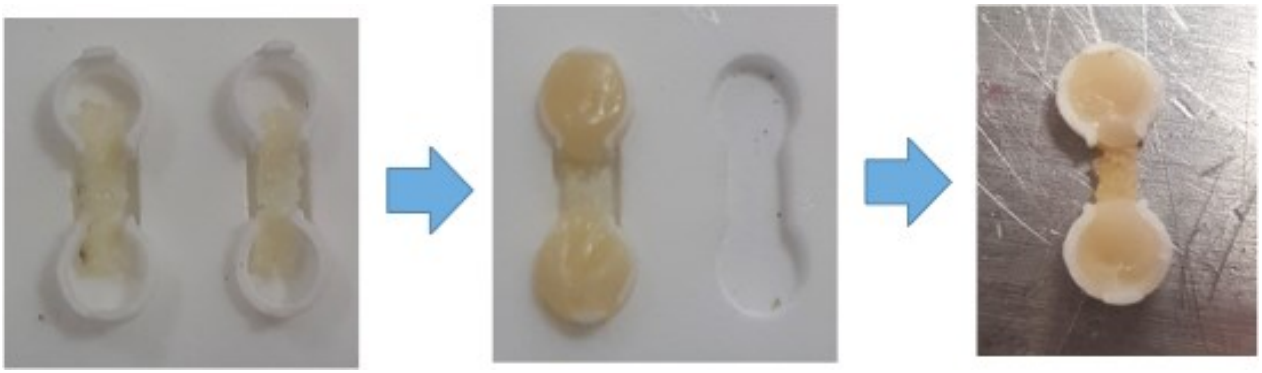

Figure 3.2.8 Process of how samples were embedded into holders.

3.2.3 Imaging nanostructure and mechanics

3.2.3.1 Synchrotron X-ray SAXD & WAXD

The embedded rectangular samples were mounted in a sealed sample chamber. These sample chambers were mounted on a 2-axis motorized linear stage on beamline I22 at Diamond Light Source (Oxfordshire, United Kingdom). A synchrotron x-ray beam (wavelength λ = 1Å, beam cross section 200µm x 200µm) was used to measure the Small-angle x-ray diffraction (SAXD) and wide-angle x-ray diffraction (WAXD) patterns. The distance between the sample and detector was 6.852 m and 0.175 m for SAXD and WAXD spectra respectively, which was verified with a calibration standard.

Samples were loaded in tension with a strain rate of $0.001s^{-1}$, corresponding to physiological loading, for about an average of 2 minutes per sample. Tensile loading was

used since the samples were taken predominantly from the tensile arcade of the femoral head. All tests were conducted at room temperature and the specimens were kept hydrated throughout testing. Video extensometry was used to capture images of the samples during testing.

The detectors used were the PILATUS 2M and RAPID, which allowed for faster measurements during in-situ mechanical testing. Samples were scanned (x-ray exposure time of 0.5 s) in real-time during testing at 2.5 second intervals.

SAXD is used to quantify deformation of collagen fibrils by tracking the changes in D-periodicity, usually about 64~67nm, of the 1st order peak of the meridional banding patterns. The peak (red arrow in Figure 3.2.9) in a SAXD image is due to the triple helical tropocollagen molecules arranged in a staggered manner. This arrangement leads to the axial periodicity in the electron density, also known as the D-periodicity. From the SAXD pattern, an integrated intensity profile of the peak was obtained like shown in Figure 3.2.9. On the other hand, WAXD is used to look at the deformations of the mineral crystals by looking at the changes in percentage changes in the (002)c-axis spacing of the hexagonal closed packed (hcp) lattice. The interplanar spacing (D-period) of mineral crystallites are about 0.1~0.3nm. Under loading, these patterns shift, allowing for the measurement of nanoscale mechanics (Gupta et al., 2006).

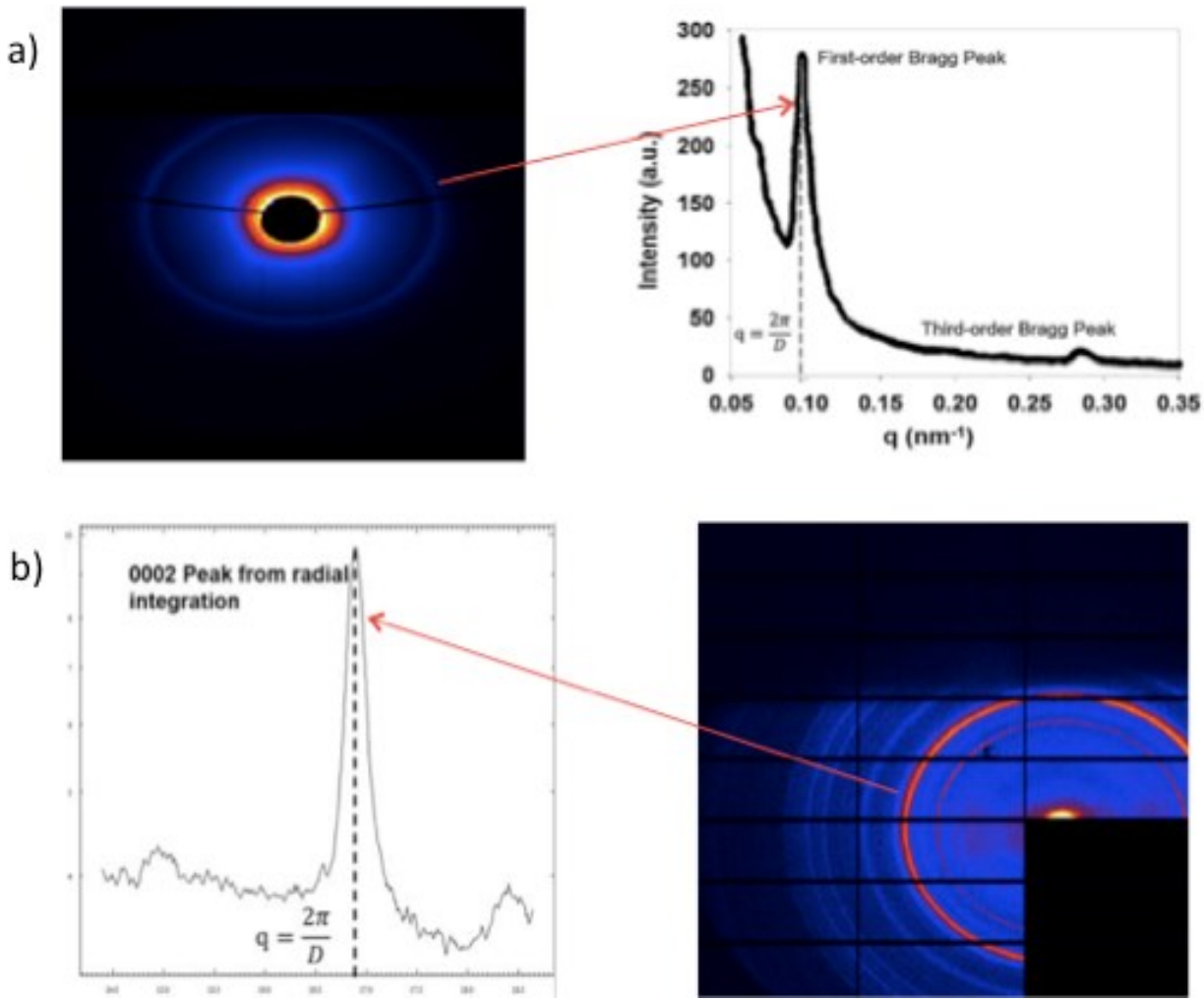

Figure 3.2.9 a) An example of an integrated intensity profile of the peak (red arrow) from a SAXD pattern. b) The integrated intensity profile of the peak (red arrow) from a WAXD pattern.

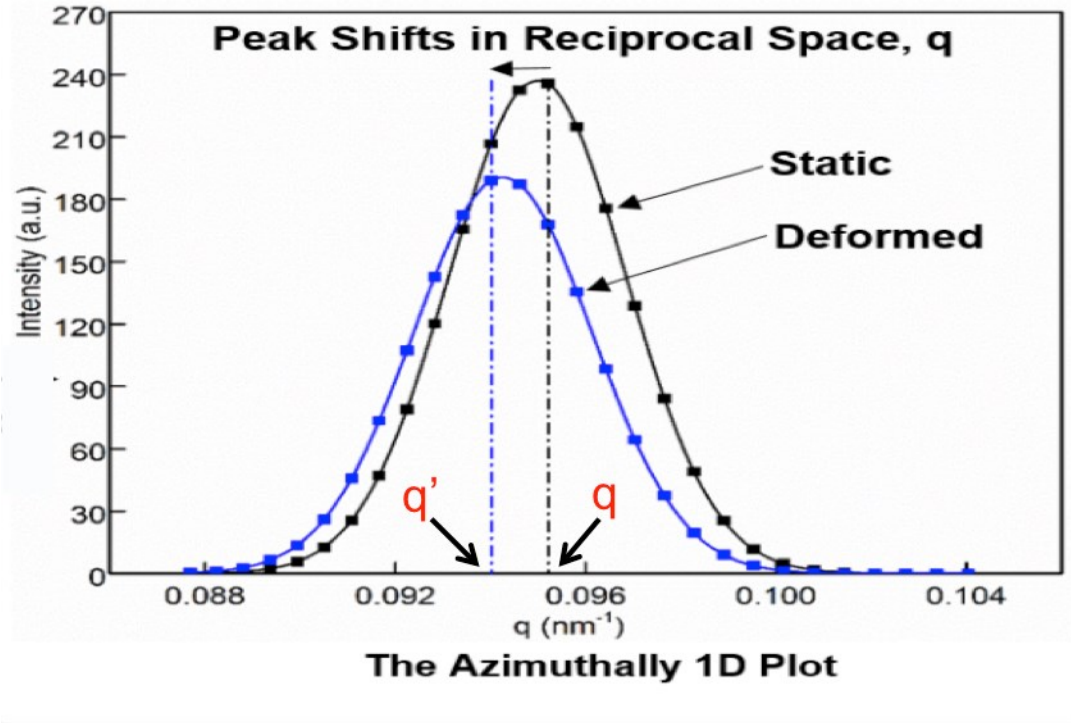

Figure 3.2.10 The shifts in the 1st order collagen peak position. These shifts are brought about when the collagen fibrils are stretched and the D period is changed, which is related to q.

From the intensity profiles, the D-period (~67nm) was calculated using Equation 3.2:

$$q = \frac{2\pi n}{D} \qquad \text{Equation 3.2}$$

where q is the distance from the centre of the beam (centre of the SAXD and WAXD patterns) to the peak, and n is the n^{th} order of the peaks of the patterns.

Fibril and mineral strains were then calculated using the changes in the D-period, as seen in Figure 3.2.10, using Equation 3.3:

$$S = \frac{\Delta d}{D}$$ Equation 3.3

where S is strain, Δd is the change in D-period and D is the original D-period before load was applied.

3.2.4 Statistical Analysis

IBM SPSS Statistics 24 (Armonk, New York) was used to perform statistical analysis and the graphs were generated with GraphPad Prism 7 (San Diego, California). The data were assessed for normality using a Q-Q plot and Shapiro-Wilk test, and were found to follow a non-Gaussian distribution. Consequently, the results were presented as median and interquartile range. Non-parametric descriptive statistics and tests used included the Kruskal-Wallis and Mann-Whitney U tests.

3.3 Results

At the tissue, fibril and mineral levels, bisphosphonate treated bone was significantly less deformable than both the untreated fracture and non-fracture controls (Figure 3.3.1). FC and BP treated fracture groups exhibited with lower strains than NFC. Moreover, the BP treated group had significantly lower tissue and mineral strains compared to FC ($p<0.01$ & $p<0.005$ respectively).

The results also suggest that there appears to be a negative correlation between tissue mechanics and BP treatment duration ($r^2 = 0.19$) and fibril mechanics and BP treatment duration ($r^2 = 0.10$), whereas there is a positive correlation between mineral mechanics and BP treatment duration ($r^2 = 0.001$), although the correlations were not strong (Figure 3.3.2).

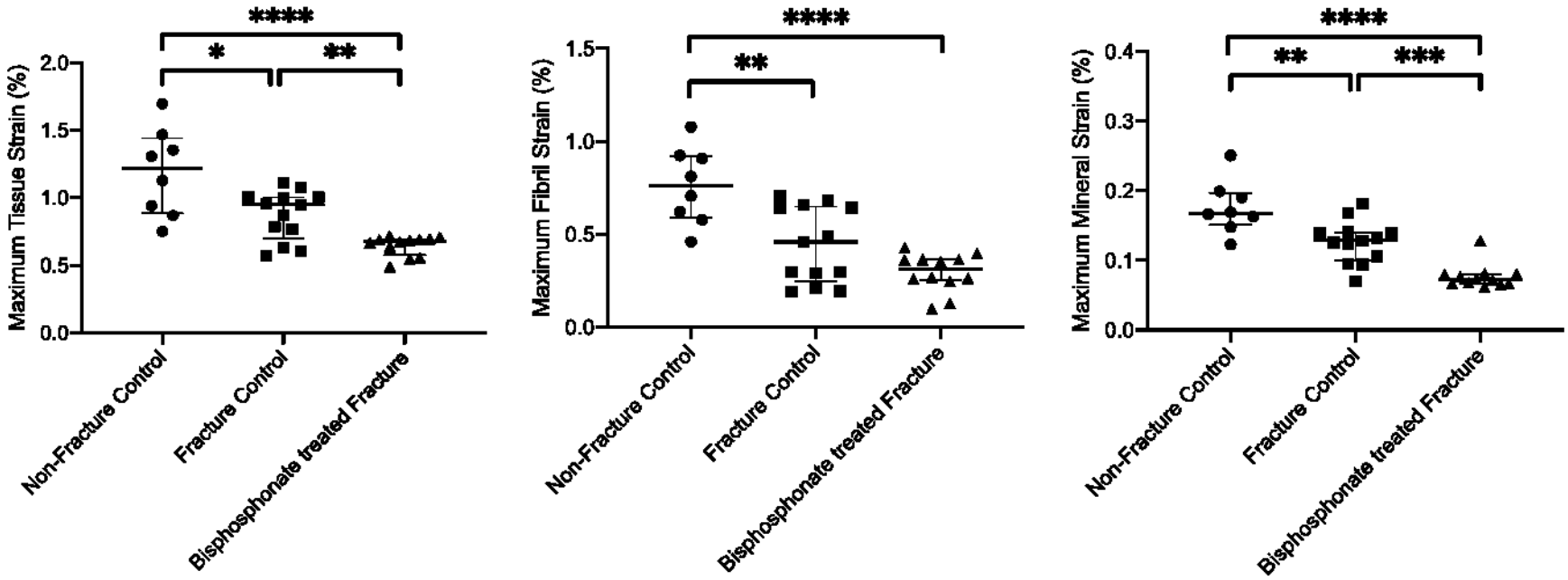

Figure 3.3.1 Comparison of tissue, fibril ad mineral strains between NFC, FC and BP treated groups. BP and FC exhibited significantly lower tissue, collagen and mineral strains than NFC. Kruskal-Wallis tests and post-hoc Mann Whitney U tests were performed to determine if differences were significant. The asterisks indicates significant pairwise differences: *p<0.05, **p<0.01, ***p<0.005, ****p<0.001.

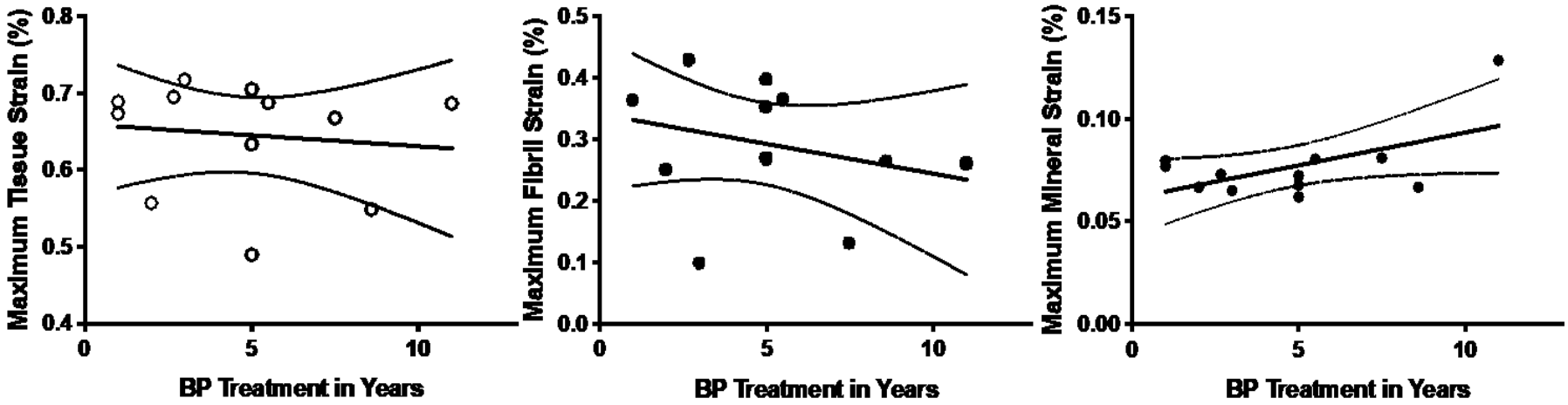

Figure 3.3.2 Analysis of the effects of BP treatment duration on tissue, fibril and mineral strains. Tissue and fibril strains tend to decrease with BP treatment duration, although not significant (r^2 = 0.19, r^2 = 0.10 respectively). However, mineral strain increased with BP treatment duration (r^2 = 0.001). The dashed lines represent the 95% confidence intervals.

3.4 Discussion

This study used synchrotron SAXD and WAXD to compare tissue, collagen fibril and mineral crystal strains across NFC, FC and BP groups. Moreover, the correlation between BP treatment duration and the nano strains was also analysed. From the data, it was apparent that the nanostructure plays an important role in tissue level bone mechanics. The results showed that irrespective of treatment, fracture patients exhibit lower collagen and mineral strain than NFC. The reduced tissue and collagen fibril strains observed in the BP treated fracture groups, negatively correlated with treatment duration (but not significantly), whilst mineral strain remained constant. Hence the findings suggest that (1) fragility fracture is associated with a loss of nanostructural integrity and (2) BP may exacerbate the loss of tissue and fibril strain associated with osteoporosis, but not mineral strain.

3.4.1 Nanocascade

It has been proposed that load transfers in bone by conveying strains from the nanoscale level to the tissue level. The results of this study showed that tissue and matrix strains were lower in the fracture patients than NFC. This confirmed previous study findings by Jin *et al.*, who measured the apparent compressive strength of bone cores collected from the same donors as this current study, and found that fracture patients had lower compressive strengths than NFC (Jin et al., 2017). As such, the lower strength in fracture patients is associated with lower strains at the nanostructure (Jin et al., 2017). This loss of

strain at the nano level potentially reduces the strain at the tissue level via a cascade effect. At the nanoscale, when the structure experiences a load, the collagen fibrils slide across one another and individual collagen molecules stretch and unwind (Gupta et al., 2006). If the collagen-mineral matrix becomes stiffer, less sliding can occur, and the collagen fibrils are resistant to stretch and unwind, thus reducing the amount of strain and in turn deformation that the bone can undergo. The lower collagen and mineral strains suggest that both the fracture groups' collagen-mineral matrices are less deformable under load. Hence, the amount of deformation the structure can undergo is reduced resulting in (1) the formation and propagation of cracks and (2) less bending of the whole bone before failure. Both mechanisms could potentially increase the risk of fracture during a bump or fall.

These findings support the theories of other researcher. Zimmerman *et al.* (2015) reviewed bone's fracture mechanics to reveal the determinants of its intrinsic resistance: the nanostructure's deformation mechanisms, which prevent crack propagation (Zimmerman et al., 2015). An easier initiation of fracture at the nano level could propagate to the other levels leading up to the tissue level due to the lack of crack resistance and potentially increasing the risk of fracture during a fall.

The key results from this current study suggest that fragility fractures are associated with low deformability at the nano level. As such an accumulation and growth of microcracks ws~~sh~~ould be expected. However, Ma *et al.* showed that bone from patients who have suffered a fragility fracture, who had not received BP treatment, had the same density of

microcracks as non-fracture controls (Ma et al., 2017). It is widely known that during remodelling, osteoclasts resorb bone, ~~thus removing material,~~ in regions that have microcracks, which arise~~s~~ as a result of physiological loading (Rumpler et al., 2012). In bone that had suffered fractures, it is expected that the lower strains at the collagen-mineral matrix would result in the formation of accumulated microcracks. However it is possible that there is increased ~~ere is increased~~ osteoclastic activity in the fractured bone, thus resorbing more cracks and bone. The study presented here used the same specimens as Ma *et al.* and builds on his work. Hence, this is a likely explanation as more perforations were observed in FC group (Ma et al., 2017).

Interestingly, our work in combination with that of Ma *et al.,* further suggests that lower nano level strains could accelerate the loss of bone mass and structure. This idea has been previously proposed by Burr *et al.*, who suggests that microcracks might upregulate remodelling and increase the loss of tissue mass and structure (Burr et al., 1997). Ma *et al.* showed that BP treated patients exhibited a higher density of microcracks than non-treated, controls which is possibly a result of lower strains at the nano level, as presented in this study (Ma et al., 2017). This suggests that BP could exacerbate the accumulation of microdamage, by supressing remodelling and removal of cracks. In combination to the ease of crack formation due to lower nano level strains, the ability to form stable damage and prevent premature microcracks is affected, thus reducing the bone's fracture toughness. This could possibly be the mechanism resulting in atypical fractures. However, it could also be argued that since this mechanism is present in all the BP

treated samples in this study, non of whom had suffered an atypical fracture, it might not be the mechanism of atypical fractures.

Moreover, with BP duration, there is a tendency for tissue and collagen strain to decrease but an increase in mineral strain. This suggests that BP treatment is unable to stop the loss of tissue and collagen strain associated with osteoporosis but might possibly stop and possibly restore the loss of mineral strain. Since there is a positive correlation between mineral strain and prolonged BP treatment, the reduction in nanostructure's deformability is more likely due to the accumulation of crosslinks, which reduces the sliding between collagen fibrils (Pachalis et al., 2001; Odetti et al., 2005).

Expanding to a clinically relevant point of view, BP therapy has been reported to have an association with reduction in fracture risks (Liberman et al., 1995; Black et al., 1996; Lyles et al., 2007). However these clinical trials typically only last 3-4 years, and patients are typically placed on treatment for over 5. Yet, there is little knowledge on how long treatment should be administered for. Ma *et al.* suggests that longer treatment duration would result in increased accumulation of microcracks, which could grow and connect, eventually leading to a fracture. However, the lack in significant decrease in the strains with increasing BP treatment duration does not support our initial theory that longer BP therapy will decrease deformability of the collagen-mineral matrix, in turn resulting in the propagation of cracks over time. As such, it brings about the question as to whether the decrease in deformability in BP bone occurs in the first 5 years of treatment, and not only after prolonged (more than 5 years) therapy.

In Figure 3.4.1, BP treated fracture group was split into 2 groups: fracture patients treated with BP for up to 5 years (short treatment) and fracture patients treated with BP for over 5 years (long treatment). The results showed that there was no significant difference in tissue, fibril and mineral strains between the short and the long treatment durations. This explains the lack of significant decrease in strain over time as seen in Figure 3.4.2. Moreover, the short term treated bone still exhibited significantly lower tissue, fibril and mineral strain than controls. This suggests that the loss in deformability in the nanostructure brought about by BP treatment occurs as early as 5 years, even though recommended drug holidays are after 3 to 5 years of treatment (Villa et al., 2016).

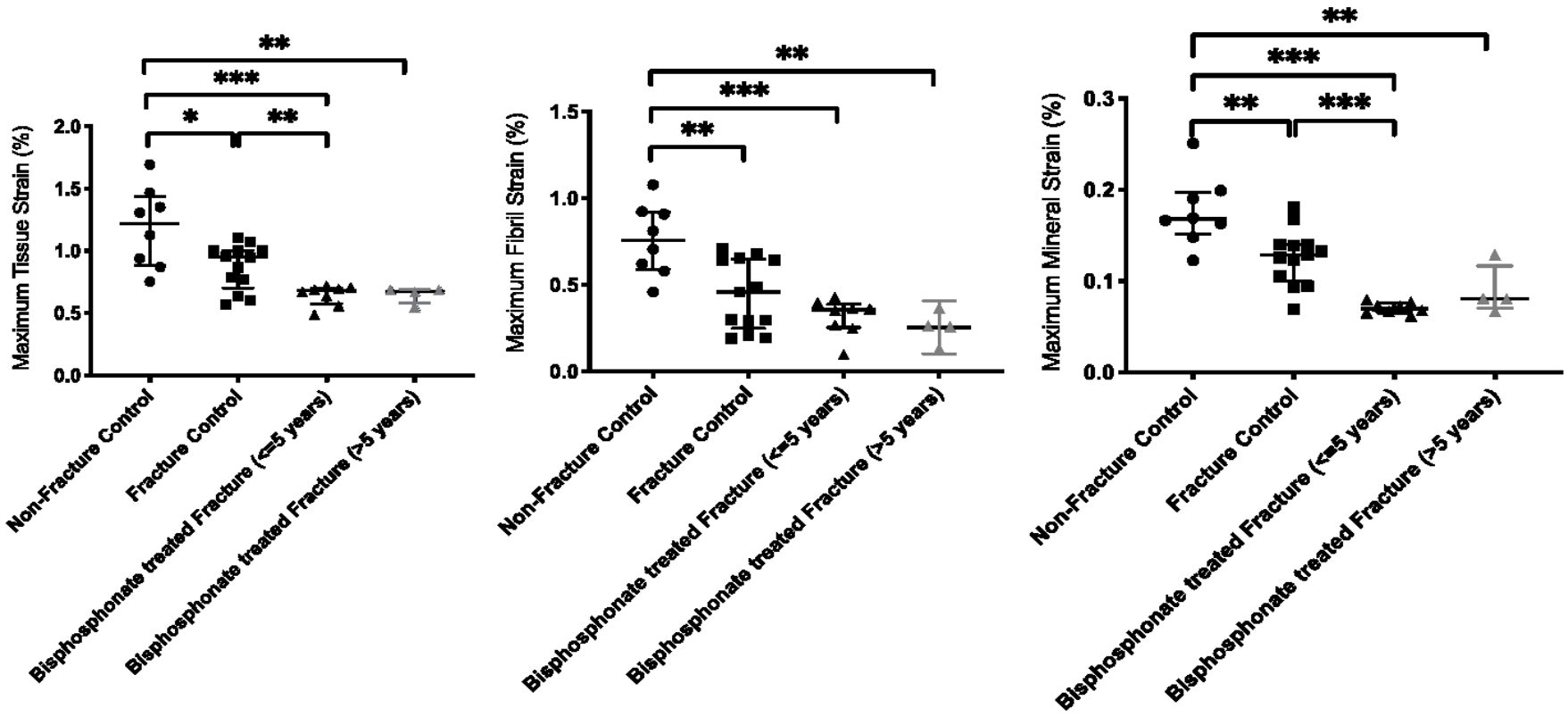

Figure 3.4.1 Comparison of tissue, fibril and mineral strains between NFC, FC, fracture group treated with BP for up to 5 years and fracture group treated with BP for more than 5 years. The fracture group treated with BP for up to 5 years exhibited with significantly lower tissue and mineral strains than controls There was also no significant difference between those treated with BP up to 5 years and more than 5 years. Kruskal-Wallis & Mann Whitney U tests were used to test for significance between the groups.

Since bisphosphonate is absorbed into bone and has a long half-life, it continues to act as an anti-resorptive even after treatment has stopped. As such, drug holidays are adopted to reduce the risks of adverse side effects such as atypical fractures (Shane et al., 2014). Research has shown that treatment holidays have been reported to be effective at reducing risks of atypical fractures (Bonnick, 2011; Adams et al., 2018). Adams et al reported that a treatment holiday after 3-5 years of BP therapy reduced fracture risks by 78%-80% compared to a reduction in fracture risk of 44% after discontinuation after a year (Adams et al., 2018). However the data from this paper's study suggests that the loss of strain, which could bring about fatigue fractures, occurs much earlier than the 3-5 year period in some patients. Thus, patients in this study could potentially benefit from an earlier treatment holiday. This is assuming that the low strains contributed to their hip fractures.

There are currently still no standards for who should receive a drug holiday and when it should be administered, but it perhaps needs to be patient specific. In order to assess patients' bone health during treatment, there would likely need to be a follow up test for patients. Currently GPs ask patients undergoing BP treatment to report groin pain in order to detect atypical fractures (National Institute for Health and Care Excellence, 2018). However, these reports are not very specific as pain is subjective. When pain is reported, follow up x-rays may reveal an atypical fracture but at that point it is already too late (National Institute for Health and Care Excellence, 2018). Thus to assess how long patients should be treated for before a treatment holiday, a trial should be conducted, measuring bone health *in-vivo* throughout treatment.

There are key limitations that should be discussed, as interpreting our results in relation to the effects of BP treatment on clinical outcome is complex since these are observational, cross-sectional data with all the potential selection biases. The BP treated samples were harvested from femoral heads of patients that were already receiving treatment because they were diagnosed to have higher fragility, and thus it could be argued that the samples already had a weaker structure than FC. However in Chapter 2, the BP treated fracture patients in fact exhibited a similar microarchitecture to the non-fracture controls. In addition, the same samples exhibited with fewer perforations as seen in Ma *et al.'s* work, suggesting that the bone is actually healthier at the microstructural level than the fracture controls (Ma et al., 2017).

More importantly, there is a lack of BMD data as it was not possible to retrospectively collect DXA scans. However it should be noted that since BP patients were most likely prescribed the medication after they had been diagnosed with osteoporosis, the BP fracture patients could safely be termed osteoporotic. With this in mind, it is possible to suggest that the groups displayed a progression in disease from the non-fracture patients to the non-treated fracture patients to the BP treated fracture patients. Thus the data does suggest that irrespective of treatment, bone that have suffered fragility fractures have lower bone strength due to the nanostructure's reduced ability to deform under load. To follow up this research, and in order to be able to make any conclusions about BP therapy, BP tissue samples from patients who had not suffered a fracture (i.e. successfully treated) should be included to reduce the limitations in comparing treated and non-treated patients.

3.5 Conclusion

The results from this chapter show that the nanostructure plays a role in tissue level mechanics and probably whole bone strength. This occurs via 2 possible mechanisms: (1) a cascade effect with a transfer of strain from the nano level to the tissue level and (2) a variation in the deformability of the nanostructure that affects the formation and propagation of cracks. This study found that, irrespective of treatment, femoral fractures are associated with a loss of nano level deformability, which could be due to increased crosslinking and mineral crystal dimensions in the collagen matrix, causing the matrix to become stiffer. Furthermore, BP treatment is associated with the exacerbation of the loss in collagen and mineral strains, possibly as a result of the suppression of remodelling. Although it is possible for BP patients' bones could have been more diseased, wider data from our lab does not support this conclusion. As such, this suggests that bisphosphonate treats the macro and micro level damage but not at the nanoscale. This could be important because the lack of repair at the nanostructure could be the reason for fragility fractures sustained even after therapy. To further understand the mechanism of the loss of nanostructure deformability, the collagen crosslinks and mineral crystals, which make up the nano matrix, should be studied with respect to disease and treatment.

Chapter 4. The Effects of Synchrotron X-ray Radiation

4.1 Introduction

With the development of synchrotron facilities, synchrotron x-ray diffraction and scattering have been used to image materials, including bone, from the macroscopic level to the nanometre scales. Synchrotron radiation covers the entire range of the electromagnetic radiation from infrared to x-rays, allowing for the imaging of parameters at multiple hierarchical levels. These high-energy beams are generated by the acceleration of electrons to almost the speed of light. At high flux, monochromatic x-ray beams can be passed allowing for detailed investigation of structure and mechanics of the bone's nanostructure while maintaining a high signal to noise ratio (Burghardt et al., 2018). It has become increasingly more common to use a combination of mechanical testing and synchrotron x-ray scattering, known as in-situ synchrotron x-ray scattering, to investigate the relationship between the nanostructure and tissue level mechanics (Gupta et al., 2005; Gupta et al., 2004; Akhtar et al., 2008; Krauss et al., 2009).

4.1.1 Radiation Effect

The main drawback of synchrotron radiation is that the high intensity x-rays can damage the tissues. However the effects of irradiation on bone's mechanical properties are often overlooked. For medical and scientific reasons, human bone can be exposed to a wide range of radiation levels.

However, several studies have reported that for doses up to 35 kGy, typically used for sterilisation of allograft bone, the post-yield properties of cortical bone were affected, in particular reduced ultimate strength and work-of-fracture (Cornu et al., 2000; Currey et al., 1997; Akkus & Belaney, 2005). Cornu *et al.* found that 25kGy of gamma irradiation on femoral heads reduced compressive ultimate strength by 42.5% and work to failure reduced by a mean of 71.8%. However, the bone that was exposed to the radiation was already processed by freeze-drying, that includes lipid extraction and exposure to chemicals, thus the decrease in mechanical strength was not only due to the irradiation (Cornu et al., 2000). Currey *et al.* exposed human bone to a range of radiation doses ranging from 17kGy to 94.7KGy. They found that radiation dose of 30KGy, even though commonly used by tissue banks, significantly affected mechanical properties and even at 17KGy, the work to fracture reduced by 50%. However, the samples were also washed with ethanol and stored at -80°C, which are likely to also have some effect on mechanical properties (Currey et al., 1997). Similarly, Akkus *et al.* reported impairment of fatigue properties when cortical bone was exposed to 36.4kGy irradiation (Akkus & Belaney, 2005). As such, the ideal safety value of 35 kGy (or below) was suggested to minimise the impact on the mechanical properties of bone while still achieving adequate sterilisation of bone grafts (Nguyen et al., 2007).

The aforementioned studies studied the effects of radiation from sterilisation, which typically include other chemical preparations that could affect the bone's properties. Although very few, there have been some studies that looked at the effects, specifically, of synchrotron radiation (Barth et al., 2010; Barth et al., 2011; Fernández et al., 2018).

Most recently, Fernández *et al.* reported that high irradiation doses did not alter the apparent mechanics of trabecular bone (Fernández et al., 2018). The study looked at the effects of synchrotron micro-CT radiation on the bone's tissue mechanics during *in-situ* mechanical testing by exposing the samples to irradiation doses between ~33 kGy to ~230 kGy. They used digital volume correlation (DVC) to detect local levels of strain and found that microcracks were not detected and bone plasticity was preserved for low irradiation doses of 33kGy. However, this study only looked at the effects at the microstructure but not at the nanoscale level.

Gamma radiation is known to adversely affect mechanical and biological properties by degrading collagen (Anderson et al., 1992; Cornu et al., 2000; Currey et al., 1997; Gibbons et al., 1991). Similarly, synchrotron irradiation has been said to affect the collagen matrix by increasing the amount of crosslinking (Barth et al., 2010). Barth *et al* exposed bone samples to 0, 0.05, 70, 210 and 630 kGy doses during synchrotron micro-CT experiments, and used Raman spectroscopy to detect changes in the collagen environment (Barth et al., 2010). Barth *et al*. reported that high exposures to synchrotron x-ray radiation results in the deterioration of the collagen mineral matrix and thus leading to degraded mechanical properties, including reduced strength, ductility and toughness in human cortical bone (Barth et al., 2010; Barth et al., 2011). However, the studies used irradiations up to 630 kGy, and plastic deformation was seen to have suppressed after 70 kGy of radiation. Typically, synchrotron diffraction experiments on bone tissue such as *in-situ* small-angle x-ray diffraction (SAXD) and wide-angle x-ray diffraction (WAXD) do not exceed the ideal value of 35 kGy, far below the 70 kGy radiation at

which plasticity was suppressed. These experiments tend to be at much lower dose rates, usually ~0.2 Gy/s, leading to typical doses ranging up to 30 KGy (Table 4.1.1).

Table 4.1.1 Typical dose rates from in-situ x-ray scattering experiments

Type of in-situ experiment	Synchrotron Location	Radiation Energy (keV)	Flux (photons/s)	Flux density (photons/s/mm^2)	Radiation dose rate (kGy/s)	Typical radiation dose (kGy)
SAXD, WAXD	Advanced Light Source (ALS), Lawrence Berkeley National Laboratory	10	2.15×10^{12}	2.2×10^{12}	5	~20
SAXD	Hamburger Synchrotron strahlungs lab (HASYLAB), Deutsches Elektronen-Synchrotron (DESY)	8.27	1×10^{9}	1.67×10^{8}	2×10^{-4}	~0.04-0.12
WAXD	Advanced Photon Source (APS), Argonne National Laboratory	80.7	1×10^{10}	1×10^{12}	0.2	~6-30
SAXD, WAXD	Diamond Light Source, I22 Beamline	12.4	6×10^{12}	1.5×10^{14}	0.3	~0.015-30

Although the amount of radiation used for SAXD and WAXD are well below the safety value there are still uncertainties on the effects of synchrotron radiation on the mechanical properties at the nanoscale level of bone (Deutsches Elektronen-Synchrotron DESY, 2018). It was thus pertinent to check that the synchrotron x-rays did not affect the mechanical integrity of the nanostructure analysed in Chapter 3.

Due to the limited amount of time allocated for synchrotron experiments (4 days) at Diamond Light Source, the radiation exposure experiments had to run concurrently with the loading experiments. Given more time, the effect of radiation should have been looked at first before conducting the loading experiments.

4.1.2 Aims & Objectives

The aim of the study was to investigate, for the first time, the influence of synchrotron diffraction irradiation-induced tissue damage on tissue, collagen and mineral strains. The hypothesis was that tissue, collagen and mineral strains were not different when exposed to low, normal and high doses of x-ray radiation.

4.2 Materials & Methods

The samples used in this experiment were sectioned and processed as described in Chapter 3. The *in-situ* tensile testing procedure was also the same as that in Chapter 3. The difference was that each specimen was exposed to different x-ray radiation doses by using variable exposure times per projection: 100ms, 500ms (the radiation dose used in Chapter 3) and full exposure until the sample fractured. These exposures were categorised as low, normal and high respectively.

To estimate the radiation dose absorbed by the sample, the radiation flux density, ψ is computed from the photon flux, ϕ:

$$\psi = \frac{\phi}{z} \qquad \text{Equation 4.1}$$

where z is the area of the x-ray beam at the sample. The flux density is then converted into energy density, E_ρ:

$$E_\rho = \psi \times 1.6 \times 10^{-19} J/eV \times E \qquad \text{Equation 4.2}$$

where E is the radiation energy of the beam in eV.

The transmission, T, of x-rays through the sample of thickness, l, is then calculated as:

$$T = e^{-\alpha\rho l} \qquad \text{Equation 4.3}$$

where α is the mass attenuation coefficient in cm^2/gm and ρ is the density.

Finally, the dose rate, D, is obtained from:

$$D = \frac{AE_\rho}{m} \qquad \text{Equation 4.4}$$

where the fraction of x-rays absorbed by the sample, A, is given as $(1 - T)$ and m is the mass of the bone absorbing the radiation.

The dose rate was calculated, using the specifications of the I22 beamline at Diamond Light Source, to be 0.3 KGy/s at the energy level 12.4 keV. The total irradiated dose received per sample was thus simply:

$$Total\ irradiation\ dose = D \times t \qquad \text{Equation 4.5}$$

where D is the dose rate and t is the time of exposure.

The amount of radiation the samples were exposed to was calculated and tabulated in Table 4.2.1.

Table 4.2.1 Total irradiation dose received by samples

	Exposure Time	Total irradiated dose
Low Exposure	100ms	0.0003 KGy
Normal Exposure	500ms	0.0015KGy
High Exposure	~100s	~30 KGy

In order to quantify and compare tissue, collagen and mineral strains, in-situ mechanical testing was conducted in conjunction with SAXD and WAXD (refer for Chapter 3 for methodology). The beam shutter, which controlled the introduction of synchrotron x-rays to the sample, was adjusted to open and close for the set exposure times.

4.3 Results

In this section, the maximum tissue, fibril and mineral strains for each group were compared across normal, low and high x-ray exposure levels.

Kruskal Wallis and pairwise Mann-Whitney U tests show that the maximum tissue, collagen and mineral strains in NFC, FC and BP treated fracture groups were not significantly different between different x-ray exposures (Figure 4.3.1, 4.3.2 & 4.3.3).

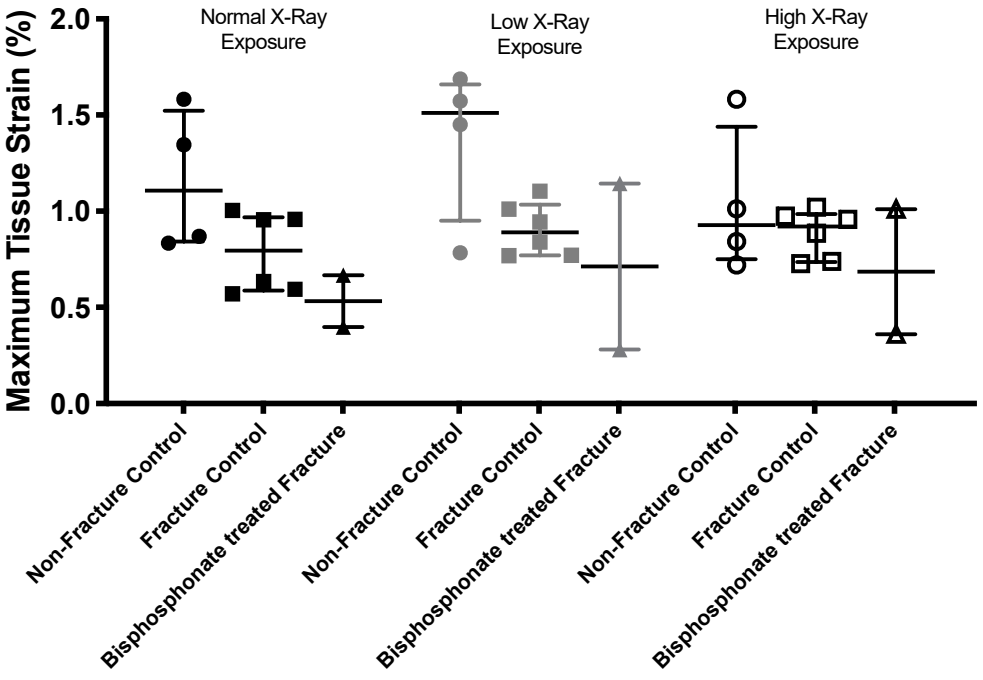

Figure 4.3.1 Comparing the maximum tissue of NFC, FC & BP groups across the different amount of x-ray exposures. There were no significant differences in maximum tissue strains among the different exposure levels. Kruskal-Wallis test and subsequent post hoc Mann-Whitney U analysis was used to find if the results of every two levels of exposures were significantly different.

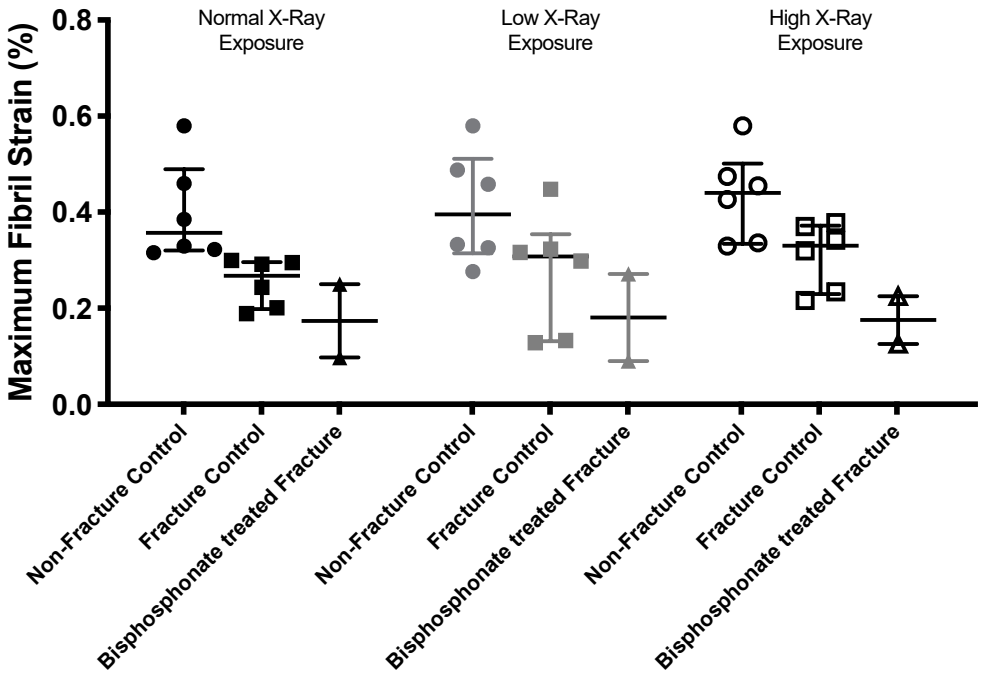

Figure 4.3.2 Comparing the maximum fibril strains of NFC, FC and BP treated fracture groups across the different amount of x-ray exposures. There were no significant differences in maximum fibril strains among the different exposure levels. Kruskal-Wallis test and subsequent post hoc Mann-Whitney U analysis were used to find if the results of every two levels of exposures were significantly different.

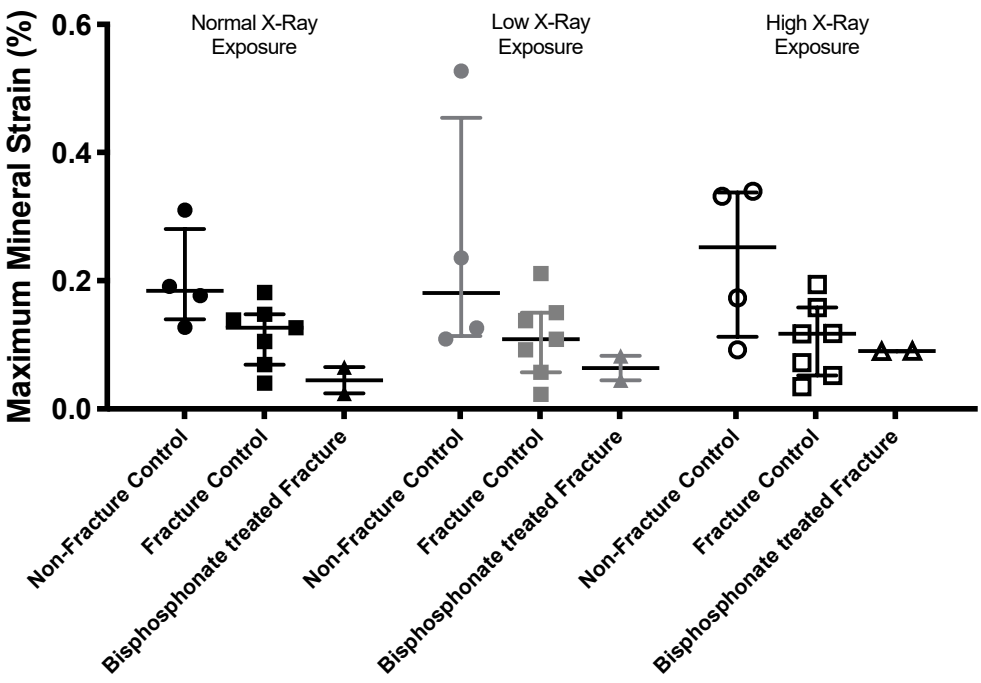

Figure 4.3.3: Comparing the maximum mineral strains of NFC, FC and BP groups across the different amount of x-ray exposures. There were no significant differences in maximum mineral strains among the different exposure levels. Kruskal-Wallis test and subsequent post hoc Mann-Whitney U analysis were used to find if the results of every two levels of exposures were significantly different.

4.4 Discussion

There were no significant differences in tissue, collagen and mineral strains between low, normal and high exposures. Thus it appeared that the amount of x-ray exposure usually used for SAXD and WAXD (exposure time of 500ms) did not degrade the mechanical properties of the collagen-mineral matrix. This finding is important as it confirms that the interpretation of the strain data in chapter 3 is reliable, that the decrease in strain seen in the fracture groups is due to nanostructural changes rather than radiation damage due to synchrotron imaging. However it is important to note that a control of no radiation exposure was not included in this experiment and as such it is not possible to conclude that no amount of radiation (even low energy) would degrade bone mechanical properties.

It could be argued that a limitation of this study is that there was no control group of unirradiated bone. This was not included in the experiment because it is impossible to measure collagen and mineral strains without synchrotron imaging. Moreover, Barth *et al*. showed that there was no difference in the collagen environment, as determined by Raman spectroscopy, between 0 and 0.05 KGy irradiation doses (Barth et al., 2010). The amount of radiation used for typical SAXD and WAXD experiments at the I22 beamline in Diamond Light Source, does not exceed 0.05 KGy (Table 4.1.1). Barth *et al*. also stated that since significant changes were only seen at higher irradiation levels, over 35 KGy, one would only need to question the results of any *in-situ* mechanical studies that involve concurrent x-ray tomography at these irradiation which with a standard 20 keV x-

ray tomography beamline would be achieved after exposure times of about 5 minutes (Barth et al., 2010). With modern detector systems such as PILATUS 2M or RAPID, which are available at Diamond Light Source, faster measurements could be made to reduce the exposure time and thus radiation dose.

In future work, it might still be of importance to compare with unirradiated bone to determine if small amounts of radiation will degrade tissue strain. The tissue strains could be compared inside and outside of the beamline, using the same loading rig. It would not be possible to test exactly the same bits of bone, however adjacent sections could be compared.

4.5 Conclusion

This study showed that the amount of x-rays exposed to bone samples from synchrotron SAXD and WAXD experiments do not seem to degrade the strains at the tissue, collagen and mineral levels. This helped us conclude that the reduction in collagen and mineral strains seen in the fracture groups are most possibly due to nanostructural changes rather than degradation due to irradiation.

Currently, synchrotron imaging is the best technique to visualise nanomechanics. It can also be used to visualise nanostructure such as collagen orientation and mineral crystal size. With the increased confidence from this chapter regarding the reliability of synchrotron imaging, the next chapter delves into other nanostructural properties.

Chapter 5. Bone Mineral Crystal Dimensions

5.1 Introduction

Traditionally fragility fractures have been attributed to the loss of bone mass and mineral density, which leads to fragility. However, researchers have long suggested that the material might also be damaged, which is possible given the apparent loss of bone mineral density (BMD) (Faibish et al., 2006). In Chapter 3, the collagen-mineral matrix mechanics was shown to be impaired in osteoporotic bone. Since BMD is decreased, and mineral crystals in the collagen mineral matrix are the only structure that accounts for mineral content, it is possible to infer the effect of mineral loss in the matrix on mechanics. Low BMD might be brought about by either changes in mineral crystal size or number, or perhaps both. However, there is little knowledge about the age-related changes in mineral crystal dimensions, or the relationship between mineral crystal dimensions and fragility fractures, even though diagnostics of osteoporotic patients rely on DXA based areal BMD measures. Moreover, the frontline therapies for osteoporosis were also specifically designed to increase BMD, yet the effects of BP therapy on mineral dimensions in humans are not known.

Studies have shown that the mineral crystals embedded in the collagen fibrillar structure play an important role in bone's mechanical behaviour (Boskey, 2003). The review by Boskey *et al*. reported that in different animal models with osteoporosis, the mineral crystal size, measured using various techniques, varied from controls. Moreover this altered mineral crystal content and size were associated with weaker mechanics, and it

was concluded that the size and distribution of mineral crystal seemed to be important to the strength of bone.

Given that bone mineral content is important, the increase in BMD brought about by BP therapy could also affect bone mechanical properties. Although the increase in BMD is only 1% to 6%, some patients still experience atypical fractures (Brown et al., 2002). It could be possible that larger mineral crystals, resulting in the increase in BMD, could affect the matrix mechanics via stronger bonding with the collagen matrix.

5.1.1 How do mineral and collagen affect matrix mechanics?

To understand how the mineral crystals affect the matrix mechanics, it is important to first understand how they attach to and interact in the matrix. Mineral crystals are embedded within the collagen fibril network in parallel layer and aligned with the length of the fibrils (Weiner et al., 1991). It has been theorised that the attachment of mineral crystals to the collagen matrix is via a mixture of three types of interfacial bonding at the collagen-mineral interface, i.e. molecular entanglement, intermolecular interactions and mechanical interlocking, as seen in Figure 5.1.1 (Stock, 2015). Kikkuchi *et al* suggested that the interaction between collagen and mineral is largely electrostatic interactions and hydrogen bonds (Kikuchi et al., 2001). This was further supported by Nair *et al,* who reported more hydrogen bonding between the mineral and collagen in the gap regions compared to non-mineralised collagen molecules, as well as electrostatic interactions between the 2 components (Nair et al., 2013). As such the interfacial bonding at the

interface is likely to be due to intermolecular interactions between the mineral crystal and collagen network.

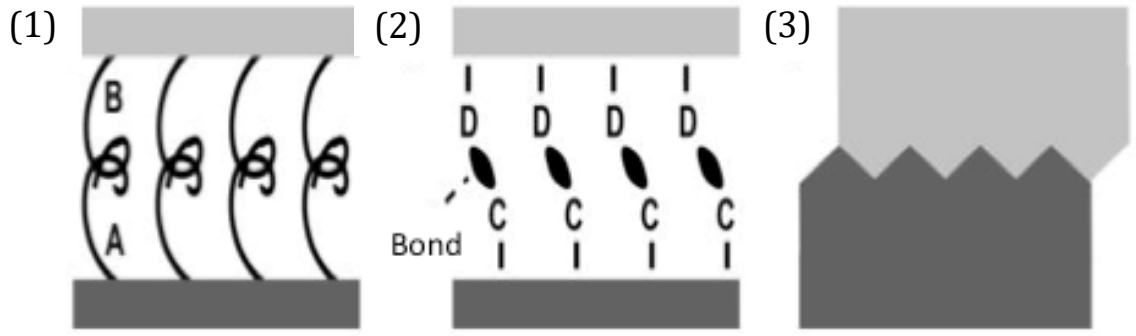

Figure 5.1.1 Schematics of the types of interfacial bonding between the collagen matrix (light grey) and the mineral crystal (dark grey). (1) Molecular entanglement: intermediary molecules, "A" & "B", that are entangled with the collagen fibrils and partly in contact with mineral crystals undergo macromolecular interaction. (2) Intermolecular interactions between mineral "C" and collagen "D" (3) Mechanical interlocking at the interface of collagen and mineral. Adapted from (Stock, 2015).

5.1.2 How do mineral crystals grow?

If the mineral crystals are attached to the collagen matrix via intermolecular interactions, the size of the crystals could affect the strength of bonding to the matrix.

The crystals develop in the spacing in the staggered arrangement of the collagen fibrils, fuse and grow within these gap regions (Figure 5.1.2) (Damon et al., 2011). Due to the organised network of collagen fibrillar structure, the nucleation and growth of mineral crystals are strongly confined by the architecture within the collagen fibril (Glimcher, 1959).

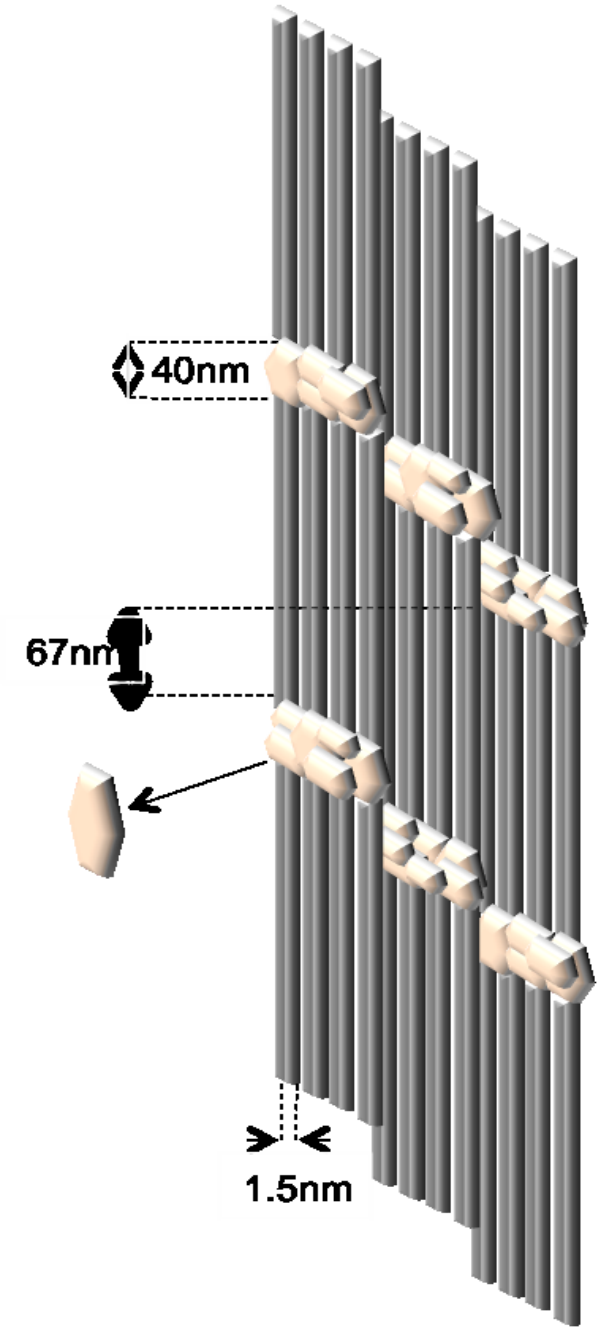

Figure 5.1.2 Simple depiction of the staggered model of the collagen fibrils and the placement of mineral crystals within the spacing of the structure.

5.1.3 Relating mineral crystal size to mechanics

Research has suggested that during healthy ageing, mineral content and crystallinity, which have been defined as the measurements of mineral crystal size and perfection by Farlay *et al.*, increase and positively correlate with bone strength and toughness (Farlay et al., 2010; Burr, 2002; Yerramshetty & O, 2008). However, there may be a plateau or drop off at high mineralisation. It has been suggested that too much mineralisation, which corresponds to a higher mineral content, could lead to weaker bone, susceptible to accumulation of microcracking and fractures.

In osteoporotic patients, increased crystal size has been observed compared to controls (Paschalis et al., 1997; Boskey et al., 2005). Paschalis *et al.* used Fourier transform infrared microspectroscopy (FTIRM) to image normal and osteoporotic bone taken from human iliac crest biopsies. They found that mineral crystals in osteoporotic were more crystalline, and thus larger, than normal in normal bone (Paschalis et al., 1997). Boskey *et al.* also found using FTIRM that bone mineral in human iliac crest biopsies of post-menopausal osteoporotic women were larger than normal controls (Boskey et al., 2005). As osteoporosis is associated with fragility fractures, the larger mineral crystal dimensions could be the factor that results in weakened bone. However, these studies examined biopsies taken from a non-loading region of bone and remodelling could differ greatly compared to loading regions. Moreover FTIRM does not give mineral crystal size values but only the amount of crystallinity, which is then inferred to be the size of mineral.

5.1.4 Measuring mineral crystal dimensions

There are many methods for assessing mineral dimensions more directly but published measurements vary 8 to 10 fold between studies with crystals ranging in length from 15 to 150 nm, in width from 10 to 80 nm, and in thickness from 2 to 5 nm (Robinson, 1952; Weiner & Price, 1986; Moradian-Oldak et al., 1991). The reason for the large range of the mineral crystal dimensions in literature is due to the lack of spatial resolution in the techniques. Traditionally, mineral crystals in bone are thought to have hexagonal shapes and grow in the spaces between the collagen fibrils (Hulmes & Miller, 1979). However, recent research has brought to light that mineral crystals do not have a regular shape but in fact have their own hierarchical structure consisting of acicular crystals, platelets, stacks of platelets and mineral aggregates (Reznikov et al., 2018).

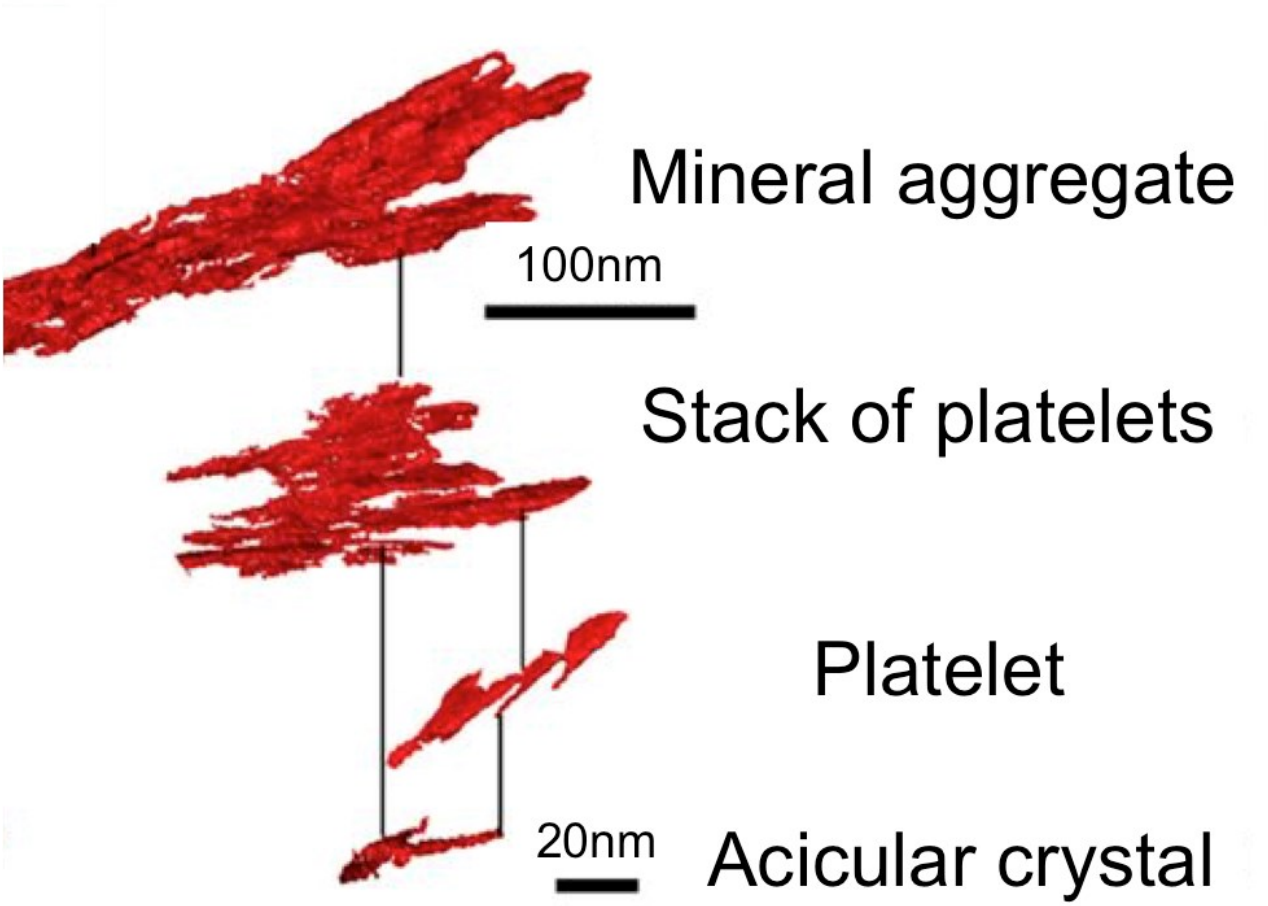

Figure 5.1.3 Depiction of the hierarchical structure of mineral crystals adapted from (Reznikov et al., 2018)

Reznikov *et al*. reported that mineral crystals have a hierarchical structure and the smallest component of a mineral crystal is an acicular crystal with lengths of about 50 to 100nm and at the largest scale they form mineral aggregates of lengths 200 to 300nm, explaining the range seen in previous literature.

The techniques used in the above studies include Raman spectroscopy and transmission electron microscopy (TEM) to measure the size of bone mineral crystals but few have used synchrotron radiation techniques, which gives the highest spatial resolution for detailed investigation of structure and orientation of mineral crystals in bone (Mandair & Morris, 2014; Arsenault, 1989). The best possible method for assessing mineral crystals size might be synchrotron imaging, which has high spatial resolution that allows for the measurement of the singular acicular crystals. However, this technique assumes that mineral crystals have a simple hexagonal-like shape, unlike the complex hierarchy as described recently by Reznikov *et al.* Moreover the synchrotron technique only gives the mean size of the crystals in a particular imaged region and not the measurement of individual crystals.

5.1.5 Aims & Objectives

This chapter aims to determine if mineral crystals were larger in fracture patients, in comparison to ageing controls, and if BP treatment is associated with increased mineral crystal dimensions. Specifically it is investigated if patients who had suffered a femoral neck fracture after undergoing BP therapy (alendronate 70mg weekly for 1-9 years, BP group) exhibit larger mineral crystals than untreated fracture control group and ageing non-fracture control group. In order to visualise and measure the mineral crystals, synchrotron x-ray scattering techniques are used in this study. Using the same imaging method and a subset of specimens as Chapter 3, the results could be matched up to fully understand the contribution of mineral crystal size to collagen-mineral matrix strains. It is possible that larger mineral crystals could result in stronger collagen-mineral interfacial bonding that results in a less deformable structure.

5.2 Materials and Methods

5.2.1 Sample Groups

For this study, trabecular bone samples were collected from the femoral heads of 3 individual groups, the NFC, the FC and the BP treated groups. Both the untreated and BP treated fracture groups' samples were obtained from patients who had suffered femoral neck fractures and had undergone hip arthroplasty surgery at Imperial College Healthcare National Service Trust in London, United Kingdom. The NFC samples were acquired from cadavers and they had no histories of hip fractures. All individuals with histories of primary bone diseases or underlying disorders, such as cancer, which could lead to secondary bone disease, were excluded from the study. Ethical approval was granted by the Imperial College Tissue Bank (R13004) for the collection of the femoral heads with additional patient consent to use their tissue for the study.

The BP treated group included patients who had suffered a femoral neck fracture after they had received BP therapy. The type of treatment undergone was with one type of BP, Alendronate, with a dosage of 70mg weekly. Only samples from patients whom had undergone treatment for a minimum of a year were included in the BP treated group.

In total, 22 female samples were attained for this study (a subset of samples in Chapter 3): 8 from BP treated fracture patients, 8 from untreated fracture patients and 6 from ageing non-fracture cadavers. The samples were adjacent samples of those outlined in Chapter 3 and scanned after the synchrotron imaging and mechanical testing had been

completed. Due to limited time at the synchrotron facility, only 22 samples of the 33 in Chapter 3 were scanned.

There was no significant difference in age present between the groups. The breakdown of the demographics for the groups is presented in Table 5.2.1.

Table 5.2.1 Demographics for the samples

Donor Group	Sex	Age	Age years (Median)	1st Quart	2nd Quart	Treatment Years
NFC	F	73	77	74	80.8	
	F	77				
	F	77				
	F	73				
	F	82				
	F	82				
FC	F	90	80	75.8	82	
	F	82				
	F	81				
	F	75				
	F	74				
	F	76				
	F	82				
	F	79				

BP	F	88	82	81.3	85	8
	F	79				5
	F	82				5
	F	82				5
	F	84				5
	F	61				2
	F	68				1
	F	79				1

5.2.2 Sample Processing

The samples were processed in the same manner as described in Chapter 3, section 3.2.2.

5.2.3 Synchrotron X-Ray Scanning SAXS & WAXS

The embedded rectangular samples were mounted in a sealed sample chamber. These sample chambers were mounted on a 2-axis motorized linear stage on beamline I22 at Diamond Light Source (Oxfordshire, United Kingdom). A synchrotron x-ray beam (wavelength λ = 1Å, beam cross section 200µm x 200µm) was used to measure the SAXS and WAXD patterns. The distance between the sample and detector was 6.852 m and 0.175 m for SAXS and WAXS spectra respectively, which was verified with a

calibration standard. SAXS and WAXS patterns were collected by moving the axis stage in X direction with a step size of 500µm in the horizontal direction.

5.2.4 Measuring length & width of mineral crystals

I(q) scattering curves were obtained by azimuthally integrating the patterns. Mineral crystal lengths and widths were derived from the WAXS curves by evaluating the c-axis (002) reflection and the ab-plane (310) reflection respectively as seen in Figure 5.2.1 (Acerbo et al., 2014; Lange et al., 2011).

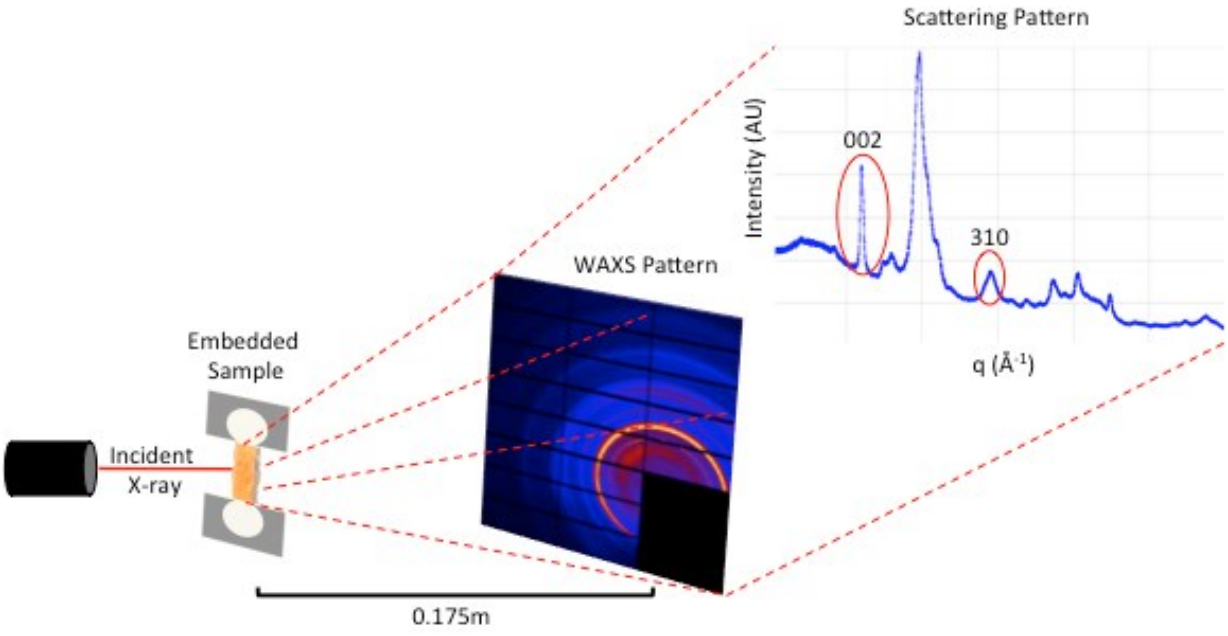

Figure 5.2.1 Schematic representation of the WAXS setup. The azimuthally integrated I(q) scattering curve is also shown here.

From the reflections, the peaks were fitted with Gaussian curves to give the total integrated area, full-width at half maximum (FWHM), and the location of the peak maxima. The crystal lengths were determined along the c-axis from the FWHM of the (002) reflection at $\Delta q \sim 1.70 - 1.82 nm^{-1}$. The crystal widths were determined at the ab-plane from the FWHM of the (310) reflection (perpendicular to the (002)) at $\Delta q \sim 2.56 - 2.77 nm^{-1}$. The crystal dimensions were calculated by plugging the FWHM values into the Scherrer's equation:

$$D = \frac{K\lambda}{\beta_{1/2}\cos(\theta)} \qquad \text{Equation 5.1}$$

where D is the average crystal dimension corresponding to the reflection, K is a constant equaling 0.9, which describes the crystal shape, λ is the x-ray wavelength, $\beta_{1/2}$ is the FWHM, and θ is the scattering angle.

5.2.5 Measuring thickness of mineral crystals

To determine the crystal thickness, the SAXS curves were evaluated by using iterative fitting of the scattering curves *I(q)* (Bunger et al., 2010).

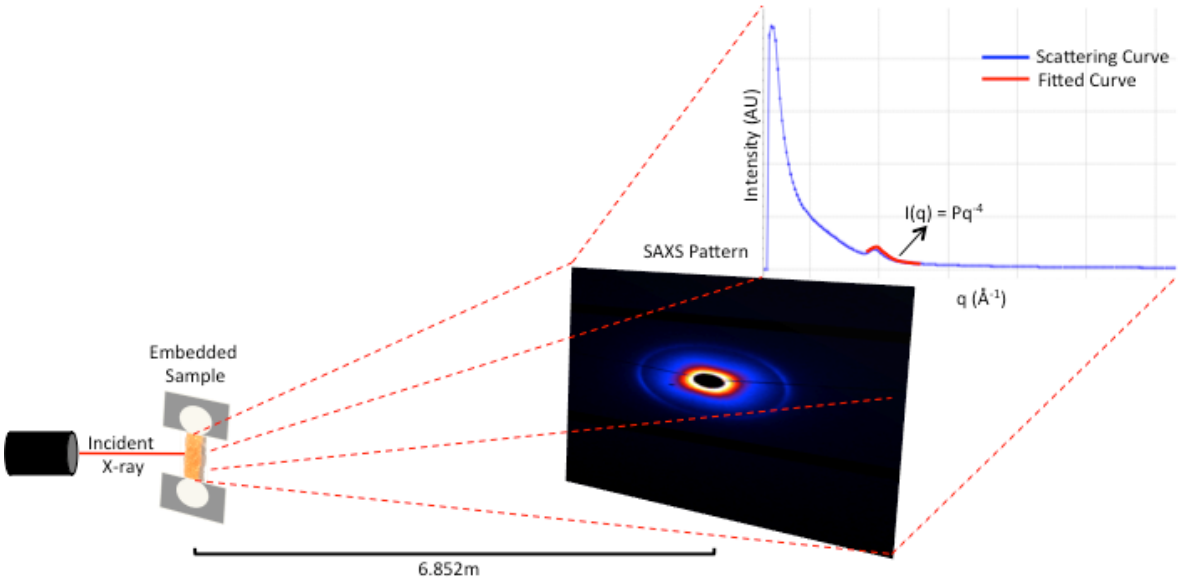

Figure 5.2.2 Schematic representation of the SAXS setup. All data follow the Porod law for high q values.

The thickness parameter is derived based on the two-phase assumption as shown in previous work also determining crystallite thickness (Fratzl et al., 1996; Rinnerthaler et al., 1999; Hauge et al., 2006). The intensity function *I(q)* follows Porod law, for large values of q (Glatter & Katky, 1982; Gauiner & Fournet, 1955):

$$I(q) = Pq^{-4} \qquad \text{Equation 5.2}$$

where the Porod constant P was determined.

To determine the average thickness, a parameter, T, is defined as:

$$T = \frac{4}{\pi P}\int_0^\infty q^2 I(q)\, dq \qquad \text{Equation 5.3}$$

T measures the ratio of crystal volume to crystal surface, with no assumption about the shape:

$$T = \frac{4v(1/v)}{\sigma} \qquad \text{Equation 5.4}$$

where v is the total volume and σ is the total surface area. Thus, if crystals are assumed to be thin platelets, then T is just the average thickness.

5.2.6 Statistical Analysis

As the data was not normally distributed as assessed by Shapiro-Wilk test ($p<0.05$), non-parametric Kruskal-Wallis tests were conducted to determine if the lengths, widths and thickness were different between the groups. Subsequently pairwise post hoc analyses (Mann-Whitney test) were also conducted to determine if there were any statistically differences in median for different pair of group combinations.

5.3 Results

In this section, 3 parameters were analysed and compared across the 3 groups, namely the lengths, the widths and the thicknesses of the mineral crystals. These parameters were also correlated with duration of therapy to assess the effects of long term BP treatment.

5.3.1 Mineral crystal length, width & thickness

The mineral crystal lengths, widths and thickness of the three groups are presented in Figure 5.3.1. The lengths and thickness of the mineral crystals between the groups were not significantly different ($p>0.05$).

The median widths of the mineral crystals in the FC and BP groups were significantly larger than those of NFC ($p<0.05$ & $p<0.01$ respectively), but there were no statistical difference between the widths in the fracture groups.

In summary, the data shows that the fracture groups have significantly wider mineral crystals than the NFC group.

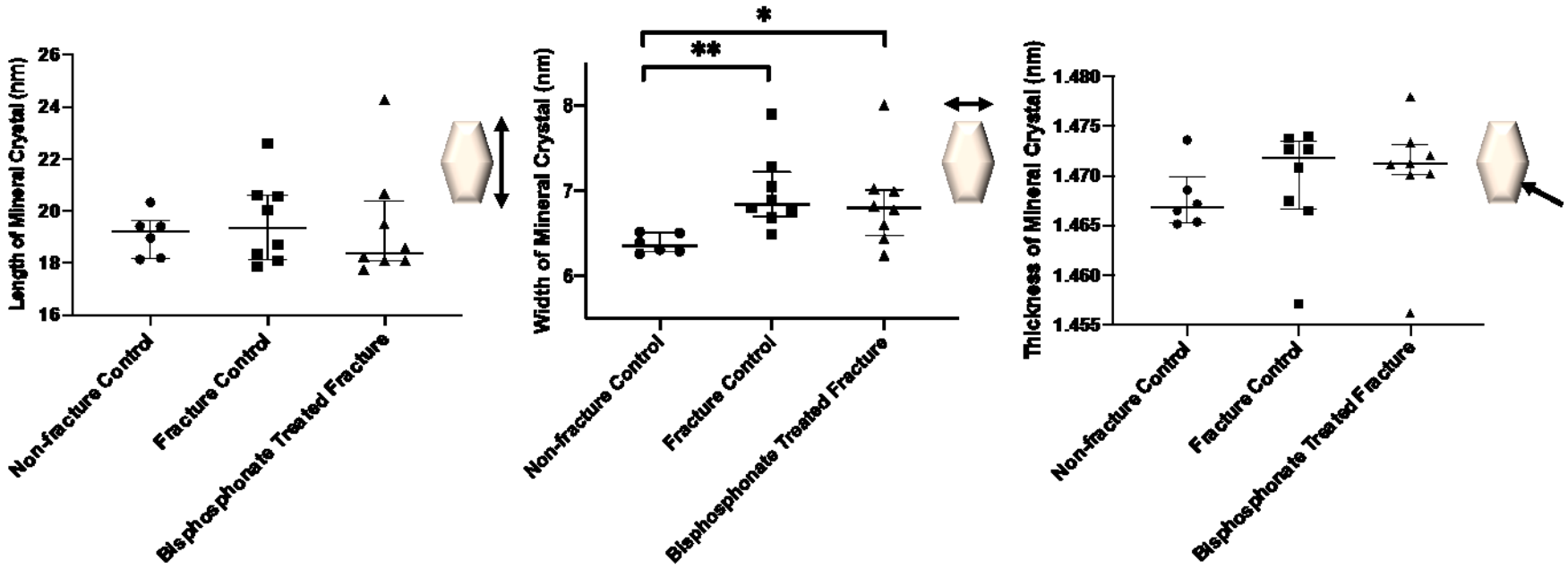

Figure 5.3.1 Comparing mineral crystal lengths among the groups, there was no significant difference between the groups. Comparing mineral crystal widths among the groups, the fracture groups exhibited with significantly wider crystals than NFC. Comparing mineral crystal thicknesses across the three groups, there were no statistically significant differences in thicknesses between the groups. Kruskal Wallis and post hoc Mann Whitney U analysis were used to find if the results of any combination of two groups were significantly different. The asterisks indicate significant pairwise differences: *p<0.05, **p<0.01.

5.3.2 Effects of BP treatment duration

Linear correlations were plotted for the mineral crystal lengths, widths and thicknesses against BP treatment durations. There were no apparent correlations of mineral crystal length, width and thickness with increasing BP treatment duration (Figure 5.4.2).

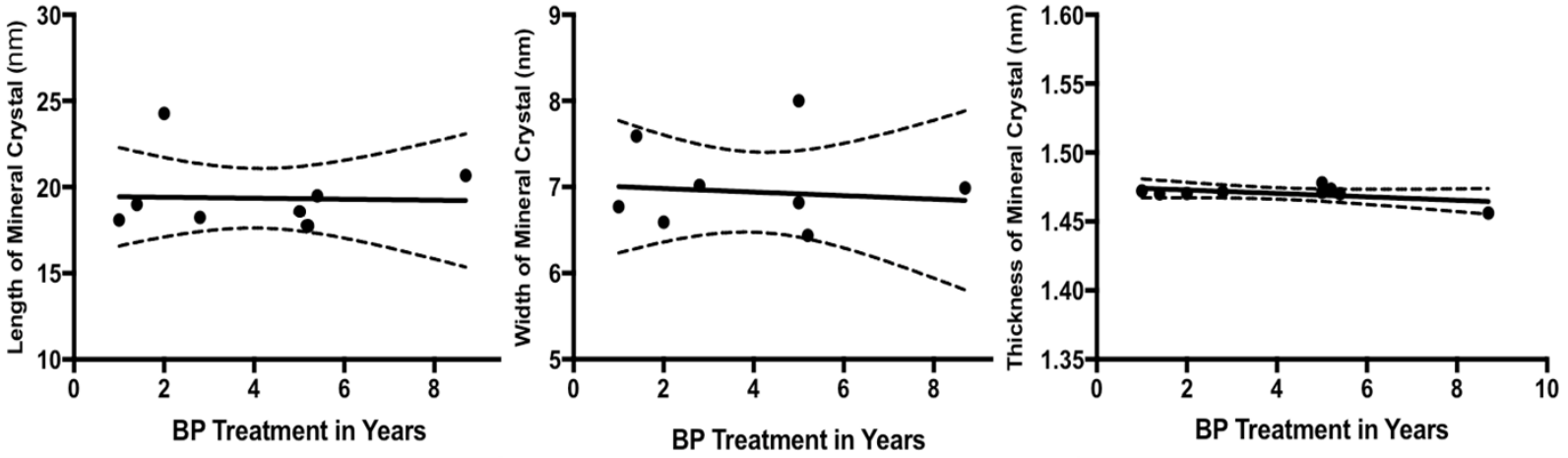

Figure 5.3.2 Mineral crystal length did not increase with BP treatment duration (r^2=0.001). There was no apparent correlation between mineral crystal width and BP treatment duration (r^2=0.008). Mineral crystal thickness did not vary with increasing BP treatment duration. The r^2 value is 0.274 and the dashed lines represent the 95% confidence intervals.

5.4 Discussion

This study applied synchrotron x-ray scattering to image and measure the mineral dimensions across ageing non-fractured, non-treated fracture and BP treated fractured bone. Trabecular bone from the BP treated fracture and non-treated fracture groups presented with crystals of similar size. Both fracture groups tended to exhibit with significantly wider mineral crystals than NFC, but the lengths and thicknesses were not significantly different (Figure 5.3.1).

This is the first study to look at the associations of BP on multiple mineral crystal dimensions, in particular looking at long-term duration. The mineral crystal dimensions did not vary significantly with BP treatment duration (0-9 years).

5.4.1 Mineral crystal dimensions

In this study the median lengths were 19.2nm for NFC group, 19.4nm for the FC group and 18.4nm for BP group, the median widths are 6.35nm for the NFC group, 6.84nm for the FC group and 6.80nm for the BP group, while the median thicknesses are 1.47nm for NFC, FC and BP groups. The mineral crystal dimensions were compared with existing literature measured using the various techniques and the lengths fall within the typical length of 15-150 nm, but fell short in width (typically from 10 to 80 nm), and in thickness (typically from 2 to 5 nm) (Robinson, 1952; Weiner & Price, 1986; Moradian-Oldak et al., 1991).

The results presented in this study were smaller than the dimensions of the acicular crystals, the smallest structural entity in the mineral hierarchy, presented by Reznikov *et al* (Reznikov et al., 2018). Reznikov *et al* used scanning transmission electron microscopy (STEM) to image and measure the individual mineral crystals, which has become the most reliable technique. However, only 2 samples were used in the study and were about 50 years of age, younger than the average age (80 years) of the samples in this research. Mineral crystal dimensions are thought to reduce with age which could explain why the crystals in this study are smaller (Burr, 2002).

Another possible reason for the differences in dimensions is that the synchrotron technique is limited to measuring the average size of the crystals in the scanned region and makes assumptions about the shape and positions of the crystals. As such, future studies should combine the synchrotron method with STEM, to get more accurate measurements of mineral crystals.

5.4.2 Why do fracture groups have significantly wider crystals

The results of the study showed that fracture groups had significantly wider mineral crystals than NFC. This supports our hypothesis that fracture patients will exhibit with larger mineral crystals than non-fracture patients. A study by Jowsey showed that with ageing, unremodelled areas of bone have increased local mineralisation, thus despite increased bone turnover, mean tissue age and levels of mineralisation in the localised areas could increase significantly (Jowsey, 1964). In compact bone, local areas of

unremodelled bone, mineralisation increased by up to 20% above normal estimates, even though there was increased remodelling and porosity in the rest of the bone (Jowsey, 1964). This finding could translate to patients with osteoporosis, who have increased bone remodelling. Burr *et al.* also showed that increased remodelling due to osteoporosis results in more mineralisation, and thus larger crystals, in areas that have not been resorbed (Burr, 2002).

In newly resorbed bone, smaller crystals will nucleate and begin to fill in the space, while crystal in unremodelled areas will continue to grow. As such compared to ageing controls, bone with increased remodelling is likely to exhibit with a greater variation in mineral crystal sizes. However in this study it was not possible to observe the variation using the data presented in as only 5 step-wise scans were made along the lengths of the samples. This gave us the average mineral crystal sizes in the scanned regions but not of the entire sample, thus lacking the data for studying variation.

Even though the mineral crystals in both fracture groups were larger NFC, the significant difference was only seen in the widths. It is possible that the lack of significant difference in length and thickness is due to the restriction of the growth of mineral crystals by the architecture of the collagen fibres, in which they are embedded. The ordered packing of the fibrils form channels, that are $\sim 1.5\, nm$ in breadth and follow a staggered arrangement with gap zones of $\sim 40\, nm$. The mineral crystals nucleate and grow within these gap regions. However, the crystals growth in width is unrestricted, overlapping

neighbouring crystals, beyond the gap regions of an individual collagen as depicted in Figure 5.1.2.

5.4.3 Does mineral crystal size affect collagen mineral interactions?

In Chapter 3, the fracture groups exhibited with lower strains than NFC. This could be attributed to stronger interface bonding with the collagen fibrils with wider mineral crystals in fracture patients as theorised by Stock *et al* (Stock, 2015). In line with this theory, wider mineral crystals could result in a larger surface area for interfacial bonding with the collagen fibrils. This increased bonding could result in less elasticity and sliding between the mineral and fibrils and could result in lower strain as seen in the fracture groups.

5.4.4 Is there an association between BP treatment duration and crystal size?

Since BP therapy increases mineral density, it was expected for the mineral crystals to be larger in BP treated fracture patients. However, there was no significance difference in any of the dimensions between FC and the BP treated group. It could be that BP therapy has does not affect mineral crystal size. Similarly, animal studies have also shown that BP either does not have effect on mineral crystal size or increase in only width (Rohanizadeh et al., 2000; Burr et al., 2003; Grynpas et al., 1992). With the use of scanning electron microscopy, TEM and electron microprobe analysis, Rohanizadeh *et al.* BP treated mice displayed slightly wider bone apatite crystals than untreated controls.

Burr *et al.* used infrared microspectroscopy, quantitative backscattered electron microscopy and x-ray diffraction to quantify the size of mineral crystals in dogs treated with BP for 1 year (Burr et al., 2003). They found that the various methods concluded that BP did not change the nature of the mineral crystal and observed no differences in mineral crystal dimensions compared to controls. Similarly, x-ray diffraction revealed that mineral crystal size changes were not observed in dogs treated with BP at various doses for a term of 1 year (Grynpas et al., 1992).

The lack of correlation between mineral crystal dimensions and BP treatment duration suggests that the increase in BMD brought about by BP therapy could instead be due to increasing number of mineral crystals in the collagen mineral matrix. However, there is currently no apparent literature on the effects of osteoporosis or treatment on mineral crystal number. In addition to an increase in collagen crosslinks, more mineral crystals could result in more areas of bonding with the collagen matrix, making the matrix less deformable under load. This would then result in lower nano strains, as seen in BP patients presented in Chapter 3. The samples used in this study were from the same femoral heads used in a study performed by Ma *et al.* that concluded that the BP treated fracture patients had an accumulation of microcracks, associated with lower compressive strengths (Ma et al., 2017). As such, the reduction in the collagen-mineral matrix's deformability increases the susceptibility to accumulation of microcracking when under load, which could grow and connect and eventually lead to a fracture.

Since the results of the study are limited to an observational, cross-sectional study, only possible associations can be made about BP therapy. However, the data can be interpreted in relation to severity of the disease. Irrespective of treatment, patients who have suffered fragility fractures have larger mineral crystals, which possibly increases the bonding with collagen fibrils and thus making the matrix stiffer and potentially impairing the mechanical properties of whole bone.

5.5 Conclusions

This study used Synchrotron x-ray scattering to image and measure the mineral dimensions across ageing controls, non-treated fracture and BP treated bone. The results of this study suggest that bone fragility is associated with larger mineral crystals, particularly in the width. Larger mineral crystals are likely to reduce the deformability of the nanostructure matrix through more interfacial bonding and potentially cause the increase in stiffness observed in Chapter 3, ultimately increasing the ease of crack initiation and growth. This would result in a greater susceptibility to fracture during a trip or fall. In addition, since mineral density increases with BP treatment, the mineral crystal dimensions were expected to be affected. However, larger mineral crystals were not observed in the BP treated group and as such the mechanism by which BP treatment increases mineral density and content could instead be due to an increase in the number of mineral crystals. Currently no apparent literature on the effect of BP therapy on the number of mineral crystals and thus further studies should use a combination of synchrotron imaging and TEM to compare the number of mineral crystals in BP treated bone and controls.

Chapter 6. Nanoindentation

6.1 Introduction

The gold standard for predicting risk of fragility fractures, a consequence of bone fragility, is the fracture risk assessment tool, which is highly dependent on the data retrieved from Dual-energy x-ray absorptiometry (DXA) scans, a measurement for a person's bone mineral density (BMD) (Harding, 2015; Kanis, 2015; Unnanuntana et al., 2010). BMD measurements are a product of bone mass, failing to account for bone chemistry and architecture. This could explain why a third of women and two thirds of men who suffer fractures had not been classified as osteoporotic based on BMD. As such, patients with high fragility risks often go underdiagnosed, as more than half of individuals who have suffered a fracture do not meet the clinical diagnosis of osteoporosis as determined by BMD measurements (Sanders et al., 2006). In the previous chapters, it has become more apparent that the hierarchical structure is important to bone strength and thus the gap in diagnosis presents an opportunity to improve diagnostics, to consider the additional parameters affecting bone strength.

In particular, the nanostructure has been discussed in Chapter 3 to possibly play an important role in whole bone mechanics via a cascade effect. It could thus be of importance to measure the material directly at the nanoscale level. A technique known as nanoindentation is able to collect such material level data. In the recent years, nanoindentation, which allows for precise measurements of local mechanical properties of individual trabeculae, has been developed for *in-situ* measurements of bone strength. In particular, the Osteoprobe has been developed as a handheld microindentation

instrument to test bone health *in vivo* (Active Life Scientific, Inc. - Research, 2019). It uses a mechanical micro-probe that allows for the simultaneous measurement of elastic modulus and hardness, with a spatial resolution of 1mm. The technique has been said to be precise and accurate and appropriate for measuring material properties of bone (Turner et al., 1999). As such, micro and nanoindentation have been extensively used to determine the micro and nano mechanical properties of bone, which result from the chemical quality of bone (Arnold et al., 2017; Hengsberger et al., 2002; Rho et al., 2002).

A systematic review by Arnold *et al*. on microindentation assessed whether the technique could accurately measure cortical stiffness. However, the review stated that only two studies had been validated against traditional mechanical testing methods, and since the results were contrasting, it was unclear if microindentation was a feasible technique (Arnold et al., 2017). For nanoindentation techniques, Hengsberger *et al.* found that nanoindentation could discriminate the elastic properties of thick and thin human bone lamellae (Hengsberger et al., 2002). Rho *et al.* also found that elastic modulus measured using nanoindenation slightly decreased with age (Rho et al., 2002). Hardness measured by indentation has also been showed to decrease with age in trabecular bone, due to the decreased trabecular density and mineral content (Zioupos et al., 2008).

However it is not currently known what the impact is, if there is any, of the hardness or elastic modulus measured by nanoindentation on fracture toughness of bone. Studies have looked at relating properties measured by nanoindentation with microstructural properties as well as with whole bone fracture toughness (Hu et al., 2015; Wu et al., 2013; Silva et

al., 2004). However, little correlation has been found in these studies. The study by Hu *et al.* further compared the micro and nano levels of bone of ovariectomised rats to show that trabecular nanomechanical properties, nanoindentation hardness, elastic modulus, and plastic deformation were not statistically different, even though at the microstructural level, there were significant differences in microarchitectural parameters (Hu et al., 2015). However the samples were dehydrated in ethanol before nanoindentation testing and this process could have affected the material properties and thus the correlation to the microarchitecture could have been underestimated. Wu *et al.* also found that bone of osteoporotic rat models that had been treated with BP did not display any differences in mechanical properties, as measured using nanoindentation, with non-treated models even though the treated models displayed with improved microarchitecture and trabecular geometry brought about by BP therapy (Wu et al., 2013). It is possible that BP treatment targets the microstructure by preserving the trabecular geometry but not the material level properties.

Moreover, the modulus determined by nanoindentation also poorly correlated with modulus from whole bone bending tests in osteoporotic mice models (Silva et al., 2004). However, the study used the Oliver-Pharr method to calculate the nanomechanical properties from indentation. The Oliver-Pharr method assumes that the sample is a perfect isotropic material (Oliver & Pharr, 1992). However, bone is a complex anisotropic solid and is heterogeneous at the material level. The mechanical properties of bone are dependent on the location's cross-section and axis (Sansalone et al., 2010). Nanoindentation also does not take into account porosity, in contrast to whole bone

bending tests, measuring the hierarchical structure, which are strongly influenced by porosity (Currey, 1988).

Since nanoindentation is a local intrinsic measure of the trabecular at a small length scale, it is possible that nanoindentation data correlates instead with nano level data, such as fibril and mineral strains. Thus the aim of this research is to assess the feasibility of measuring bone health using a nanoindenter. In order to achieve this aim, two objectives have been highlighted:

1. Determine whether nanoindentation can distinguish ageing controls from fracture patients by comparing nanoindentation mechanical parameters between non-fracture control (NFC), fracture control (FC) and BP treated fracture groups (BP)
2. Establish whether nanoindentation mechanical parameters capture nano strains by correlating nanoindenter data the nano level strain data collected in Chapter 3.

It is hypothesised that BP treated fracture bone would display weaker mechanical properties than FC and NFC bone measured with the indenter, and the nanoindentation parameters will correlate with fibril and mineral strains.

6.2 Material and Methods

6.2.1 Sample Groups

Similar to previous chapters, trabecular bone samples were collected from the femoral heads of 3 individual groups, the NFC, the FC and the BP treated group. Fracture groups' samples were obtained from patients who had suffered femoral neck, while NFC samples were acquired from cadavers who had no histories of fractures. Ethical approval was granted by the Imperial College Tissue Bank (R13004) for the collection of the femoral heads with additional patient consent to use their tissue for the study.

In total, 15 female samples used for this study: 6 from BP treated fracture patients, 5 from untreated fracture patients and 4 from ageing non-fracture cadavers. They were adjacent samples to those in Chapter 3 and a subset of those in Chapter 3 as samples were lost during the preparation of the samples. There was no significant difference in age present between the groups. The breakdown of the demographics for the groups is presented in Table 6.2.1.

Table 6.2.1 Demographics for samples

Donor Group	Sex	Age	Age years (Median)	1st Quart	2nd Quart	Treatment Years
NFC	F	73	77	76	78.3	
	F	77				
	F	77				
	F	82				
FC	F	90	82	76	82	
	F	82				
	F	75				
	F	76				
	F	82				
BP	F	88	79	70.8	81.2	8
	F	79				5
	F	82				5
	F	61				2
	F	68				1
	F	79				1

6.2.2 Sample Processing

Halved core shaped samples were cut from the caps of the femoral heads that were removed in Chapter 2 using an EXAKT saw (Figure 6.2.1). A diamond saw was used to first make a cut down the centre of the cap before being drilled by a diamond drill bit (DK Holdings, UK) (Figure 6.2.2). This produced 2 halved core-like samples drilled from the centre of the femoral cap as seen in Figure 6.2.3.

Figure 6.2.1 Cap of a femoral head removed using a EXAKT saw.

Figure 6.2.2 Diamond saw and diamond drill used to cut and drill into the cap to produce the desired samples

Figure 6.2.3 The left over cap with the hole drilled in the centre to produce final halved core-like samples.

In order to remove fat and marrow from the samples, the half cores were pressure washed with hot water and spun in plastic tubes for 36 hours in 1:1 chloroform/methanol solution and then for 12 hours in 99% ethanol. The sections were then dried at room temperature and embedded in epoxy resin (Metprep Kleer- Set Type SSS). The embedded samples were left to cure for 24 hours before being grounded and polished to a flat surface using an automatic Struers RotoPol-15 with 203 mm silicon carbide abrasive disks grinding paper of decreasing grit size (400, 800, 1200, 2500) on a MasterTex cloth with Alumina 3B 6OZ.

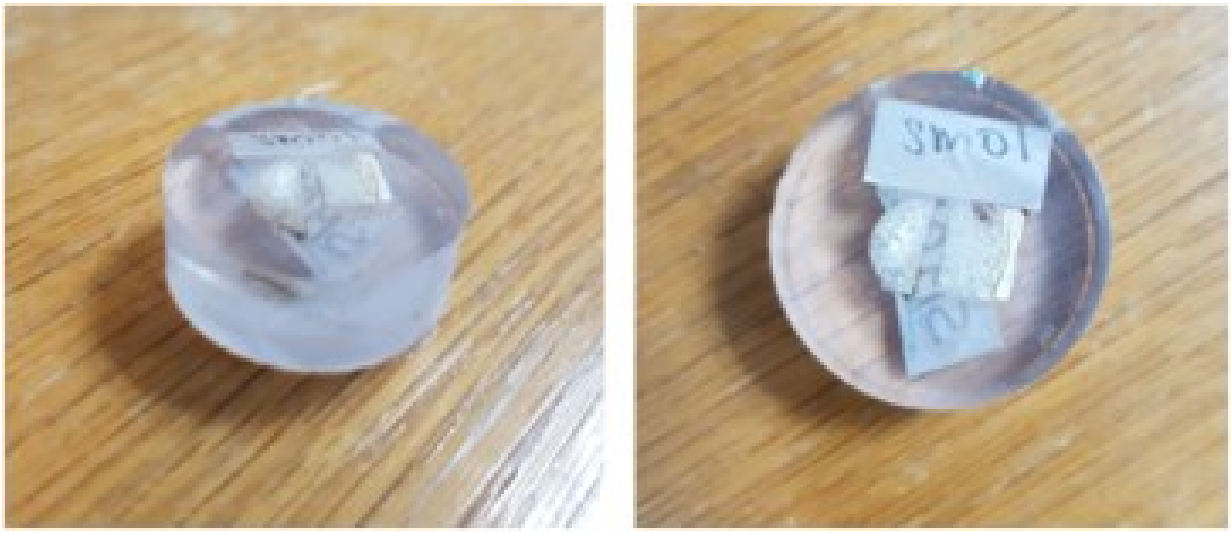

Figure 6.2.4 Embedded samples in resin that have been polished to produce the flat, smooth surfaces for indentation.

6.2.3 Methodology

Nanoindentations were conducted using a CSM-Nano Hardness tester (system v.3.75, CSM, 2034 Peseux, Switzerland) (Figure 6.2.5). The load was controlled to 10mN with a linear loading and unloading rates of 30s with a 30s pause. For each specimen 10 indentations were carried out in 4 sites, 3 in the transverse region and 1 in the vertical region (Figure 6.2.7). A single trabeculae in each of the sites was identified and selected under an optical microscope to achieve precise location of indentations (Figure 6.2.6).

The hardness (HIT in MPa), indentation modulus (EIT in GPa, assuming a Poisson's ratio value of $\nu = 0.3$), indentation creep (CIT in %) and elastic part of indentation work (ηIT in %) were measured by advanced protocol using the method suggested by Oliver and Pharr (Oliver & Pharr, 1992).

The hardness (H) was measured by dividing the maximum load (P_{max}) by the indentation area (A_r).

$$H = \frac{P_{max}}{A_r} \qquad \text{Equation 6.1}$$

The indentation modulus, E_s, was measured by looking at the slope of the load-displacement curve (Figure 6.2.8). The slope is indicative of the stiffness of contact, S, and the reduced modulus, E_r, is related to S as expressed in equations 6.2-6.3.

$$E_r = \frac{1}{\beta}\frac{\sqrt{\pi}}{2}\frac{S}{\sqrt{A_p h_c}} \qquad \text{Equation 6.2}$$

where $A_p h_c$ is the projected area of indentation of contact depth h_c, and $A_p h_c$ is defined as:

$$A_p h_c = C_0 h_c^2 + C_1 h_c^1 + C_2 h_c^{1/2} + \cdots + C_8 h_c^{1/128} \qquad \text{Equation 6.3}$$

where C_0 for a Berovich tip is 24.5.

The indentation modulus is then related to the reduced modulus by equation 6.4:

$$\frac{1}{E_r} = \frac{(1-v_i^2)}{E_i} + \frac{(1-v_s^2)}{E_s} \qquad \text{Equation 6.4}$$

i is related to the property of the indenter material and v is Poisson's ratio. For a diamond indenter, E_i is 11406 Pa, v_i is 0.07 and v_s is 0.3.

Indentation creep is calculated as the proportional increase in depth while load is held at P_{max}, and finally the elastic part of indentation work is calculated from the area under the graph where the force is decreasing.

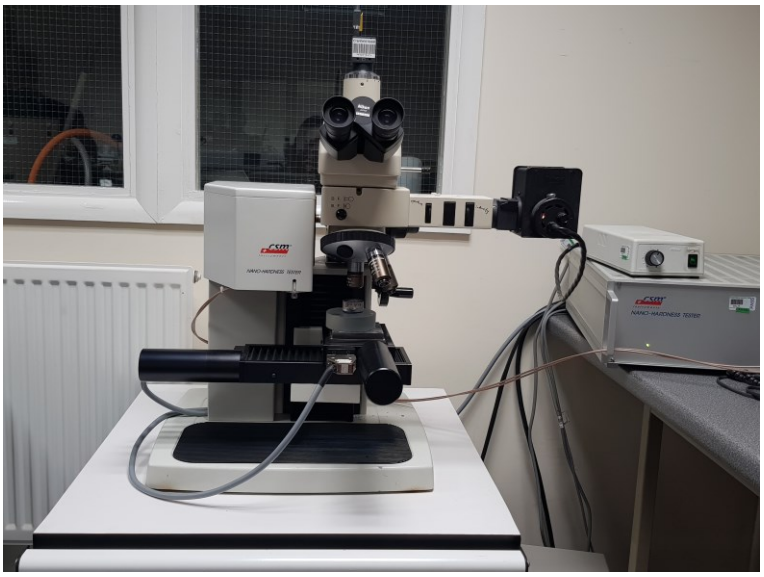

Figure 6.2.5 Image of the CSM-Nano Hardness tester complete with a microscope and diamond indenter to image and indent samples.

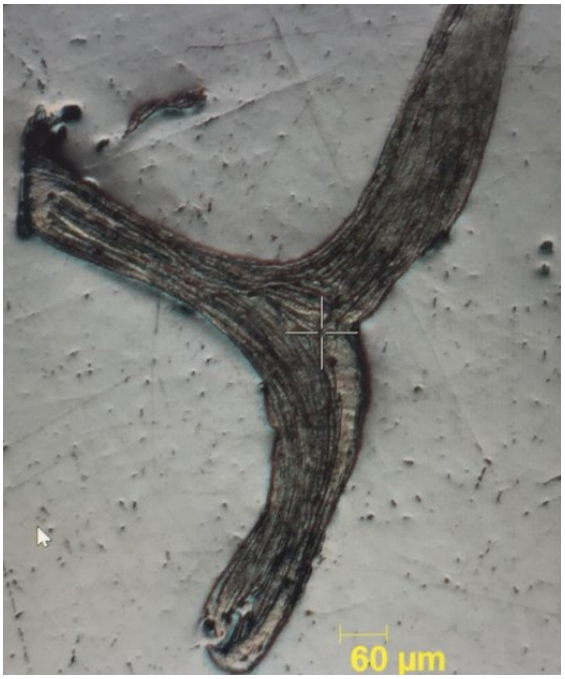

Figure 6.2.6 Image of a single trabeculae imaged using 10x objective in the nanoindenter. Using the image, indentations can be made at specific positions on the sample.

Figure 6.2.7 Magnified image of the 10 triangular indentations (circled) made on one of the sites of the trabecular samples.

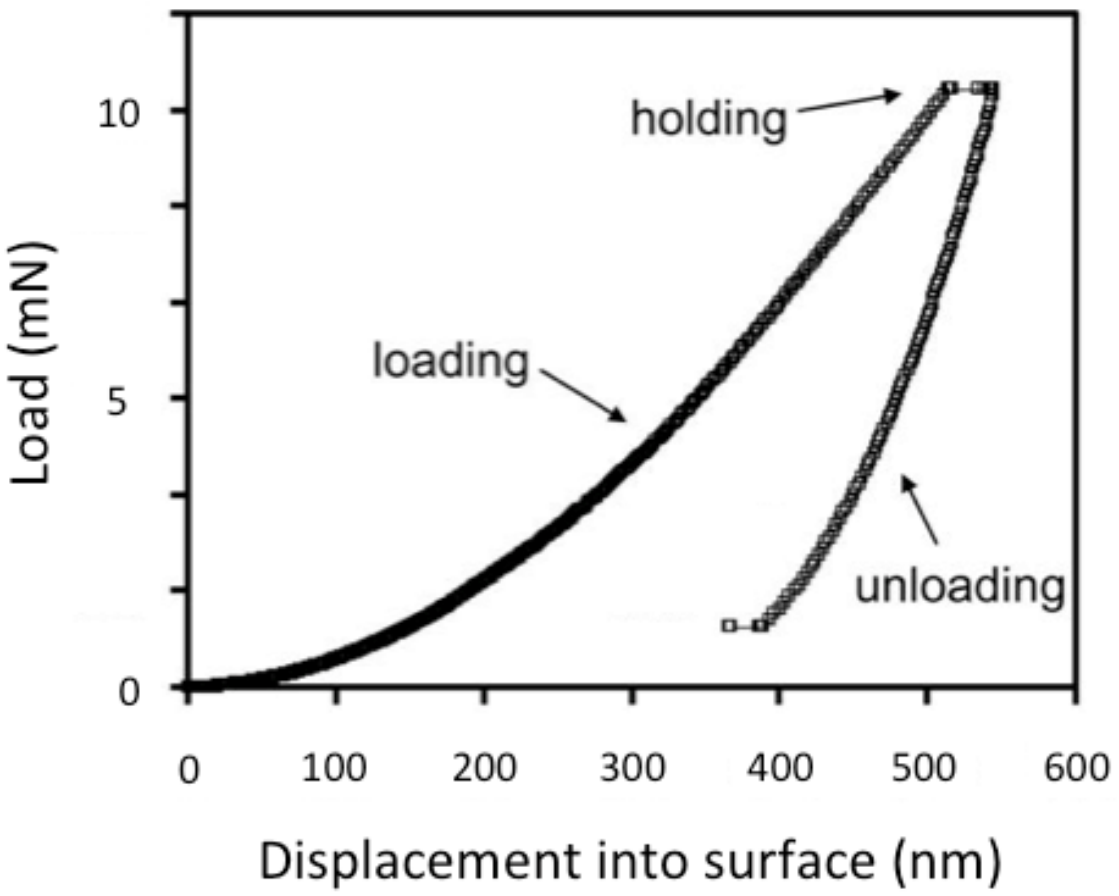

Figure 6.2.8: Representative nanoindentation load-displacement curve for 600 nm indent with controlled load of 10mN. Berkovich diamond tip loaded into the surface at a rate of 30s, with maximum load held for 30s. Hardness and elastic modulus were calculated from the unloading portion of the curve. Adapted from (Tjhia et al., 2011; Tjhia et al., 2011).

6.2.4 Statistical Analysis

Non-parametric Kruskal-Wallis tests were conducted to analyse the data between the groups and subsequent post hoc Mann-Whitney tests were conducted to determine if there were any statistical differences in median for different pairs of group combinations. Pearson's correlation was performed to establish the correlation between the nanoindentation parameters with fibril and mineral strains.

6.3 Results

In this section, 4 nanomechanical parameters as determined using nanoindentation were analysed and compared across the 3 groups, namely the hardness, the indentation modulus, the indentation creep and work done in the elastic part of indentation. There were no differences in hardness, indentation modulus, indentation creep and work done in the elastic part of indentation between the 3 groups. Moreover, no significant correlations were found with any of the nanoindentation parameters and nano strains ($p>0.05$).

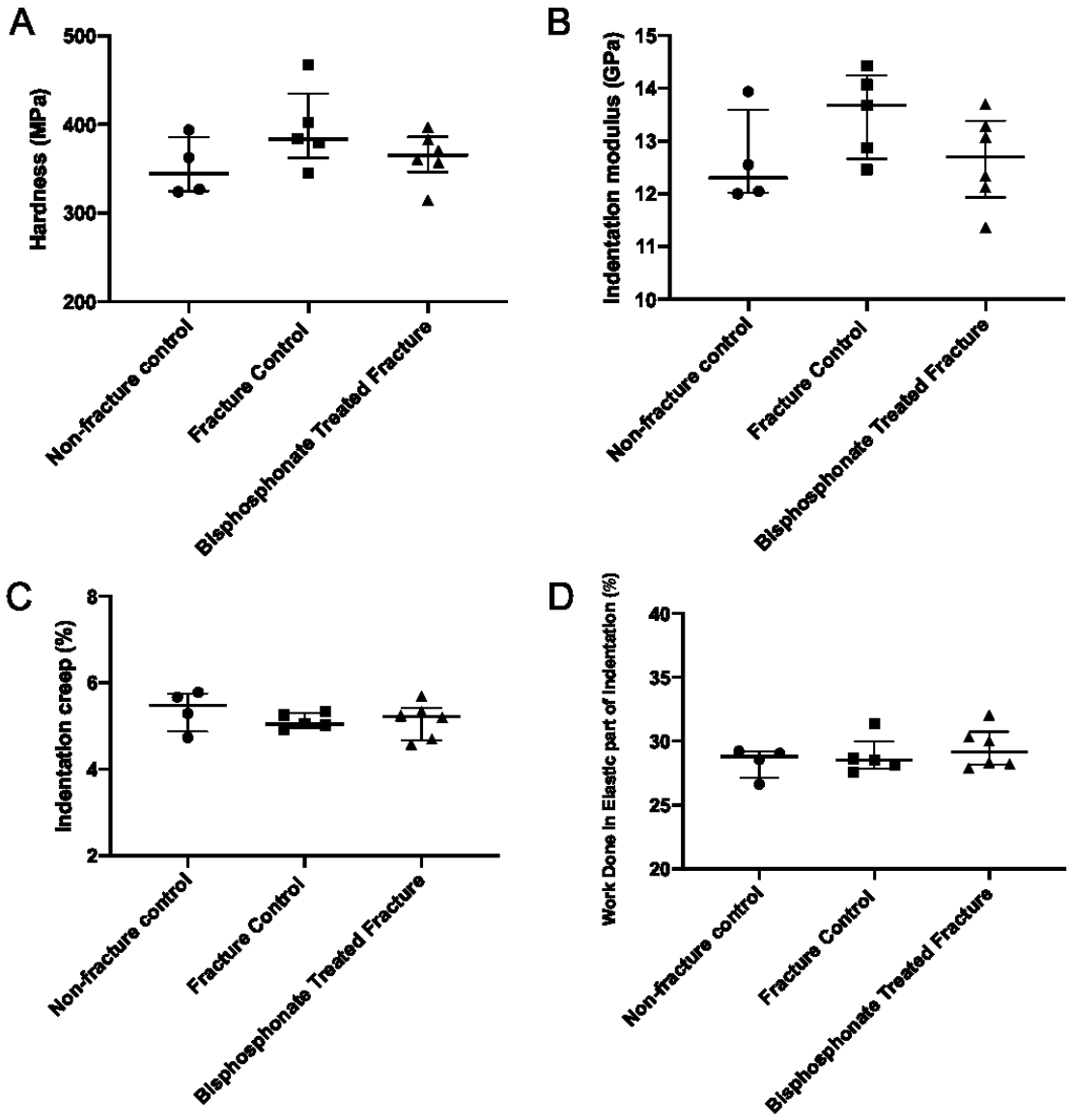

Figure 6.3.1 Comparing hardness, indentation modulus, indentation creep and work done in the elastic part of indentation among the groups. The hardness, indentation modulus, indentation creep and elastic part of indentation were not statistically different between the groups. Kruskal-Wallis test and subsequent post hoc analysis was used to find if the results of any combination of two groups were significantly different.

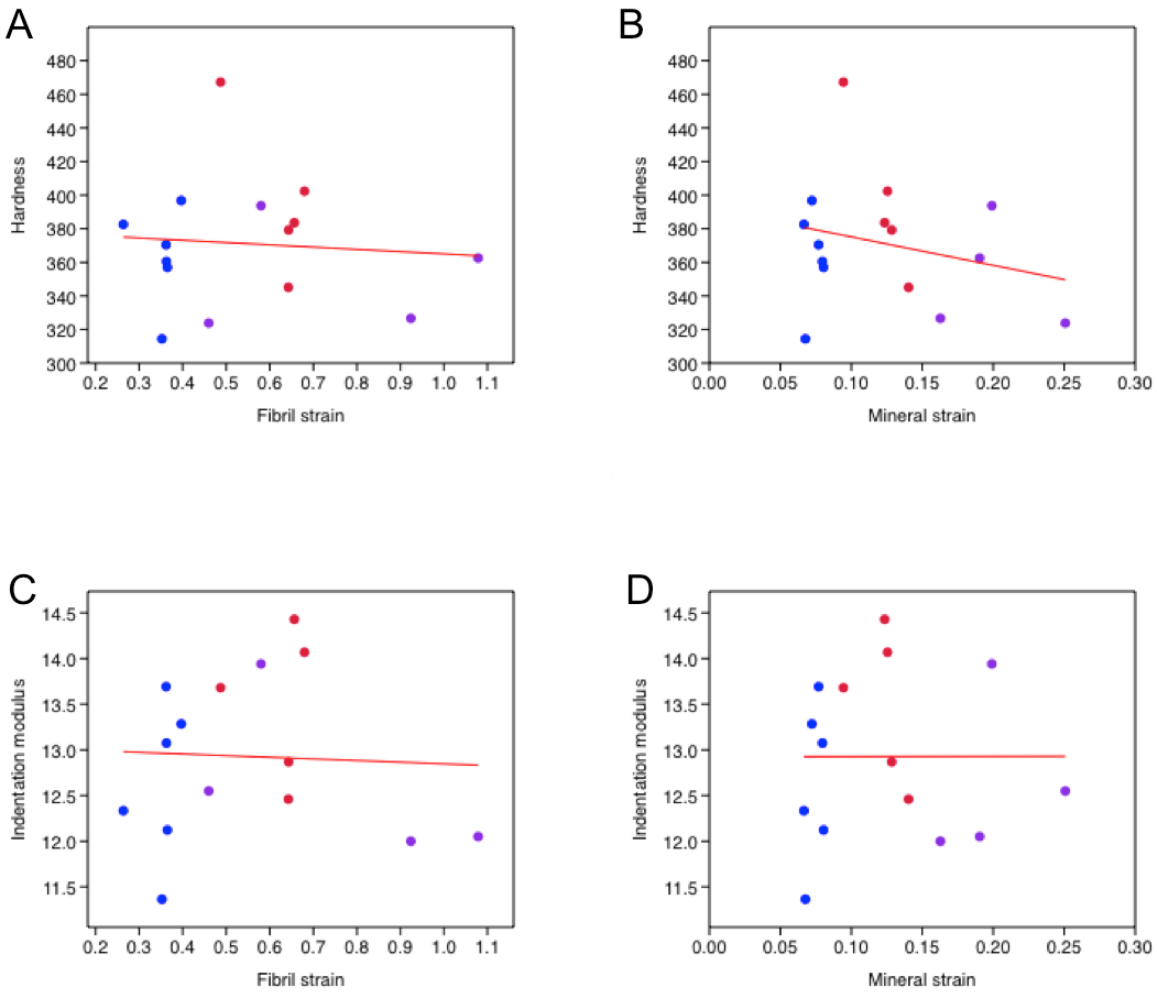

Figure 6.3.2 Hardness (A & B) and indentation modulus (C & D) as functions of fibril and mineral strains respectively for all groups. In all regressions, the slope constants were not significantly different from zero ($p>0.05$), showing no significant correlations between the nanoindentation mechanical parameters and the nano level strains. NFC is tagged in purple, FC in red and BP in blue.

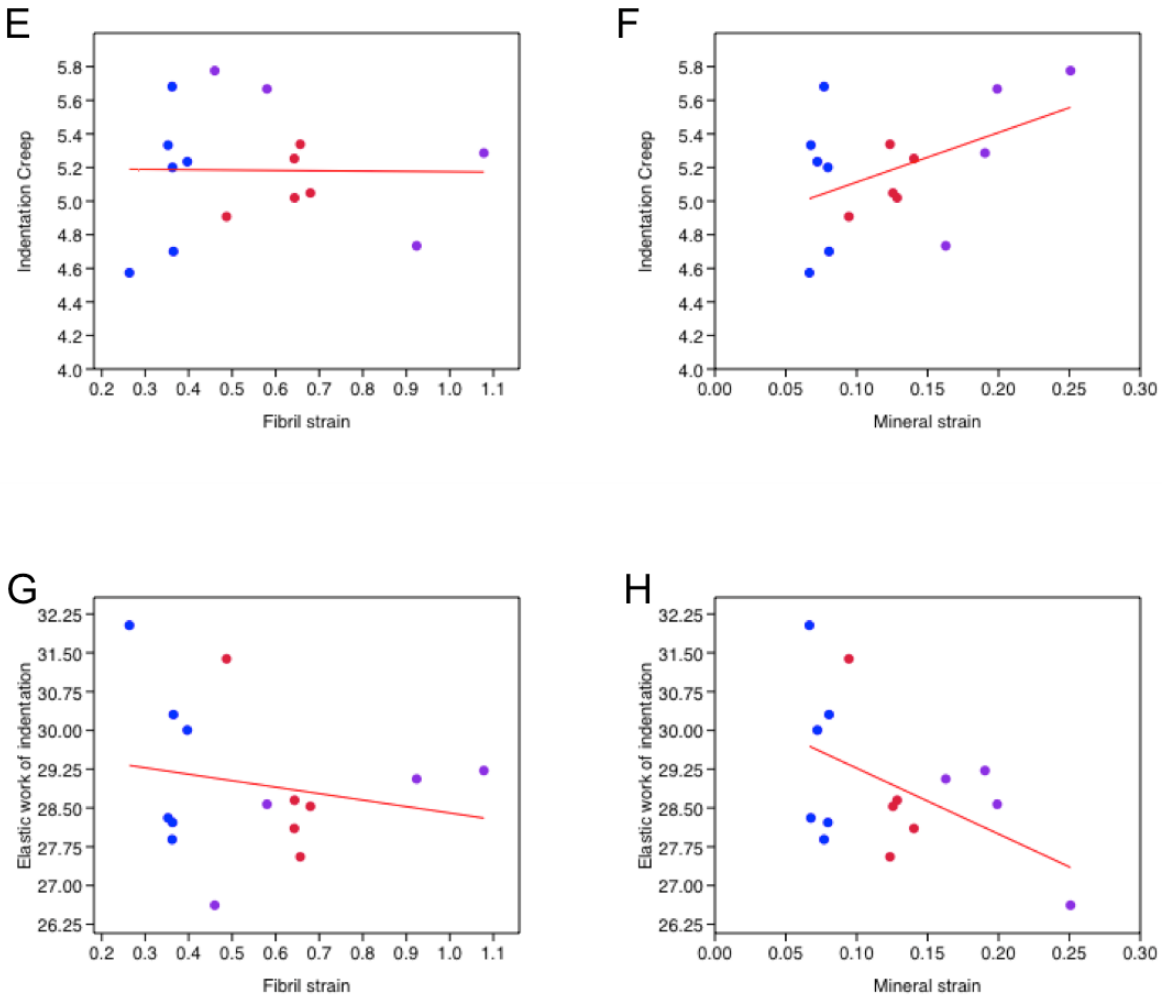

Figure 6.3.3 Indentation creep (E & F) and elastic part of indentation (G & H) as functions of fibril and mineral strains respectively for all groups. In all regressions, the slope constants were not significantly different from zero ($p>0.05$), showing no significant correlations between the nanoindentation mechanical parameters and the nano level strains. NFC is tagged in purple, FC in red and BP in blue

6.4 Discussion

This study used nanoindentation to compare the nanomechanical properties, in particular the hardness, the indentation modulus, the indentation creep and elastic part of indentation, across NFC, FC and BP treated samples. This is the first study to correlate nanoindentation data with nano level strain data collected using synchrotron imaging. The data showed that there were no differences in hardness, indentation modulus, indentation creep and work done in the elastic part of indentation between the groups. Moreover, the indentation parameters did not correlate significantly with fibril and mineral strains.

In the earlier chapters, the importance of the bone's nanostructure has been laid out. The aim of this chapter is to determine if nanoindentation could distinguish between the groups. The results in this study show that there are no differences between non-fractured controls, non-treated fracture and BP treated bone.

However, the data in this study contrasts a longitudinal study by Pienkowski *et al*. Their study found that both Young's modulus and hardness increased with BP treatment (Pienkowski et al., 2019). They collected biopsies of bone samples consecutively from osteoporotic women who were treated with BP for 1-20 years and used nanoindentation to measure the nanomechanics of the samples. However, the biopsies were taken from the iliac crest, which is a non-loading region. Moreover since biopsies cannot be taken exactly from the same place each time, the study cannot be considered a longitudinal one. Another study by Tjhia *et al.* compared BP treated patients with non-treated osteoporotic patients and healthy controls, and reported that BP treated bone had harder trabecular bone compared to the other groups, which was associated with higher mineral density

(Tjhia et al., 2011). However these samples were also taken from the iliac crest and have lower mineral content than the samples in this study, which are taken from the loading region, the femoral head. Moreover, the BP treated samples were not controlled for other bone-related diseases and thus the results could not be directly attributed to BP therapy.

The data from the study also showed no correlation between nanoindenter data and fibril and mineral strains. Studies have additionally shown little correlation to micro level and whole bone properties (Hu et al., 2015; Wu et al., 2013; Silva et al., 2004). The lack of correlation to the different level mechanical and structural properties that have been measured by validated techniques suggests that nanoindentation technique is not reliable for measuring material properties.

Moreover, many other studies have found no differences in the parameters measured using nanoindentation between osteoporotic patients and healthy ageing patients (Guo & Goldstein, 2000; Lane et al., 2003; Polly et al., 2012; Hu et al., 2015; Wang et al., 2008). Guo and Goldstein measured the hardness and elastic modulus of osteoporotic rate models and found no differences with the healthy models (Guo & Goldstein, 2000). Lane *et al.* also made the same conclusion, measuring the nanomechanics in the trabecular tibia of osteoporotic rats (Lane et al., 2003). However bone remodelling in rat models tend to differ from osteoporotic human patients. Polly *et al.* and Wang *et al.* found the same results in human bone by comparing biopsies from fracture patients and normal healthy patients (Polly et al., 2012; Wang et al., 2008). Further these biopsies were taken from non-loading iliac crests and mineral content is lower than in the femoral head.

A limitation of this study is that the nanoindentations were performed on samples that had been dehydrated and embedded, a procedure that could modify the mechanical properties of the bone matrix and affect the correlations with the nanostrains (Rodriguez-Florez et al., 2013). Hardness measured under wet conditions have been shown to be to be 30-40% lower than in dry conditions, while the modulus measured using a nanoindenter has been shown to be about 30% lower in bone that had been indented under wet conditions (Dall'ara et al., 2007; Wolfram et al., 2010). However, since all the specimens in the groups had undergone uniform processing, interspecimen comparisons could still be made, and the results showed that the samples did not display significant differences in the hardness or modulus as measured by nanoindentation.

The relation of the nanostructure and its material property still needs to be understood in relation to fracture toughness. Since nanoindentation does not appear to measure material property at the nanoscale accurately, research on other techniques, needs to be done to allow for such investigations. One such technique could be *in-vivo* Raman spectroscopy, in particular Spatially Offset Raman Spectroscopy (SORS), which has been developed to measure human tissue, including bone, *in vivo* (Matousek et al., 2005). Since nanoindentation does not consider other important aspects of the nanostructure such as collagen crosslinking, Raman might be a better method for capturing the bone's material as it allows for the measurements of crosslinks and mineral crystal dimensions.

6.5 Conclusion

The results from this chapter indicate the ineffectiveness of the use of nanoindentation to measure nano level mechanics. With the lack of correlations to nano, micro and macro level mechanics and structure, even with the development of *in-situ* nanoindentation techniques, it is unlikely to give any information that could predict fracture toughness or meaningful measured of bone health that could be used in clinical practice.

Chapter 7. Conclusion – The Nano Cascade Effect

7.1 Introduction

This thesis developed with the idea that the basic building blocks of bone, namely the collagen-mineral matrix at the nanoscale, are important for whole bone strength. Many authors have suggested that the nanostructures are key determinants of whole bone mechanics (Wang ZX, 2016; Wen et al., 2015; Burstein et al., 1975; Ammann & Rizzoli, 2003). However, there was no clear published evidence of the impact of nanoscale structures on tissue or macroscale mechanics. Moreover there is a lack of research on how disease and treatment affects bone at the nano level and if there are subsequent effects at the macroscale. As such, the overall aim of the research was to investigate how the different levels of bone, in particular the nanostructure, differed in bone that had suffered a fracture and non-fractured bone, as well as the effects of bisphosphonate treatment on bone at these levels.

The results from each chapter have already been discussed and compared with other studies. This chapter is aimed at discussing the outcomes, the potential limitations of the research and impacts the results have on current and future research.

7.2 Effect of nanostructure on macromechanics

The thesis began by investigating the trabecular microstructures of the different groups. The fracture groups had significantly larger trabecular spacing, lower total bone surface density and lower connectivity than the non-fracture control. The chapter then look at how the microstructure related to overall compressive strength. Mechanical testing previously conducted by Jin showed that the bisphosphonate-treated fracture group had lower compressive strengths than the non-fracture control (Jin, 2016). However, multiple regression analysis showed that less than 50% of the variability in microstructure could account for bone strength. This suggests, as many other studies have, that some aspect of bone strength and fragility is accounted for by the bone's material. This lack of predictability of mechanical strength using microarchitecture thus led to study at the nanostructural level.

Chapter 2 on nanostrains brought about a theory of a nano-cascade effect, initially suggested by Gupta *et al.* (Gupta et al., 2006). The study investigated the differences in tissue, collagen and mineral strains in human samples between BP treated and non-treated controls, and the findings suggest that bone fragility is associated with loss of nanostructural integrity and this loss could contribute to the loss of strength and stiffness and therefore resulting in fragility. Perhaps wider mineral crystals provide a larger area for interfacial bonding with the collagen fibrils and preventing the fibrils from sliding and unwinding, resulting in a less deformable matrix overall and thus lower nanostrains, which in turn reduces tissue level (and macroscopic) strength. This can occur either directly by limiting the ability of a whole-bone to bend and absorb energy during a trip or

fall, or indirectly by reducing the energy required to form microcracks in the collagen-mineral matrix. The cracks could accumulate and propagate, reducing the bone's fracture toughness. Hence the loss of strain nanostructure associated with bone fragility might cascade up to the whole bone level and reduce the ability to resist fracture during a trip or fall.

7.3 Reliance on cross-sectional studies

The results must be interpreted with caution since these are observational, cross-sectional data with the potential selection biases that could not have been adjusted for. It is plausible, however, to suggest that the groups display a continuum of 'healthy', since without BMD data it is also possible that the non-fracture controls could have been facing an imminent fracture following a fall, towards disease from non-fractured control, fractured control and BP treated fracture. As such, the results from the thesis can show a correlation with the severity of bone fragillity.

With regards to any interpretations about BP therapy, the assumption that the patients had been compliant with therapy had been made. Letters from general practitioners (see Appendix) had been collected to determine length of prescription of BP treatment but there was no data on compliance with therapy.

7.4 Association of nanostructure with impaired mechanics

Firstly the fracture groups are associated with the loss of collagen and mineral strains. This loss of strain at the nanoscale level comes alongside reduced strength and stiffness at the macroscale level. The lower nanostrain in fracture patients could be due to an association of larger mineral crystals, as reported in the mineral crystal size chapter. Larger mineral crystals could result in stronger interfacial bonding with the collagen fibrils, resulting in less elasticity of the structure and thus lower nanostructural strains seen in the fracture patients compared to non-fracture control (Stock, 2015).

The loss in nanostructure deformation could also be due to more crosslinks between the collagen fibres resulting in the restricted sliding mechanism the collagen-mineral matrix usually undergoes during loading (Garnero, 2012; Bailey et al., 1998). The review by Garnero presented several studies that reported increased crosslinks resulting in reduced fracture toughness of bone. Moreover, patients who had suffered hip fractures exhibited with increased crosslinks. Bailey *et al.* also reviewed the ageing of collagen, describing the mechanism of increasing crosslinks that resulted in the ageing of the collagenous tissue.

Ageing and bone fragility seem to be associated with both larger mineral crystals and more collagen crosslinking. Since they are both part of the same matrix, there could possibly be a relationship between the two components. Although limited, research has reported the influence of crosslinking on the mineralisation of bone (Banes et al., 1983; Huesa et al., 2011). Banes *et al* reported that non-mineralised bone exhibited with a higher concentration of crosslinks than mineralised bone (Banes et al., 1983). This

suggests that either the mineralisation process prevents collagen maturation and the formation of crosslinks, or that increased crosslinking results in decreased intermolecular distances between collagen chains, reducing the space needed for mineral crystal formation. Comparing hypomineralised bone and controlled mice models, Raman microscopy found that the ratio of immature and mature crosslinks were different between the groups, suggesting that the mineralisation of bone alters the maturation process of crosslinks (Huesa et al., 2011). However, the relationship between mineral crystals and collagen crosslinks is still not well known. Research in this area could be of importance to understand the loss of nanostructure integrity in diseased bone.

7.5 A new component of bone fragility

In terms of bone fragility, there is an indication that bone that had suffered fragility fractures are associated with poorer bone quality at the nanoscale level in addition to a loss in bone mass. This suggests that the nanostructure is crucial for fragility as inferior nanomechanical properties lead to weaker bone via easier initiation of microdamage and inability to sustain pre-existing cracks.

It could also be of importance for treatment, as BP therapy seems to affect the nanostructure, and therefore the macroscale level of bone. The lack of significant correlation of strains with long-term BP therapy brought about the question of the appropriate length of therapy. Drug holidays are usually recommended after 3 to 5years of treatment, to reduce the risks of adverse effects like atypical fractures (Shane et al., 2014). However the data in the nanostrain chapter suggests that the loss in nanoscale deformability could occur within 5 years of treatment in some patients (Villa et al., 2016). In addition to the suppressed remodelling, the ease of crack initiation due to the less deformable nanostructure could bring about the mechanism for atypical fractures, possibly as early as 5 years after treatment.

Current guidelines for the length of BP treatment suggest reviewing the need for treatment after 5 years, however it does not take into account nano level bone health (National Institue for Health and Care Excellence (NICE), 2019). As such, a trial should be conducted, using *in-vivo* bone health measurements in order to assess ideal treatment durations, which is likely to be patient specific.

7.6 Impact

The thesis has brought about a new understanding of how bones fracture, the pathophysiology of fragility as well as the potential long-term effects of osteoporosis treatment. The newfound importance of the nanostructure could be used to fill the current gaps in diagnostics and treatment.

7.6.1 Current diagnostics

The current gold standard for measuring the risk of fragility fractures, an effect of bone fragility, is the fracture risk assessment tool (FRAX) (Harding, 2015; Kanis, 2015; Unnanuntana et al., 2010). FRAX is highly dependent on the data retrieved from Dual-energy x-ray absorptiometry (DXA) scans, a measurement for a person's bone mineral density (BMD) a seemingly accurate diagnostic since fragility fractures are associated with the loss of bone mass.

However, there are key problems associated with diagnosing and treating bone fragility, with inaccurate diagnostics, often leading to patients with high fragility risks going underdiagnosed, as well as ineffective treatments, which only reduce fractures by 30-50% (Sanders et al., 2006; Chavassieux et al., 1997; Bone et al., 2004). With an increasingly ageing population, there is a growing need to break the barrier in osteoporotic care to produce accurate and affordable diagnostics and treatment plans that can effectively reduce fracture risks.

7.6.2 Current treatment

The most current form of treatment is bisphosphonates. However, this form of treatment does not completely prevent fractures, only reducing fracture risk in the vertebral by 50% in postmenopausal women aged 55 to 80 (Chanurlat & Delmas, 2006).

Many factors contribute to the ineffectiveness of treatment, including the possibility that half of patients receive therapy only after experiencing a fracture, due to lack of screening for osteoporosis or the inadequacy of diagnostics (Gleason et al., 2012). There is also the lack of compliance with therapy due to factors such as the strict regimen for drug therapy to avoid inefficacy of the drug and damage to the esophagus due to improper intake as well as gastrointestinal side effects (Cooper et al., 2006; Cramer et al., 2007; Lekkerkerker et al., 2007; van den Boogaarda et al., 2006). It is also possible that current treatments are not targeting the correct underlying problems.

1 in 1000 patients undergoing BP therapy is associated with weakness and fatigue fractures due to microcracking (Shane et al., 2014). A recent study by Ma *et al.* showed that BP treatment, although effective at reducing perforations, is associated with the accumulation of microcracks that lead to a decrease in the bone's structural integrity and mechanical strength in both tension and compression (Ma et al., 2017; Jin et al., 2017).

With bone fragility affecting 200 million people worldwide, and the lack of effectiveness in diagnosis and treatments, it is possible that the gaps stem from the current lack of understanding of why bones break (Johnell & Kanis, 2006).

7.7 Pathways to impact

Currently, both diagnostics and treatments do not take into account any information about the nanostructure. In order for the gap to be filled, there are needs for more and better research designed to further understand the effects of disease and treatment on the nanostructure.

Future studies could continue cross-sectional studies, but include BP treated patients who had not fractured, to fully understand the role of treatment. It would be even better if a longitudinal study could be done to actually track the disease as well as long-term therapy. However it is currently not possible to perform a longitudinal study as there is no way of measuring bone strength *in-vivo*. The nanoindentation chapter had shown that the technique is not feasible at measuring useful nanomechanical properties but there are other methods that could be worth researching such as *in-vivo* Raman spectroscopy.

An *in-vivo* device could measure the mechanical integrity of bone and this data could be added into the current risk assessments, which could then also be used to follow up on patients on therapy to assess the optimal treatment duration for individual patients.

In addition to bisphosphonates, other newer treatments of osteoporosis target the underlying molecular mechanisms of the bone remodelling cycle (Kenkre & Bassett, 2018). As such, in addition to the effects at the structural levels, there is a growing need to look at pathophysiology of the disease in order to provide targets for pharmacological interventions.

7.8 Overall Summary

There is a growing consensus that bone's nanostructure and material contribute to whole bone strength and stiffness, specifically the collagen fibrils and mineral crystals. Indeed, at the start of this study the bone volume and microstructure were found to not entirely account for bone strength and stiffness, even when novel microarchitectural variable such as ITS was considered.

The theory that the basic building blocks of bone play a role in whole bone mechanics makes logical sense but it has never really been tested. Little is known about the mechanics at the nanoscale because the behaviour of collagen and mineral under loading and the way collagen fibrils slide, twist or unwind then break away from the mineral is so hard to visualise. To put the size into perspective, imagine one nanometre by imagining shrinking the sun down to the size of a football and then again by the same magnitude. Recent development of state-of-the-art synchrotron scanning now makes it possible to image the nanoscale structure and mechanics whilst simultaneously measuring tissue level (i.e. macro) mechanics, whilst also capturing the mineral crystal dimensions.

The nanoscale mechanics and structure of human bone from ageing controls was compared with ageing fracture patients, half of whom had been treated with BP and half not. Irrespective of treatment, fracture patients exhibited lower tissue strength and stiffness, in combination with lower collagen and mineral strains than non-fracture patients (i.e. the bone material was less deformable). Fracture patients also exhibited with larger (significantly wider) mineral crystals. Bisphosphonate seemed to exacerbate this

loss as BP treated patients exhibited with lower tissue and mineral strains than untreated fracture patients.

Hence it seems plausible that bone fragility is a result of impaired nanomechanical properties of bone, which in turn reduces the tissue level properties. The lower strain in the collagen-mineral matrix would be a result of less sliding and unwinding of the collagen, thus reducing the deformation the structure can undergo which cascade up to the whole bone level via (1) the formation and propagation of microcracks and (2) less bending of the whole-bone under load.

Due to the limitations of the study, results must be interpreted with caution because these are observational, cross-sectional data with all the potential selection biases that cannot be adjusted for. The study is also limited by the lack of DXA data in the fracture groups. We do not know whether the donors were osteoporotic, although they had suffered fragility fractures. However, studies of osteoporosis, which is a risk factor for fractures, have produced similar findings (Zimmerman et al., 2016). As osteoporotic patients are likely to suffer from fragility fractures, the changes in their nanostructures may mirror the changes observed in the fractured groups in this study.

Overall though, the pattern of decreasing strength at the macroscale and strain at the nanoscale from NFC to FC and BP suggest that fragility fractures are associated with loss of material properties at the nanoscale, which contribute to loss of whole bone strength, and therefore increased bone fragility. The newfound importance of the nanostructure to whole bone strength and stiffness could fill the gaps in current diagnostics and treatment if it is possible to measure material properties *in vivo*.

The study found that nanoscale deformations are important to the bone's ability to bend and resist loads. *In-vivo* nanoindentation techniques have been developed to measure such deformations. Data from a benchtop nanoindentation system were correlated with nanostrain data, but no correlation was found with fibril and mineral strains. Moreover there was also a lack of correlation with microstructure and whole bone strength and stiffness. Thus, it appears that the nanoindentation techniques do not measure the material properties accurately. Perhaps there are other alternatives such as Raman spectroscopy, which have been developed *in-vivo* to measure bone health.

Assessing the effect of nanomechanics on whole bone strength was a grand challenge from both scientific and technical perspectives requiring expertise in particle accelerator physics, advanced imaging and computing and bone biomechanics. The new fundamental research resolved how bone is strengthened from the nanoscale up. Hence the positive impact of this thesis is new knowledge, skills and expertise for us and the bone research community.

Bibliography

Acerbo, A.S. et al., 2014. Alterations in collagen and mineral nanostructure observed in osteoporosis and pharmaceutical treatments using simultaneous small- and wide-angle x-ray scattering. *Calcified Tissue International*, 95, pp.446-56.

Active Life Scientific, Inc. - Research, 2019. *Osteoprobe*. [Online] Available at: http://research.activelifescientific.com/osteoprobe/ [Accessed 17 July 2019].

Adams, A.L. et al., 2018. Bisphosphonate Drug Holiday and Fracture Risk: A Population-Based Cohort Study. *Journal of Bone and Mineral Research*, 33(7), pp.1252-59.

Akhtar, R., Daymond, M.R., Almer, J.D. & Mummery, P.M., 2008. Elastic strains in antler trabecular bone determined by synchrotron x-ray diffraction. *Acta Biomaterialia*, 4(6), pp.1677-87.

Akhter, M.P., Lappe, J.M., Davies , K.M. & Recker, R.R., 2007. Transmenopausal changes in the trabecular bone structure. *Bone*, 41(2007), pp.111-16.

Akkus, O. & Belaney, R.M., 2005. Sterilization by gamma radiation impairs the tensile fatigue life of cortical bone by two orders of magnitude. *Journal of Orthopaedic Research*, 23, p.1054.

Allen, M.R. et al., 2008. Bisphosphonates alter trabecular bone collagen cross-linking and isomerization in beagle dog vertebra. *Osteoporosis International*, 19(3), pp.329-37.

Altman, A.R. et al., 2015. Enhanced Individual Trabecular Repair and Its Mechanical Implications in Parathyroid Hormone and Alendronate Treated Rat Tibial Bone. *J Biomech Eng*, 137(1), pp.0110041–48.

Ammann, P. & Rizzoli, R., 2003. Bone strength and its determinants. *Osteoporosis International*, 14(3), pp.13-18.

Andersen, T. et al., 2009. A physical mechanism for coupling bone resorption and formation in adult human bone. *Am J Pathol.* , 14(1), pp.239-47.

Anderson, M.J., Keyak, J.H. & Skinner, H.B., 1992. Compressive mechanical-properties of human cancellous bone after gamma irradiation. *J Bone Joint Surg Am*, 74A, p.747.

Arnold, M. et al., 2017. Microindentation – a tool for measuring cortical bone stiffness? *Bone & Joint Research*, 6(9), pp.542-549.

Arsenault, A.L., 1989. A comparative electron microscopic stidy of apatite crystals in collagen fibrils of rat bone, dentin and calcified turkey tendons. *Bone and Mineral*, 6, pp.165-77.

Bailey, A.J., Paul, R.G. & Knott, L., 1998. Mechanisms of maturation and ageing of collagen Allen. *Mechanisms of Ageing and Development*, 106, pp.1-56.

Banes, A.J., Yamauchi, M. & Mechanic, G.L., 1983. Nonmineralized and mineralized compartments of bone: the role of pyridinoline in nonmineralized collagen. *Biochem Biophys Res Commun*, 113(3), pp.975-81.

Barth, H.D. et al., 2010. On the effect of x-ray irradiation on the deformation and fracture behavior of human cortical bone. *Bone*, 46, pp.1475-85.

Barth, H.D. et al., 2011. Characterization of the effects of x-ray irradiation on the hierarchical structure and mechanical properties of human cortical bone. *Biomaterials*, 32, pp.8892-904.

Black, D.M. et al., 1996. Randomised trial of effect of alendronate on risk of fracture in women with existing vertebral fractures. Fracture Intervention Trial Research Group. *Lancet*, 348(9041), pp.1535-41.

Boivin, G. et al., 2008. The role of mineralization and organic matrix in the microhardness of bone tissue from controls and osteoporotic patients. *Soumis*.

Bone, H.G. et al., 2004. Ten Years' Experience with Alendronate for Osteoporosis in Postmenopausal Women. *The New England Journal of Medicine*, 350, pp.1189-99.

Bonnick, S.L., 2011. Going on a druf holiday? *J Clin Densitom*, 14(4), pp.377-83.

Boskey, A., 2003. Bone mineral crystal size. *Osteoporosis International*, 14, pp.16-21.

Boskey, A.L. et al., 2005. Comparison of mineral quality and quantity in iliac crest biopsies from high—and low-turnover osteoporosis: an FT-IR microspectroscopic investigation. *Osteoporosis International*, 16(12), pp.2031-38.

Brandi, M.L., 2009. Microarchitecture, the key to bone quality. *Rheumatology*, 48(4), pp.iv3–v8.

Brown, J.P., Josse, R.G. & Osteoporosis Society of Canada, T.S.A.C., 2002. 2002 clinical practice guidelines for the diagnosis and management of osteoporosis in Canada. *CMAJ*, 167(10), pp.s1–s34.

Bunger, M.H. et al., 2010. Strontium and bone nanostructure in normal and ovariectomized rats investigated by scanning small-angle x-ray scattering. *Calcified Tissue International*, 86, pp.294-306.

Burge, R.T. et al., 2001. The cost of osteoporotic fractures in the UK: projections for 2000–2020. *Journal of Medical Economics*, 4(1-4), pp.51-62.

Burghardt, A.J., Krug, R. & Majumdar, S., 2018. Chapter 55 - High-Resolution Imaging Techniques for Bone Quality Assessment. In *Vitamin D*. 4th ed. San Francisco, California, USA: Academic Press. pp.1007-41.

Burr, D.B., 2002. Bone material properties and mineral matrix contributions to fracture risk or age in women and men. *Journal of Musculoskeletal Neuronal Interactions*, 2(3), pp.201-04.

Burr, D.B. et al., 1997. Bone Microdamage and Skeletal Fragility in Osteoporotic and Stress Fractures. *Journal of Bone and Mineral Research*, 12(1), pp.6-15.

Burr, D. et al., 2003. Tissue mineralization is increased following 1-year treatment with high doses of bisphosphonates in dogs. *Bone*, 33(6), pp.960-69.

Burstein, A.H., Zika, J.M., Heiple, K.G. & Klein, L., 1975. Contribution of collagen and mineral to the elastic- plastic properties of bone. *J. Bone Joint Surg*, 57A, pp.956-61.

Capulli, M., Paone, R. & Rucci, N., 2014. Osteoblast and osteocyte: games without frontiers. *Arch Biochem Biophys*, 561, pp.3-12.

Chanurlat, R.D. & Delmas, P.D., 2006. Drug insight: Bisphosphonates for postmenopausal osteoporosis. *National Clinical Practice Endocrinology & Metabolism*, 2, pp.211-19.

Charles, J. & Aliprantis, A., 2014. Osteoclasts: more than 'bone eaters'. *Trends Mol Med.*, 20(8), pp.449-59.

Chavassieux, P.M. et al., 1997. Histomorphometric assessment of the long-term effects of alendronate on bone quality and remodeling in patients with osteoporosis. *The Journal of Clinical Investigation*, 100(6), pp.1475–80.

Chen, H., Shoumura, S., Emura, S. & Bunai, Y., 2008. Regional variations of vertebral trabecular bone microstructure with age and gender. *Osteoporosis International*, 19(10), pp.1473-83.

Cooper, A., Drake, J. & Brankin, E., 2006. Treatment persistence with once-monthly ibandronate and patient support vs. once-weekly alendronate: results from the PERSIST study. *International Journal of Clinical Practice*, 60, pp.896-905.

Cornu, O. et al., 2000. Effect of freeze-drying and gamma irradiation on the mechanical properties of human cancellous bone. *Journal of Orthopaedic Research*, 18, p.426.

Corte, A., Giorgio, I. & Scerrato, D., 2019. A review of recent developments in mathematical modeling of bone remodeling. *Proceedings of the Institution of Mechanical Engineers Part H Journal of Engineering in Medicine, 234(3), pp.273-281*.

Cowin, S., 2009. *Bone mechanics handbook*. New York: CRC Press.

Cramer, J.A., Gold, D.T. & Silverman, S.L., 2007. A systematic review of persistence and complaince with bisphosphonates for osteoporosis. *Osteoporosis International*, 18, pp.1023-31.

Cummings, S.R. et al., 1998. Effect of alendronate on risk of fracture in women with low bone density but without vertebral fractures: results from the Fracture Intervention Trial. *JAMA*, 280(24), pp.20772-82.

Cummings, S., Karpf, D. & F, H., 2002. Improvement in spine bone density and reduction in risk of vertebral fractures during treatment with antiresorptive drugs. *Am J Med*, 112, pp.281-89.

Currey, J.D., 1984. Effects of differences in mineralization on the mechanical properties of bone. *Philos Trans R Soc Lond B Biol Sci*, 304(1121), pp.509-18.

Currey, J.D., 1988. The effect of porosity and mineral content on the Young's modulus of elasticity of compact bone. *Journal of Biomechanics*, 21, pp.131-39.

Currey, J.D., 2003. The many adaptations of bone. *J Biomech*, 36(10), pp.1487-95.

Currey, J.D. et al., 1997. Effects of ionizing radiation on the mechanical properties of human bone. *Journal of Orthopaedic Research*, 15, p.111.

Dall'ara, E., Ohman, C., Baleani, M. & Viceconti, M., 2007. The effect of tissue condition and applied load on Vickers hardness of human trabecular bone. *Journal of Biomechanics*, 40(14), pp.3267-70.

Dalle Carbonare, L. & Giannini, S., 2004. Bone microarchitecture as an important determinant of bone strength. *J Endocrinol Invest.*, 27(1), pp.99-105.

Damon, P., Paul, T. & Mckittrick, J., 2011. Minerals form a continuum phase in mature cancellous bone. *Calcified Tissue International*, 88, pp.351-61.

Depalle, B., Qin, Z., Shefelbine, S.J. & Buehler, M.J., 2015. Influence of cross-link structure, density and mechanical properties in the mesoscale deformation mechanisms of collagen fibrils. *Journal of the Mechanical Behavior of Biomedical Materials*, 52, pp.1-13.

Deutsches Elektronen-Synchrotron DESY, 2018. *DESY*. [Online] Available at: http://photon-science.desy.de/ [Accessed 27 Nov 2018].

Diamond Light Source, 2018. *Small Angle Scattering I22 Technical Specifications*. [Online] Available at: https://www.diamond.ac.uk/Instruments/Soft-Condensed-Matter/small-angle/I22/specs.html# [Accessed 27 Nov 2018].

Ding, M. et al., 2003. Canine cancellous bone microarchitecture after one year of high-dose bisphosphonate. *Calcified Tissue International*, 72(6), pp.737-44.

Doube, M. et al., 2010. BoneJ: Free and extensible bone image analysis in ImageJ. *Bone*, 47(6), pp.1076-79.

Drake, M.T., Clarke, B.L. & Khosla, S., 2008. Bisphosphonates: Mechanism of Action and Role in Clinical Practice. *Mayo Clin Proc*, 83(9), pp.1032-45.

Eastell, R. & Walsh, J.S., 2018. Microarchitecture of bone predicts fractures in older women. *Bone*, 14(2018), pp.255-56.

Faibish, D., Ott, S. & AL, B., 2006. Mineral Changes in Osteoporosis A Review. *Clin Orthop Relat Res*, 443, pp.28-38.

Fantner, G. et al., 2007. Nanoscale ion mediated networks in bone: osteopontin can repeatedly dissipate large amounts of energy. *Nano Lett.* , 7(8), pp.2491-98.

Fantner, G. et al., 2005. Sacrificial bonds and hidden length dissipate energy as mineralized fibrils separate during bone fracture. *Nature Materials*, 4(8), pp.612-16.

Farlay, D. et al., 2010. Mineral maturity and crystallinity index are distinct characteristics of bone mineral. *Journal of Bone and Mineral Metabolism*, 28(4), pp.433-45.

Fernández, M.P. et al., 2018. Effect of SR-microCT radiation on the mechanical integrity of trabecular bone using in situ mechanical testing and digital volume correlation. *Journal of the Mechanical Behavior of Biomedical Materials*, 88, pp.109-19.

Florencio-Silva, R. et al., 2015. Biology of Bone Tissue: Structure, Function, and Factors That Influence Bone Cells. *Biomed Res Int*, 2015, p.421746.

Franz-Odendaal, T., Hall, B. & Witten, P., 2006. Buried alive: how osteoblasts become osteocytes. *Dev Dyn.* , 235(1), pp.176-90.

Fratzl, P. et al., 1992. Mineral crystals in calcified tissues: A comparative study by SAXS. *Journal of Bone and Mineral Research*, 7(3), pp.329-34.

Fratzl, P., Schreiber, S. & Klaushofer, K., 1996. Bone minerilzation as studied by small-angle x-ray scattering. *Connective Tissue Research*, 34, pp.247-54.

Garnero, P., 2012. The contribution of collagen crosslinks to bone strength. *Bonekey Reports*, 1(182).

Gauiner, A. & Fournet, G., 1955. Small angle scattering of x-rays. *John Wiley, New York*.

Gibbons, M.L. et al., 1991. Effects of gamma irradiation on the initial mechanical and material properties of goat bone – patellar tendon – bone allografts. *J Orthop Res*, 9, p.209.

Glatter, O. & Katky, O., 1982. Small angle x-ray scattering. *Academic Press, New York*.

Gleason, L. et al., 2012. Diagnosis and Treatement of Osteoporosis in High-Risk Patients Prior to Hip Fracture. *Geriatric Orthopaedic Surgery and Rehabilitation*, 3(2), pp.79-83.

Glimcher, M.J., 1959. Molecular biology of mineralized tissues with particular reference to bone. *Reviews of Modern Physics*, 31, pp.359-93.

Gourion-Arsiquaud, S. et al., 2010. Bisphosphonate treatment modifies canine bone mineral and matrix properties and their heterogeneity. *Bone*, 46(3), pp.666-72.

Grynpas, M.D. et al., 1992. Changes in bone mineralization, architecture and mechanical properties due to long-term (1 year) administration of pamidronate (APD) to adult dogs. *Osteoporosis International*, 2(2), pp.74-81.

Guo, X.E. & Goldstein, S.A., 2000. Vertebral trabecular bone microscopic tissue elastic modulus and hardness do not change in ovariectomized rats. *J Orthop Res*, 18(2), pp.333-36.

Gupta, H.S. et al., 2004. Synchrotron diffraction study of deformation mechanisms in mineralized tendon. *Phys Rev Lett*, 93, p.4.

Gupta, H.S. et al., 2006. Cooperative deformation of mineral and collagen in bone at the nanoscale. *PNAS*, 103(47), pp.17741-46.

Gupta, H.S. et al., 2005. Nanoscale deformation mechanisms in bone. *Nano Lett*, 5, p.2108.

Harding, M., 2015. *Osteoporosis*. [Online] (31) Available at: http://patient.info/doctor/osteoporosis-pro [Accessed 3 March 2017].

Harris, S.T. et al., 1999. Effects of risedronate treatment on vertebral and nonvertebral fractures in women with postmenopausal osteoporosis: a randomized controlled trial. Vertebral Efficacy With Risedronate Therapy (VERT) Study Group. *JAMA*, 282(14), pp.1344-52.

Hauge, B.M. et al., 2006. Nanostructure of the neurocentral growth plate: insight from scanning small angle x-ray scattering, atomic force microscopy and scanning electron microscopy. *Bone*, 39, pp.530-41.

Hemmatian, H., Bakker, A., Klein-Nulend, J. & van Lenthe, G., 2017. Aging, Osteocytes, and Mechanotransduction. *Current Osteoporosis Reports*, 15(5), pp.401-11.

Hengsberger, S., Kulik, A. & Zysset, P., 2002. Nanoindentation discriminates the elastic properties of individual human bone lamellae under dry and physiological conditions. *Bone*, 30(1), pp.178-84.

Hert, J., Fiala, P. & Petertyl, M., 1994. Osteon orientation of the diaphysis of the long bones in man. *Bone*, 15, pp.269-77.

Hodge, A.J. & Petruska, J.A., 1963. Recent studies with the electron microscope on ordered aggregates of the tropocollagen molecule. *G.N. Ramachandran (Ed.), Aspects of protein structure, Academic Press, New York*, pp.289-300.

Huesa, C. et al., 2011. PHOSPHO1 is essential for mechanically competent mineralization and the avoidance of spontaneous fractures. *Bone*, 48(5), pp.1066-74.

Hu, S. et al., 2015. Micro/Nanostructures and Mechanical Properties of Trabecular Bone in Ovariectomized Rats. *Int J Endocrinol*, 2015, p.252503.

Hulme, P.A., Boyd, S.K. & Ferguson , S.J., 2007. Regional variation in vertebral bone morphology and its contribution to vertebral fracture strength. *Bone*, 41(6), pp.946-57.

Hulmes, D. & Miller, A., 1979. Quasi-hexagonal molecular packing in collagen fibrils. *Nature*, 282, pp.878-80.

International Osteoporosis Foundation, 2017. *Facts and Statistics*. [Online] IOF Available at: https://www.iofbonehealth.org/facts-statistics [Accessed 16 July 2019].

Jin, A., 2016. *The effect of bisphosphonates on bone microstructure and strength (Doctoral Dissertation)*. Retrieved from https://spiral.imperial.ac.uk/handle/10044/1/49791.

Jin, A. et al., 2017. The effect of long-term bisphosphonate therapy on trabecular bone strength and microcrack density. *Bone Joint Res.*, 6(10), pp.602–09.

Johnell, O. & Kanis, J.A., 2006. An estimate of the worldwide prevalence and disability associated with osteoporotic fractures. *Osteoporosis Internationa;*, 17, p.1726.

Jowsey, J., 1964. *Variations in bone mineralization with age and disease*. Boston: In Bone Biodynamics.

Kanis, J.A., 2015. *FRAX® - WHO Fracture Risk Assessment Tool*. [Online] (1) Available at: http://patient.info/doctor/fraxr-who-fracture-risk-assessment-tool [Accessed 3 March 2017].

Keene, D.R., Sakal, L.Y. & Burgeson, R.E., 1991. Human bone contains type III collagen, type VI collagen, and fibrillin: type III collagen is present on specific fibers that may mediate attachment of tendons, ligaments, and periosteum to calcified bone cortex. *J Histochem Cytochem*, 39, pp.59-69.

Kenkre, J.S. & Bassett, J.H.D., 2018. The bone remodelling cycle. *Annals of Clinical Biochemistry: International Journal of Laboratory Medicine*, 55(3), pp.308-27.

Kikuchi, M. et al., 2001. Self-organization mechanism in a bone-like hydroxyapatite/collagen nanocomposite synthesized in vitro and its biological reaction in vivo. *Biomaterials*, 22(13), pp.1705-11.

Kinney, J.H. & Ladd, A.J.C., 1998. The Relationship Between Three-Dimensional Connectivity and the Elastic Properties of Trabecular Bone. *Journal of Bone and Mineral Research*, 13(5), pp.839-45.

Krauss, S. et al., 2009. Inhomogeneous fibril stretching in antler starts after macroscopic yielding: indication for a nanoscale toughening mechanism. *Bone*, 44, p.1105.

Lane, N.E. et al., 2003. Both hPTH(1-34) and bFGF increase trabecular bone mass in osteopenic rats but they have different effects on trabecular bone architecture. *J Bone Miner Res*, 18(12), pp.2105-15.

Lange, C. et al., 2011. Fetal and postnatal mouse bone tissue contains more calcium than is present in hydroxyapatite. *Journal of Structural Biology*, 176, pp.159-67.

Lekkerkerker, F., Kanis, J.A. & Alsaved, N., 2007. Adherence to treatment for osteoporosis: a need for study. *Osteoporosis International*, 18, pp.1311-17.

Liberman, U.A. et al., 1995. Effect of oral alendronate on bone mineral density and the incidence of fractures in postmenopausal osteoporosis. The Alendronate Phase III Osteoporosis Treatment Study Group. *The New England Journal of Medicine*, 333, pp.1437-44.

Liu, X.S. et al., 2010. Individual Trabeculae Segmentation (ITS)–Based Morphological Analysis of High-Resolution Peripheral Quantitative Computed Tomography Images Detects Abnormal Trabecular Plate and Rod Microarchitecture in Premenopausal Women With Idiopathic Osteoporosis. *J Bone Miner Res*, 25(7), pp.1496–505.

Liu, X. et al., 2008. Complete Volumetric Decomposition of Individual Trabecular Plates and Rods and Its Morphological Correlations With Anisotropic Elastic Moduli in Human Trabecular Bone. *Journal of bone and mineral research*, 23(2), pp.223-34.

Lyles, K.W. et al., 2007. Zoledronic acid and clinical fractures and mortality after hip fracture. *The New England Journal of Medicine*, 357(18), pp.1799-809.

Ma, S. et al., 2017. Long-term effects of bisphosphonate therapy: perforations, microcracks and mechanical properties. *Scientific Reports*, 7, p.43399.

Majumdar, S. et al., 1997. Correlation of trabecular bone structure with age, bone mineral density, and osteoporotic status: in vivo studies in the distal radius using high resolution magnetic resonance imaging. *Journal of Bone Mineral Research*, 12(1), pp.111-18.

Mandair, G.S. & Morris, M.D., 2014. Contributions of Raman spectroscopy to the understanding of bone strength. *BoneKEy Reports*, 4, p.620.

Manolagas, S., 2000. Birth and death of bone cells: basic regulatory mechanisms and implications for the pathogenesis and treatment of osteoporosis. *Endocr Review*, 21(2), pp.115-37.

Matousek, P. et al., 2005. Non-invasive Raman spectroscopy of human tissue in vivo. *Central Laser Facility Annual Report*, pp.133-35.

McClung, M.R. et al., 2001. Effect of risedronate on the risk of hip fracture in elderly women. Hip Intervention Program Study Group. *N Engl J Med*, 344(5), pp.333-40.

microCT world, n.d. *microCT world*. [Online] Available at: http://microctworld.net/trabecular-thickness-tb-th-trabecular-spacing-tb-sp-trabecular-number-tb-n/ [Accessed 2019].

Miller, S., de Saint-Georges, L., Bowman, B. & Jee, W., 1989. Bone lining cells: structure and function. *Scanning Microsc*, 3(3), pp.953-60.

Moradian-Oldak, J. et al., 1991. Electron imaging and diffraction study of individual cyrstals of bone, mineralized tendon and synthetic carbonate apatite. *Connective Tissue Research*, 25(219-228).

Morgan, S., Poundarik, A.A. & Vashishth, D., 2016. Do Non-Collagenous Proteins Affect Skeletal Mechanical Properties? *Calcified Tissue International*, 97(3), pp.281-91.

Mosley, J., 2000. Osteoporosis and bone functional adaptation: mechanobiological regulation of bone architecture in growing and adult bone, a review. *J Rehabil Res Dev*, 37(2), pp.189-99.

Nair, A.K., Gautieri, A., Chang, S.W. & Buehler, M.J., 2013. Molecular mechanics of mineralized collagen fibrils in bone. *Nature Communications*, 16(4), p.1724.

Nanci, A., 1999. Content and distribution of noncollagenous matrix proteins in bone and cementum: relationship to speed of formation and collagen packing density. *Journal of Structural Biology*, 126(3), pp.256-69.

National Institue for Health and Care Excellence (NICE), 2019. *Osteoporosis*. [Online] Available at: https://www.nice.org.uk/guidance/qs149/chapter/Quality-statement-4-Long-term-follow-up [Accessed 5 July 2019].

National Institute for Health and Care Excellence, 2018. *Alendronic Acid*. [Online] Available at: https://bnf.nice.org.uk/drug/alendronic-acid.html [Accessed 12 December 2018].

National Institutes of Health Osteoporosis and Related Bone Diseases National Resource Center, 2018. *What is Bone?* [Online] Available at:

https://www.bones.nih.gov/sites/bones/files/pdfs/whatisbone-508.pdf [Accessed 10 July 2019].

Nazarian, A. et al., 2007. Densitometric, morphometric and mechanical distributions in the human proximal femur. *J Biomech*, 40(11), pp.2573-79.

Nguyen, H., Morgan, D.A.F. & Forwood, M.R., 2007. Sterilization of allograft bone: effects of gamma irradiation on allograft biology and biomechanics. *Cell Tissue Bank*, 8, pp.93-105.

Odetti, P. et al., 2005. Advanced Glycation End Products and Bone Loss during Aging. *Annals of the New York Academy of Sciences*, 1043, pp.710-17.

Oliver, W.C. & Pharr, G.M., 1992. An improved technique for determining hardness and elastic modulus using load and displacement sensing indentation experiments. *Journal of Materials Research*, 7(6), pp.1564-83.

Owen, R.L., Holton, J.M., Schulze-Briese, C. & Garman, E.F., 2009. Determination of x-ray flux using silicon pin diodes. *J. Sync. Rad.*, 16, pp.143-51.

Pachalis, E.P. et al., 2001. Spectroscopic Characterization of Collagen Cross-Links in Bone. *Journal of Bone and Mineral Research*, 16(10), pp.1821–28.

Paschalis, E.P. et al., 1997. FTIR microspectroscopic analysis of human iliac crest biopsies from untreated osteoporotic bone. *Calcified Tissue International*, 61(6), pp.487-92.

Pienkowski, D., Wood, C.L. & Malluche, H.H., 2019. Young's modulus and hardness of human trabecular bone with bisphosphonate treatment durations up to 20 years. *Osteoporosis International*, 30(2), pp.277-85.

Polly, B.J. et al., 2012. Intrinsic material properties of trabecular bone by nanoindentation testing of biopsies taken from healthy women before and after menopause. *Calcif Tissue Int.*, 90(4), pp.286-93.

Raisz, L.G. & Rodan, G.A., 2003. Pathogenesis of osteoporosis. *Endocrinol Metab Clin North Am*, 32(1), pp.15-24.

Reznikov, N. et al., 2018. Fractal-like hierarchical organization of bone begins at the nanoscale. *Science*, 360(6388).

Rho, J.Y., Khun-Spearing, L. & Zioupos, P., 1998. Mechanical properties and the hierarchical structure of bone. *Medical Engineering & Physics*, 20(2), pp.92-102.

Rho, J.Y., Zioupos, P., Currey, J.D. & Pharr, G.M., 2002. Microstructural elasticity and regional heterogeneity in human femoral bone of various ages examined by nano-indentation. *Journal of Biomechanics*, 35, pp.189-98.

Rinnerthaler, S. et al., 1999. Scanning small angle x-ray scattering analysis of human bone sections. *Calicified Tissue International*, 64, pp.422-29.

Robey, P.G., 1995. Biochemistry of Bone. In B.L. Riggs & L.J. Melton, eds. *Osteoporosis: etiology, diagnosis and management*. Philadelphia: Lippincott-Raven Publishers. pp.41-66.

Robinson, R., 1952. An electron-microscopic study of the crystalline inorganic component of bone and its relationship to the organic matrix. *The Journal of Bone & Joint Surgery*, 34(2), pp.389–476.

Rodriguez-Florez, N., Oyen, M. & SJ, S., 2013. Insight into differences in nanoindentation properties of bone. *J Mech Behav Biomed Mater*, 18, pp.90-99.

Rohanizadeh, R. et al., 2000. Ultrastructural properties of bone mineral of control and tiludronate-treated osteoporotic rat. *Calcified Tissue International*, 67, pp.330-36.

Rudman, K.E., Aspden, R.M. & Meakin, J.R., 2006. Compression or tension? The stress distribution in the proximal femur. *Biomedical Engineering*, 20, pp.5-12.

Rumpler, M. et al., 2012. Microcracks and Osteoclast Resorption Activity In Vitro. *Calcified Tissue International*, 90(3), pp.230-38.

Saha, P.K. & Chaudhuri, B.B., 1994. Detection of 3-D simple points for topology preserving transformations with application to thinning. *IEEE Trans. Pattern Anal.*, 16(1994), pp.1028-32.

Saha, P.K., Chaudhuri, B.B., Chanda, B. & Majumder, D.D., 1994. Topology preservation in 3d digital space. *Pattern Recogn*, 27(1994), pp.295-300.

Saito, M. & Marumo, K., 2010. Collagen cross-links as a determinant of bone quality: a possible explanation for bone fragility in aging, osteoporosis, and diabetes mellitus. *Osteoporosis International*, 21, pp.195–214.

Saito, M. et al., 2008. Collagen maturity, glycation induced-pentosidine, and mineralization are increased following 3-year treatment with incadronate in dogs. *Osteoporosis International*, 19(9), pp.1343-54.

Salmon, P.L., Ohlsson, C., Shefelbine, S.J. & Doube, M., 2015. Structure model index does not measure rods and plates in trabecular bone. *Front. Endocrinol*, 6(162).

Sanders, K.M. et al., 2006. Half the burden of fragility fractures in the community occur in women without osteoporosis. When is fracture prevention cost-effective? *Bone*, 38(5), pp.694-700.

Sansalone, V. et al., 2010. Determination of the heterogeneous anisotropic elastic properties of human femoral bone: from nanoscopic to organ scale. *J Biomech*, 43(10), pp.1857-63.

Shane, E. et al., 2014. Atypical subtrochanteric and diaphyseal femoral fractures: second report of a task force of the American Society for Bone and Mineral Research. *Journal of Bone Mineral Research*, 29(1), pp.1-23.

Silva, M.J., Brodt, M.D., Fan, Z. & Rho, J.Y., 2004. Nanoindentation and whole-bone bending estimates of material properties in bones from the senescence accelerated mouse SAMP6. *Journal of Biomechanics*, 37(11), pp.1639-46.

Stock, S.R., 2015. The Mineral–Collagen Interface in Bone. *Calcified Tissue International*, 97(3), pp.262-80.

Thürlimann, B., 2012. *Bisphosphonates in Clinical Oncology: The Development of Pamidronate*. 1st ed. Springer Science & Business Media.

The National Osteoporosis Society, 2016. *The National Osteoporosis Society*. [Online] Available at: https://nos.org.uk/ [Accessed 26 February 2017].

Thomsen, J.S., Ebbesen, E.N. & Mosekilde, L.I., 2002. Age-related differences between thinning of horizontal and vertical trabeculae in human lumbar bone as assessed by a new computerized method. *Bone*, 31(1), pp.136-42.

Tjhia, C. et al., 2011. Mechanical property and tissue mineral density differences among severely suppressed bone turnover (SSBT) patients, osteoporotic patients, and normal subjects. *Bone*, 49(6), pp.1279-89.

Traub, W., Arad, T. & Weiner, S., 1989. Three dimensional ordered distribution of crystals in turkey tendon collagen fibers. *Proc Natl Acad Sci USA*, 86, pp.9822-26.

Turner, C.H. et al., 1999. The elastic properties of trabecular and cortical bone tissues are similar: results from two microscopic measurement techniques. *Journal of Biomechanics*, 32, pp.437-41.

Unnanuntana, A., Gladnick, B.P., Donnelly, E. & Lane, J.M., 2010. The Assessment of Fracture Risk. *The Journal of Bone and Joint Surgery*, 92(3), pp.743-53.

van den Boogaarda, C. et al., 2006. Persistent bisphosphonat use and the risk of osteoporotic fractures in clinical practice: a database analysis study. *Current Medical Research and Opinion*, 22(9), pp.1757-64.

van der Linden, J.C., 2007. Effects of microarchitecture on bone strength. *Current Osteoporosis Reports*, 5(2), pp.56-61.

Vashishth, D., 2007. The role of collagen matrix in skeletal fragility. *Current Osteoporosis Reports*, 5(2), pp.62-66.

Villa, J.C., Gianakos, A. & Lane, J.M., 2016. Bisphosphonate Treatment in Osteoporosis: Optimal Duration of Therapy and the Incorporation of a Drug Holiday. *HSS Journal*, 12(1), pp.66-73.

Walker, M.D. et al., 2013. Premenopausal and postmenopausal differences in bone microstructure and mechanical competence in Chinese-American and white women. *J. Bone Miner. Res*, 28(2013), pp.1308-18.

Wang ZX, L.A.B.J.G.-A.S.D.E., 2016. Altered distributions of bone tissue mineral and collagen properties in women with fragility fractures. *Bone*, 84, pp.237-44.

Wang, X., Shen, X., Li, X. & Agrawal, C.M., 2002. Age-related changes in the collagen network and toughness of bone. *Bone*, 31(1), pp.1-7.

Wang, X. et al., 2008. Human iliac crest cancellous bone elastic modulus and hardness differ with bone formation rate per bone surface but not by existence of prevalent vertebral fracture. *J Biomed Mater Res B Appl Biomater*, 85(1), pp.68-77.

Weiner, S., Arad, T. & Traub, W., 1991. Crystal organization in rat bone lamallae. *Federation of European Biochemical Sciences*, 285(1), pp.49-54.

Weiner, S. & Price, P., 1986. Disaggregation of bone into crystals. *Calcified Tissue International*, 39, pp.365-75.

Wen, X.X. et al., 2015. Time Related Changes of Mineral and Collagen and Their Roles in Cortical Bone Mechanics of Ovariectomized Rabbits. *PLoS One*, 10(6), p.e0127973.

Wolfram, U., Wilke, H. & Zysset, P., 2010. Rehydration of vertebral trabecular bone: influences on its anisotropy, its stiffness and the indentation work with a view to age, gender and vertebral level. *Bone*, 46(2), pp.348-54.

Wu, Y. et al., 2013. Compositional and Material Properties of Rat Bone after Bisphosphonate and/or Strontium Ranelate Drug Treatment. *J Pharm Pharmaceut Sci*, 16(1), pp.52-64.

Yerramshetty, J.S. & O, A., 2008. The associations between mineral crystallinity and the mechanical properties of human cortical bone. *Bone*, 48(3), pp.476-82.

Yosibash, Z., Padan, R., Joskowicz, L. & Milgrom, C., 2007. A CT-based high-order finite element analysis of the human proximal femur compared to in-vitro experiments. *Journal of Biomechanical Engineering*, 129(3), pp.297-309.

Zimmerman, E.A., Barth, H.D. & Ritchie, R.O., 2012. The Multiscale Origins of Fracture Resistance in Human Bone. *JOM*, 64(2), pp.486-93.

Zimmerman, E.A., Busse, B. & Ritchie, R.O., 2015. The fracture mechanics of human bone: influence of disease and treatment. *BoneKEy Reports*, 4(743), pp.1-13.

Zimmerman, E. et al., 2016. Intrinsic mechanical behavior of femoral cortical bone in young, osteoporotic and bisphosphonate-treated individuals in low- and high energy fracture conditions. *Scientific Report*, 6(21072).

Zioupos, P., Cook, R. & Coats, A.M., 2008. Bone quality issues an matrix properties in OP cancellous bone. *Stud Health Technol Inform*, 133, pp.238-45.

Appendix

9.1 GP Letter

Imperial College London
Faculty of Medicine
Room 7L21, Floor 7, Laboratory Block
St Dunstan's Road, Charing Cross Campus
London, W6 8RP.
E: richard.abel@imperial.ac.uk
07760 168 197/020 3313 4489

Dr XXX
Address
Address

DATE

Dear Dr. XXX,

Request for patient information on bone health

We are writing to ask you for help with your patient named below who underwent hip surgery at St Mary's Hospital/Northwick Park Hospital. With the patients consent we have collected the femoral head for a study into the effect of long-term bisphosphonate use on fracture risk, which has been ethically approved (Imperial College Tissue Bank application number R11030).

Name: XXX
Date of Birth: XX/XX/XXX
Hospital Number: XXXXXX

The majority of patients who take bisphosphonates show improved bone strength and reduced fracture risk during the first 3-5 years of treatment. However, a small proportion (1-2%) exhibit rare stress fractures in the lateral proximal femur, often referred to as 'a-typical'. This may occur because bisphosphonates reduce the rate of natural bone repair (i.e. remodelling), which prevents the bone wastage associated with osteoporosis but may also cause unrepaired micro-cracks to accumulate and coalesce into a brittle fracture. Accordingly we are comparing bone collected from patients prescribed bisphosphonate therapy and naïve controls. We aim to determine *whether bisphosphonates can increase the risk of rare stress fractures in some patients?*

We are fully aware of the substantial demands upon your time and apologise for the inconvenience but we would like to request some patient info for the project. Please could you fill out the attached form and return it in the enclosed stamped addressed envelope.

Many thanks for your time
Yours sincerely

Dr. Richard Abel
Lecturer in Musculoskeletal Science

Prof. Justin Cobb
Chair in Orthopaedic Surgery

Name: XXX
Date of Birth: XX/XX/XXXX
Hospital Number: XXXXXX

Research Sample ID: XXXXX

1. Is the patient known to suffer from any of the following conditions?
   Osteoporosis Yes No
   Osteopenia Yes No
   Hip osteoarthritis Yes No
   Other major illness (es): _____

2. Has the patient taken / been taking bisphosphonates? Yes No
   If yes, Indication for treatment: _____
   Type of bisphosphonate: _____
   Dosage: _____
   The date treatment started: _MM_ /__Y Y Y Y_
   The date treatment discontinued: _MM_ /__Y Y Y Y_
   Reason for discontinuation:_____

3. Has the patient had a previous fracture? Yes No
   If yes, Site(s) of fracture(s): _____
   Date of fracture(s): _MM_ /__Y Y Y Y_

4. Has the patient received / been receiving hormone replacement therapy? Yes No
   If yes, Type of HRT: _____
   Dosage: _____
   The date treatment started: _MM_ /__Y Y Y Y_
   The date treatment discontinued: _MM_ /__Y Y Y Y_
   Reason for discontinuation:_____

5. Has the patient taken / been taking calcium supplementation? Yes No
6. Has the patient taken / been taking Vitamin D supplementation? Yes No
7. Is the patient known to have cancer? Yes No
   If yes, Type of cancer: _____
   Treatment received: _____
8. Has the patient had a history of smoking: Yes No

   If yes, current smoker: Yes No; or Time since quitting: _____